UNIVERSIDAD COMPLUTENSE DE MADRID

FACULTAD DE CIENCIAS MATEMÁTICAS

DEPARTAMENTO DE MATEMÁTICA APLICADA

TESIS DOCTORAL

A Mathematical Model for the Progression of Dental Caries

(Un Modelo Matemático para la Progresión de Caries Dentales)

MEMORIA PARA OPTAR AL GRADO DE DOCTOR

PRESENTADA POR

Lázaro René Izquierdo Fábregas

Director

Jacob Rubinstein

Madrid, 2014

UNIVERSIDAD COMPLUTENSE DE MADRID

FACULTAD DE CIENCIAS MATEMÁTICAS

Departamento de Matemática Aplicada

A Mathematical Model for the Progression of Dental Caries

(Un Modelo Matemático para la Progresión de Caries Dentales)

Tesis doctoral realizada por:

Lázaro René Izquierdo Fábregas

Bajo la dirección de:

Jacob Rubinstein

Madrid, March 10, 2014

"Funny quote"

A little boy was taken to the dentist. It was discovered that he had a cavity that would have to be filled. "Now, young man," asked the dentist, "what kind of filling would you like for that tooth?" "Chocolate, please," replied the youngster.

"Important quotes on the develop of this project"

Natural-born process in darkness...
In a postgraduate course at the FisyMat program professor Miguel A. Herrero told me a sentence which I translated in the following way:
"*The key in the mathematics applied to biology is to find a practical application in life and then, try to make a theory and not a theory in order to find practical application.*"

Two months later, and partly also as consequence of an unforgettable toothache suffered during childhood, a decision was taken to explore dental caries in an attempt to find some initial mathematical models.

Growing up from the darkness toward the light...
The idea was born in Granada, Spain, but it was not until May of 2011, in Haifa, Israel, that it began to grow, under the supervision of professor Koby Rubinstein. The main idea was to follow the advice offered by Professor Rubinstein:
"*The goal is to understand the phenomenon as dentist [sic] and later on we will be able to observe the processes that we can modelling [sic], but, we shouldn't force the theory in order to describe the dental caries process.*"

COMPLUTENSE UNIVERSITY OF MADRID

Abstract

Faculty of Mathematics
Department of Applied Mathematics

Doctor of Philosophy

by Lázaro René Izquierdo Fábregas

The study of tooth decay could be one of a range of next-generation research which will directly affect quality of life worldwide over the next few decades. The level of commercial development in this area is significant, with many international pharmaceutic companies wishing to develop better products (gel dentifrice, antiseptic mouthwash, etc) in order to prevent dental caries. There are two important processes in tooth decay formation, mineralization and demineralization, and both play a vital part in our life and the environment around us. Therefore, the study of dental caries has many important applications around it. One of the most famous and close applications is bone remodelling, because the tooth is a bone, and the enamel is one of the hardest tissue of the body. Also, demineralization and remineralization (if it took place) has been used by different scientific disciplines including the following: demineralized bone allograft, dental anthropology, remineralization of biomaterials, biotechnology, ageing techniques (demineralization of vertebrae and otolith) etc. In other words, the beneficial impact on society as a result of the availability of such studies to both personal health and environmental quality is immense. In consequence, carrying out an investigation which contributes to a better understanding of the prevention of dental caries, which improves pharmaceutical products or which reduces the cost of these, reveals alternative system designs and subsequently increases the rate at which new dentifrice gels or antiseptic mouthwashs etc., can be brought to the market, is of the utmost importance. In particular, mathematical modelling, analysis and simulation a virtual experimentation is a relatively inexpensive and yet powerful tool for scientific analysis and prediction.

An intuitive knowledge about dental caries implies creation of a cavity in the teeth after eating, however, further research reveals that tooth decay is the process where the mineral components of the tooth dissolve and break down. The underlying process starts with bacteria in the mouth that digest foodstuff such as sucrose, and converts them into acidic material such as lactic acid. Hydrogen ions that dissolve from the lactic acid penetrate into the tooth and react with its mineral compounds such as enamel or dentin. As the enamel dissolves, the tooth become mechanically weak and susceptible to local collapse, which leads to the formation of cavities.

Nature is very wise and curious, because, from a geometrical and structural point of view, it provided the mammalian species with a very well organized structure and the hard part of the body in order to realize the mechanical function of eating, teeth. Teeth, the so-called hardest substance in the human body (Avery et al. (2002); Chandra et al. (2007)), are structured with the general three layers: Enamel, Dentin and Pulp

Since ancient times humans have known that dental caries is the process by which enamel is worn away. This process starts when sugar consumed by the person (or animal) is digested by certain oral bacteria. The bacteria form a biofilm on the tooth surface. Since the teeth are naturally abased, for instance by tooth brushing, these biofilms typically are created in protected areas such as pits and grooves on the tooth surface or near the junction of the tooth and the gums. The common terminology in the literature is to call the area near the pit *occlusal surface*, while the area at the lower part of the tooth is sometimes termed *approximal surface*. The biofilm is typically quite small and concentrated near the pit, while it is spread when it forms at an approximal surface.

The bacteria convert the sugar into lactic acid. This acid reduces the pH level, that is, increases the concentration of hydrogen ions, near the tooth. The ions diffuse into the tooth, thus creating a high acidity environment inside the tooth. This leads to a reaction of the solid (mineral) enamel according to

$$\underset{\text{Hydroxyapatite (HAP)}}{Ca_{10}(PO_4)_6(OH)_{2(s)}} + 8\,H^{+}_{(aq)} \underset{k_{-1}}{\overset{k_1}{\rightleftharpoons}} 10\,Ca^{2+}_{(aq)} + 6\,HPO^{2-}_{4(aq)} + 2\,H_2O_{(l)} \tag{1}$$

This reaction is reversible, but when the pH level drops to about 5.5 or below, it proceeds mostly to the right. As the enamel is reacting and is demineralized, material is lost and later cavities form in the enamel. Indeed, one of the most challenging tasks for the odontologist research community is based on the improvement of a methodology to prevent the wearing-away of the teeth or increase the low remineralization of the tooth. From a chemical point of view and trying to find a new approach to prevent the creation and propagation of tooth decay, there is a research line which propagates the addition of fluoride into toothpaste or antiseptic mouthwashes.

As the enamel dissolves, visible lesions can be observed. Focus here will be on the formation of such lesions where mineral is lost and the porosity increases. Consideration is not given here to the formation of cavities, which is a total mechanical breakdown that occurs after too much mineral is lost.

In the demineralization line, in the last two decades the propagation of lesions was studied by a number of techniques. The most common early approach was development in the nature of an experiment in vitro. A number of important in vitro experiments have been developments by the authors (Anderson et al. (1998); Bollet-Quivogne et al. (2005); Patel et al. (1987a); Poole et al. (1981); ten Cate (1997)) in order to gain a better understanding of the lesion progression.

There is a long history of mathematical models for the initial stages of dental caries, and almost all of them consider appropriate conditions in order to apply Fick's Laws Gray (1962); Holly and Gray (1968); Patel et al. (1987a,b); Wu et al. (1976); Zimmerman (1966a,b,c), etc. Zimmermand's (Zimmerman (1966c)) and Patel's (Patel et al. (1987b))

works in particular will be referred to in order to illustrate the general theories of mathematics applied to the propagation of tooth decay. These models and the others differ in the level of complexity (e.g. the number of compounds) and details of the reaction.

The diffusion of chemical species in a solution, porous medium or a combination of them, usually are assumed with the fact that *the flow goes from regions of high concentration to regions of low concentration*, i.e., a gradient of concentration in accordance with Fick's first and second law.

Fick's first law: The flux $\mathcal{J}_i$ of chemical specie i is proportional to the concentration gradient

$$\mathcal{J}_i = -D_i \nabla u_i \tag{2}$$

where $\nabla = \left(\partial_x, \partial_y, \partial_z\right)$, D_i the diffusion coefficient of specie i, and $\partial_x = \partial/\partial x$ and so on for ∂_y and ∂_z.

However, the Fick's first law is basic for diffusive transport and there is a more fundamental basis for diffusive process, and the explanation appears in the works of Quigley et al. (1987), Daniel and Shackelford (1988) and others. Two important relationships are the so-called Einstein relation for the kinetic theory, connecting the mobility of a particle with the diffusion coefficient $D_i = \mu_i k_B T$, and the Stokes-Einstein relation, for large spherical molecules in a liquid with low Reynolds number $D_i = k_B T/6\pi\eta r_i$, where k_B is Boltzmann's constant, T the the absolute temperature, μ_i is the "mobility" of the particle i, η is the viscosity of the liquid and r_i the radius of the molecules. In addition, if the concentrations changes with time, we can induce the second Fick's law

The goal in the model of Zimmerman is studying the behaviour of the solubility of synthetic HAP in chemical solutions controlled with a mathematical model. In order to make more easy the mathematical analysis the following assumptions are taken into account: Diffusion is assumed one-dimensional with a flow parallel to the prisms directions; The enamel is regarded as a granular base (surface) and the Fick's laws are applicable.

The goals of Patel's work was to set out a theorical understanding between the dissolution behaviour of HAP and its chemical components in the demineralization process on in vitro experiment with teeth and the numerical simulations of a constructed mathematical model for describe the propagation of dental caries.

The goal of this research is to derive a mathematical model for the first part of this process, namely the dissolution of the enamel. The model starts from the local transport equations on the microscopic scale. The local equations are averaged via the method of homogenization to create a macroscopic model. The model proposed in this thesis takes into account key factors such as the anisotropic geometry of the enamel and the time evolution of the microstructure due to demineralization and remineralization.

Chapter 1 provides some background material which includes the motivation for studying tooth decay as well as an elementary description of their structure and functionality. This chapter also includes a background history of the mathematical models applied to the progression of dental caries.

Enamel has a periodic distribution of crystals into the inter-rod, therefore, in order to consider the geometry of the solid structure, Chapter 2 is dedicated to introducing the basic ideas of the homogenization method and the domain decomposition methods.

The results are presented in Chapter 3 with the microscopic equations. These equations will be homogenized to take into account the evolution of the microgeometry in space and time. An evolution equation for the microstructure is therefore derived. The macroscopic equations involve averaged diffusion coefficients. In addition, the parameters involved in the local enamel dissolution process are considered in some detail. Finally, adding the influence of the outer layer of the enamel to the model, a second model (a version of the first one) is postulated.

Chapter 4 presents a simplified version of the model assuming that the amount of hydrogen ions lost to the reaction is small compared to their total amount and a rectangular geometry that mimic the in vitro experiments. In addition, two examples are provided to describe the method of estimate of the effective diffusion coefficient for two different cell problems. These coefficients are determined by solving certain canonical differential equations. The difficult task of estimating the effective diffusivities in a varying local geometry is also discussed. A number of numerical examples are then presented and contrasted with a number of experiments results.

In Chapter 5 the model used for this research is presented and the underlying assumptions behind it are explained. The equations are solved in a three-dimensional rectangular domain. The model is also upgraded to account for the resilient outer layer of the enamel, and inspect its effect on caries progress. Furthermore, discussion of the important and controversial issue of what is the progression rate of caries solving the equations in a two-dimensional geometry that mimics a realistic tooth shape is provided. In particular consideration is given to the shape of the lesion, in terms of where it starts along the tooth boundary. The chapter finishes with a discussion of the model and the simulations therein.

A summation of the basic ideas of the work will be presented in Chapter 6, which will also reveal the version of general model in general curvilinear coordinates. Finally, a summary of the work from the previous chapters is given in this chapter.

Chapter 7 offers suggestions for future extensions of the model. First, the paradox of Cate in relation to the influence of the fluoride in the process of caries in order to ilustrate the possible extension of the model is provided. In addition, a possible second extension of the model to the bone remodeling process is suggested.

Finally, in Appendix A, a number of geometrical identities required are derived. Appendix B and Appendix C provide the mathematic frameworks for the numerical solutions of the examples undertaken. An extensive and detailed bibliography is provided at the end of the thesis.

UNIVERSIDAD COMPLUTENSE DE MADRID

Resumen

Facultad de Matemáticas
Departamento de Matemáticas Aplicadas

Doctor en Filosofía

por Lázaro René Izquierdo Fábregas

El estudio de las caries dentales es una de las líneas de investigacón de última generación que afectá directamente la calidad de vida en todo el mundo. El nivel de desarrollo comercial en esta área es importante, con muchas compañías internacionales farmacéuticas que desarrollan mejores productos (de dentífrico en gel, enjuague bucal antiséptico, etc) con el fin de prevenir las caries dentales. Hay dos procesos importantes en la formación de la caries dentales, la mineralización y desmineralización, y ambos juegan un papel vital en nuestra vida y el medio ambiente que nos rodea. Por lo tanto, el estudio de la caries dentales tiene muchas aplicaciones importantes que lo rodean. Una de las aplicaciones más famosas es la remodelación ósea, debido a que el diente es un hueso, y el esmalte es uno de los tejidos más duros del cuerpo humano. También, la desmineralización y remineralización (si tiene lugar) ha sido utilizado por diferentes disciplinas científicas como las siguientes: antropología dental, remineralización de los biomateriales , la biotecnología, las técnicas de envejecimiento (desmineralización de vértebras y otolitos), etc. En otras palabras, el impacto beneficioso en la sociedad como consecuencia de la disponibilidad de dichos estudios para la salud personal y la calidad ambiental es inmenso. En consecuencia, la realización de una investigación que contribuye a una mejor comprensión de la prevención de la caries dentales, lo que mejora los productos farmacéuticos o que reduce el costo de estos, revela diseños de sistemas alternativos y, posteriormente, aumenta la velocidad a la que los nuevos geles dentífricos o enjuagues bucales antisépticas etc., se pueden poner en el mercado, es de suma importancia. En particular, los modelos matemáticos , análisis y simulación de una experimentación virtual es una herramienta relativamente barata y potente para el análisis científico y la predicción.

Desde la antigüedad los seres humanos han sabido que la caries dental es el proceso por el que el esmalte se disuelve. Este proceso comienza cuando el azúcar consumida por las personas (o animales) se digiere por ciertas bacterias orales. Las bacterias forman una biopelícula sobre la superficie del diente. Dado que los dientes son, naturalmente, degradados, por ejemplo, al cepillarse los dientes, estos biofilms normalmente se crean en las áreas protegidas, tales como pozos y surcos en la superficie del diente, o cerca de la unión del diente y la encía. La terminología común en la literatura es llamar a la zona cerca de la superficie oclusal pozo, mientras que el área en la parte inferior del diente se

denomina a veces la superficie proximal. La biofilm es normalmente bastante pequeño y se concentra cerca del hoyo, mientras que se transmite cuando se forma en una superficie proximal.

Las bacterias convierten el azúcar en ácido láctico. Este ácido reduce el nivel de pH, que aumenta la concentración de iones de hidrógeno, cerca del diente. Los iones se difunden en el diente, creando así un ambiente de alta acidez dentro del diente. Esto conduce a una reacción del sólido (mineral) de esmalte según

$$\underset{\text{Hydroxyapatite (HAP)}}{Ca_{10}(PO_4)_6(OH)_{2(s)}} + 8\,H^{+}_{(aq)} \underset{k_{-1}}{\overset{k_1}{\rightleftharpoons}} 10\,Ca^{2+}_{(aq)} + 6\,HPO^{2-}_{4(aq)} + 2\,H_2O_{(l)}$$

Esta reacción es reversible, pero cuando el nivel de pH cae a aproximadamente hasta 5.5 o por debajo, la reacción avanza sobre todo a hacia la derecha. A medida que el esmalte está reaccionando y se desmineraliza, el material se pierde y cavidades posteriores se forman en el esmalte. De hecho, una de las tareas más difíciles para la comunidad de investigación odontóloga se basa en la mejora de una metodología para evitar el desgaste de los dientes o de aumentar el bajo nivel de remineralización del diente. Desde un punto de vista químico y tratando de encontrar un nuevo enfoque para prevenir la creación y propagación de caries dentales hay una línea de investigación para la adición de fluoruro en la pasta de dientes o enjuagues bucales antisépticos.

A medida que el esmalte se disuelve, lesiones visibles se pueden observar. El enfoque de este trabajo es la formación de tales lesiones em las que se pierde mineral y la porosidad aumenta. No se considerará la formación de cavidades, que es un desglose mecánico total que se produce después de que se pierde demasiada cantidad de mineral.

En el campo de la desmineralización, en las dos últimas décadas la propagación de las lesiones ha sido estudiada por un número de técnicas. El enfoque temprano más común es el desarrollo en la naturaleza de un experimento in vitro. Un número importante de los experimentos in vitro han sido los desarrollos por los autores (Anderson et al. (1998); Bollet-Quivogne et al. (2005); Patel et al. (1987a); Poole et al. (1981); ten Cate (1997)) con el fin de obtener una mejor comprensión de la propagación de la lesión.

Hay una larga historia de los modelos matemáticos para las etapas iniciales de la caries dental, y casi todos ellos consideran las condiciones apropiadas para la aplicación de las Leyes de Fick, por ejemplo Gray (1962); Holly and Gray (1968); Patel et al. (1987a,b); Wu et al. (1976); Zimmerman (1966a,b,c). En particular haciendo referencia a los trabajos de Zimmermand (Zimmerman (1966c)) y Patel (Patel et al. (1987b)) popdemos decir que las teorías generales de la matemática aplicada a la propagación de las caries dentales pueden ser mejoradas significativamente haciendo nuevas aportaciones en el nivel de complejidad de los modelos con relación a los experimentos realizados.

La difusión de las sustancias químicas en una solución, medio poroso o una combinación de ellos, por lo general se supone con el hecho de que *el flujo va desde las regiones de alta concentración a regiones de baja concentración*, es decir, un gradiente de concentración como consecuencia de la primera y la segunda ley de Fick.

Primera ley de Fick: El flujo $\mathcal{J}_i$ de una sustancia química i es proporcional al gradiente de concentración

$$\mathcal{J}_i = -D_i \nabla u_i \tag{3}$$

donde $\nabla = \left(\partial_x, \partial_y, \partial_z\right)$, D_i *el coeficiente de difusión de la sustancia i,* $\partial_x = \partial/\partial x$, ∂_y *y* ∂_z.

Sin embargo, la primera ley de Fick es básica para el transporte por difusión y existe una base fundamental para el proceso de difusión, y la explicación aparece en las obras de Quigley et al. (1987), Daniel and Shackelford (1988) y otros. Dos relaciones importantes son la denominada relación de Einstein de la teoría cinética, la conexión de la movilidad de una partícula con el coeficiente de difusión $D_i = \mu_i k_B T$, y la relación de Stokes-Einstein, para grandes moléculas esféricas en un líquido con bajo número de Reynolds $D_i = k_B T/6\pi\eta r_i$, donde k_B es la constante de Boltzmann, T la temperatura absoluta, μ_i es la "movilidad" de la partícula i, η es la viscosidad del medio y r_i el radio de las moléculas. Además, si las concentraciones cambia con el tiempo, se puede inducir la segunda ley de Fick.

El objetivo en el modelo de Zimmerman es estudiar el comportamiento de la solubilidad de HAP sintética en soluciones químicas controladas con un modelo matemático. Con el fin de hacer más fácil el análisis matemático se toman las siguientes suposiciones en cuenta: La difusión se supone unidimensional con un flujo paralelo a las direcciones de los prismas; El esmalte se considera como una base granular (superficie) y las leyes de Fick son aplicables. Por otro lado, los objetivos del trabajo de Patel es establecer una comprensión teórica entre el comportamiento de la disolución de HAP y sus componentes químicos en el proceso de desmineralizaciín en la experimentación in vitro con los dientes y las simulaciones numéricas de un modelo matemático construido para describir la propagación de las caries dentales.

El objetivo de esta investigación es obtener un modelo matemático para la primera parte de este proceso, es decir, la disolución del esmalte. El modelo parte de las ecuaciones de transporte local en la escala microscópica. Las ecuaciones locales se promedian a través del método de homogeneización para crear un modelo macroscópico. El modelo propuesto en esta tesis tiene en cuenta factores claves como la geometría anisotróopica del esmalte y la evolución temporal de la microestructura debido a la desmineralización y la remineralización.

El Capítulo 1 proporciona los antecedentes que incluye la motivación y descripción del porque estudiar la progresión de las caries dentales, así como una descripción elemental de su estructura y funcionalidad. Este capítulo también incluye la historia de los anteriores modelos matemáticos aplicados a la progresión de las caries dentales.

El esmalte tiene una distribución periódica de los cristales en el medio inter-cristal, por lo tanto, con el fin de tener en cuenta la geometría de la estructura sólida, Capítulo 2 está dedicado a la introducción de las ideas básicas del método de homogeneización y el método de descomposición de dominios.

Los resultados que se presentan en la Capítulo 3 comienza con la deducción de las ecuaciones microscópicas. Estas ecuaciones son homogeneizadas para tener en cuenta la evolución de la microgeometría en el espacio y el tiempo. Por consiguiente, se deriva una

ecuación de evolución de la microestructura. Las ecuaciones macroscápicas implican coeficientes de difusión promediados. Además, los parámetros que intervienen en el proceso de disolución del esmalte local son considerados con cierto detalle. Finalmente, se postula un segundo modelo (una versión del primero) mediante la adición de la influencia de la capa exterior de esmalte para el modelo.

En el Capítulo 4 se presenta una versión simplificada del modelo suponiendo que la cantidad de iones de hidrógeno perdidos en la reacción es pequeña en comparación con su cantidad total y una geometría rectangular que imitan los experimentos in vitro. Además, se proporcionan dos ejemplos para describir el método de estimación del coeficiente de difusión eficaz para dos problemas diferentes de células. Estos coeficientes son determinados por la solución de ciertas ecuaciones diferenciales. También se discute la difícil tarea de estimar los coeficientes de difusividad efectiva en una geometrÃŋa local variable. Un número de ejemplos numéricos son presentados en contratraste con los resultados de experimentos.

En el Capítulo 5, se presentan y los supuestos que subyacen detrás del modelo utilizado para esta investigación. Las ecuaciones se resuelven en un dominio rectangular tridimensional . El modelo también se actualiza para tener en cuenta para la capa externa del esmalte , e inspeccionar su efecto sobre la progresión de las caries. Además, se proporciona la discusión del tema importante y controvertido relacionado con la tasa de progresión de las caries resolviendo las ecuaciones en una geometría bidimensional que imita la forma realista del diente. En particular la consideración de la forma de la lesión, en términos de dónde se inicia a lo largo de la frontera de los dientes. El capítulo termina con una discusión sobre el modelo y las simulaciones del mismo.

Un resumen de las ideas básicas de la obra será presentada en el Capítulo 6, que también permitirá conocer la versión del modelo general en coordenadas curvilíneas generales. Por último , un resumen de lo realizado en los capítulos anteriores. El Capítulo 7 ofrece sugerencias para futuras extensiones del modelo . En primer lugar, la paradoja de Cate en relación con la influencia del fluoruro en el proceso de las caries con el fin de proporciona una posible extensión y aplicación industrial del modelo. Además, se sugiere una posible segunda extensión del modelo del proceso de remodelación ósea.

En el Apéndice A, una serie de identidades geométricas requeridas se derivan. Por otro lado en el Apéndice B y Apéndice C se proporciona el marco matemático para la soluciones numéricas de los ejemplos realizados. Por último, para finalización de la tesis se muestra la amplia y detallada bibliografía que se utilizó para el desarrollo de este trabajo.

Acknowledgements

Foremost, I would like to express my sincere gratitude to my advisor Prof. Jacob Rubinstein for the continuous support of my Ph.D study and research, for his patience, motivation, enthusiasm, and immense knowledge. His guidance helped me in all the time of research and writing of this thesis. Thank you for encouraging my research and for allowing me to grow as a research scientist. Your advice on both research as well as on my career have been priceless.

I would also like to thank my international referees, professor Chris Budd, professor Hermenegildo Borges de Oliveira and professor Jesús Ildefonso Díaz Díaz, for his professional reviews. I would like to express the deepest appreciation to my committee members, professor Jean-Michel Coron, professor Juan Francisco Padial Molina, professor Alfonso Carlos Casal Piga, professor Angel Ramos, professor Gerardo Oleaga, professor José Ignacio Tello del Castillo, professor L. Tello, professor Gregorio Díaz Díaz and specially to my project manager and committee president, the professor Jesús Ildefonso Díaz Díaz, for his support and help. In addition, my immense gratitude to the professor Miguel ángel Herreo for their advice and mentorship.

A special thanks to my family. Words cannot express how grateful I am to my mother-in law, father-in-law, my mother, my father and brothers for all of the sacrifices that you have made on my behalf. I would also like to thank all of my friends who supported me in writing, and incented me to strive towards my goal. At the end I would like express appreciation to my beloved wife Aniya who spent sleepless nights with and was always my support in the moments when there was no one to answer my queries.

Contents

List of Figures

List of Tables

To my Grandparents

Chapter 1

Introduction and Background

1.1 Why study tooth decay?

The study of tooth decay could be one of a range of next-generation research which will directly affect quality of life worldwide over the next few decades. The level of commercial development in this area is significant, with many international pharmaceutic companies wishing to develop better products (gel dentifrice, antiseptic mouthwash, etc) in order to prevent dental caries. There are two important processes in tooth decay formation, mineralization and demineralization, and both play a vital part in our life and the environment around us. Therefore, the study of dental caries has many important applications around it. One of the most famous and close applications is bone remodelling, because the tooth is a bone, and the enamel is one of the hardest tissue of the body. Also, demineralization and remineralization (if it took place) has been used by different scientific disciplines including the following: demineralized bone allograft, dental anthropology, remineralization of biomaterials, biotechnology, ageing techniques (demineralization of vertebrae and otolith) etc. In other words, the beneficial impact on society as a result of the availability of such studies to both personal health and environmental quality is immense. In consequence, carrying out an investigation which contributes to a better understanding of the prevention of dental caries, which improves pharmaceutical products or which reduces the cost of these, reveals alternative system designs and subsequently increases the rate at which new dentifrice gels or antiseptic mouthwashs etc., can be brought to the market, is of the utmost importance. In particular, mathematical modelling, analysis and simulation a virtual experimentation is a relatively inexpensive and yet powerful tool for scientific analysis and prediction.

An intuitive knowledge about dental caries implies creation of a cavity in the teeth after eating, however, further research reveals that tooth decay is the process where the mineral components of the tooth dissolve and break down. The underlying process starts with bacteria in the mouth that digest foodstuff such as sucrose, and converts them into acidic material such as lactic acid. Hydrogen ions that dissolve from the lactic acid penetrate into the tooth and react with its mineral compounds such as enamel or dentin. As the enamel dissolves, the tooth become mechanically weak and susceptible to local collapse, which leads to the formation of cavities.

1.2 Structure of teeth

Nature is very wise and curious, because, from a geometrical and structural point of view, it provided the mammalian species with a very well organized structure and the hard part of the body in order to realize the mechanical function of eating, teeth. Teeth, the so-called hardest substance in the human body (Avery et al. (2002); Chandra et al. (2007)), are structured with the general three layers: Enamel, Dentin and Pulp Figure. 1.1(a).

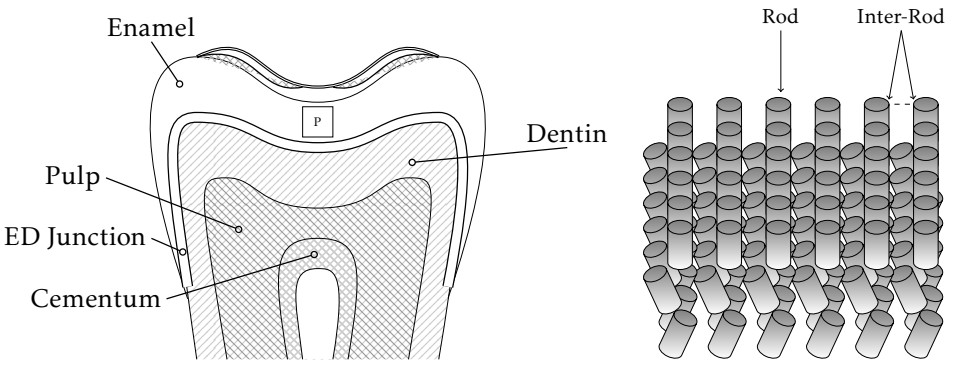

(a) Tooth (b) Enamel Layers

Figure 1.1: (a) Diagram showing the anatomy of the tooth, structured for the fundamental layers and the junction of the enamel and the dentin (ED junction). (b) Representation of the three different layers of the enamel (zoom in P, figure (a)) structured by the rod and the inter-rod.

The outer layer of the tooth is formed of enamel. This is a mineral consisting of a packed array of rods, called sometimes enamel prisms. The radius of a rod is about $2\mu m - 3\mu m$ and the distance between rods is about $1\mu m - 3\mu m$ Jeng et al. (2009); Radlanski and Renz (2004). The rods are elongated, essentially parallel to each other. Their length varies between $20\mu m - 1000\mu m$ Radlanski and Renz (2004). Each rod consists of hydroxyapatite crystals. Enamel is created in the human body at infanthood. It is not

generated later in life. However, even upon demineralization through caries, the process is reversible, and remineralization can take place. In the tooth the rods are arranged roughly in layers, where the long axis is perpendicular to the tooth surface Figure 1.1(b). The inter-rod domain consists of pores and of material that has the same chemical composition as enamel, but the crystal orientation is not ordered as in the rods themselves. It is known that diffusion in the enamel is mostly along the prisms (rods). General reviews on enamel's physical, geometrical and chemical properties can be found in a number of texts, e.g. Avery et al. (2002) and Thylstrup and Fejerskov (1986).

Looking at the Figure 1.1(b), we can see some kind of organization in the three layers mixed by the enamel prism which can give the impression of order or a sense thereof. The issue here is that one of the main roles of the rods is how is its organization by different layers ordered, focusing the attention in the so-called "outer layer", where the demineralization process take place in the early instant. Following the papers cited by Dumont (1995, 1996); Maas and Dumont. (1999) the patterns of the enamel prism in mammalian are organized in three basic categories based on their prism shape and the packing patterns. The pattern of the prism 1 (PP1) consists of prisms with complete limits that are disposed in the displaced horizontal rows relating to the axis cervical apico of the tooth, see Figure 1.2(a). On the other hand, prisms take the shape of an arc and are arranged in vertical rows of displacement separated by a difference between rows of sheets, this is the pattern of the prism 2 (PP2), see Figure 1.2(b), and as to third pattern (PP3), the prisms are shaped in an arc and are arranged in horizontal rows of compensation, see Figure 1.2(c).

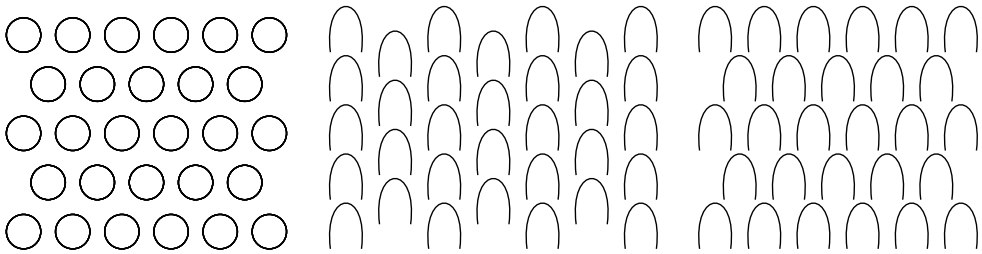

(a) PP1 (b) PP2 (c) PP3

Figure 1.2: Sketches of three different patterns of the prism, displaying three different unique spatial organization and enamel prism shape. (a) Prism pattern 1 (PP1); (b) Prism pattern 2 (PP2); (c) Prism pattern 3 (PP3).

Dentin is the material just below the enamel. It is not as hard as enamel, but also not completely different from it. Dentin consists of 70 percent hydroxyapatite crystals, 20 percent organic material, and water. The mineral part of the dentin is not organized in rods as in enamel. However, dentin also has a microscopic structure. It has many tiny

channels, dentinal tubules, containing fluid that extend from the exterior part of it (the enamel-dentin border) to the inner part of the tooth (pulp).

The pulp is the only soft tissue in the tooth and occupies a cavity located in the center of the tooth Fig. 1.1(a), and it's formed by cells, tiny blood vessels, and a nerve Chandra et al. (2007). The pulp chamber is a cavity centric excavated in complete dentine, than from the point of view morphologic reproduce the dentinal element shape, for what's changing according to the anatomy of the teeth. The stimulation of pulpar nerve fibers through heat or cold, mechanical or chemical action, produces a painful sensation âĂŞ a toothache.

1.3 Tooth decay formation.

Since ancient times humans have known that dental caries is the process by which enamel is worn away. This process starts when sugar consumed by the person (or animal) is digested by certain oral bacteria. The bacteria form a biofilm on the tooth surface. Since the teeth are naturally abased, for instance by tooth brushing, these biofilms typically are created in protected areas such as pits and grooves on the tooth surface or near the junction of the tooth and the gums. The common terminology in the literature is to call the area near the pit *occlusal surface*, while the area at the lower part of the tooth is sometimes termed *approximal surface*. The biofilm is typically quite small and concentrated near the pit, while it is spread when it forms at an approximal surface.

The bacteria convert the sugar into lactic acid. This acid reduces the pH level, that is, increases the concentration of hydrogen ions, near the tooth. The ions diffuse into the tooth, thus creating a high acidity environment inside the tooth. This leads to a reaction of the solid (mineral) enamel according to

$$\underset{\text{Hydroxyapatite (HAP)}}{Ca_{10}(PO_4)_6(OH)_{2(s)}} + 8\,H^{+}_{(aq)} \underset{k_{-1}}{\overset{k_1}{\rightleftharpoons}} 10\,Ca^{2+}_{(aq)} + 6\,HPO^{2-}_{4(aq)} + 2\,H_2O_{(l)} \tag{1.1}$$

This reaction is reversible, but when the pH level drops to about 5.5 or below, it proceeds mostly to the right. As the enamel is reacting and is demineralized, material is lost and later cavities form in the enamel. Indeed, one of the most challenging tasks for the odontologist research community is based on the improvement of a methodology to prevent the wearing-away of the teeth or increase the low remineralization of the tooth. From a chemical point of view and trying to find a new approach to prevent the creation

and propagation of tooth decay, there is a research line which propagates the addition of fluoride into toothpaste or antiseptic mouthwashes.

As the enamel dissolves, visible lesions can be observed. Focus here will be on the formation of such lesions where mineral is lost and the porosity increases. Consideration is not given here to the formation of cavities, which is a total mechanical breakdown that occurs after too much mineral is lost.

1.3.1 In vitro and in vivo experiments

In the demineralization line, in the last two decades the propagation of lesions was studied by a number of techniques. The most common early approach was development in the nature of an experiment in vitro. A number of important in vitro experiments have been developments by the authors (Anderson et al. (1998); Bollet-Quivogne et al. (2005); Patel et al. (1987a); Poole et al. (1981); ten Cate (1997)) and in order to gain a better understanding, this section will proceed with a brief summary of two of these in vitro experiments.

Pole and colleagues experiment: They took some teeth from the different species of primate Pan Troglodytes (Chimpanzee), Macaca Fascicularis, Macaca Mulatta and Papio Cynocephalus depicted in the Figure 1.3, with different ages and from children of aged 10-14 yr, where all the removed teeth are caries-free.

After performing some specific chemical technics in order to obtain the adequate experimental environment for each extracted tooth and remove the soft tissue, the teeth are introduced in a special gels at a fixed pH, and it were removed at intervals from the gels in order to measure the depths induced by the acid-gels on the teeth.

(a) Pan Troglodytes (b) Macaca Fascicularis (c) Macaca Mulatta (d) Papio Cynocephalus

Figure 1.3: Drawings of different species of primates used for extracting the necessary teeth for the experiments of Pool and colleagues.

Anderson and colleagues experiment: They prepared some enamels blocks from humans, varnishing all the cut surfaces of the blocks in order to expose only the natural surfaces, besides,

the varnished surfaces depend of the form to measure the deepness of the lesion in the enamel block, Figure 1.4(a).

After introducing the cut block in to a special chamber with a special acid gel to a fixed pH=4.5, as show in Figure 1.4(b), Anderson and colleagues proceeded to measure the demineralization process and the lesions using a X-ray photons counter, getting very good statistical measurements with a very good correctness.

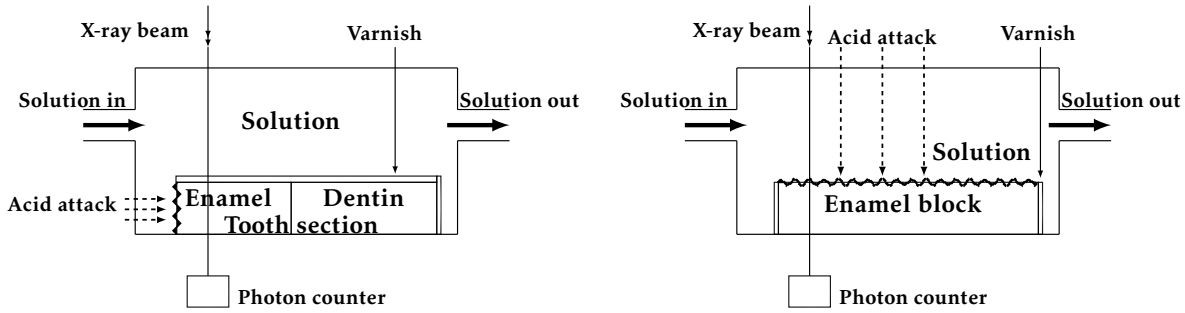

(a) Perpendicular microradiography (b) Parallel microradiography

Figure 1.4: Diagrams showing the two different special chambers using in the Anderson and colleagues experiment for measuring the loss enamel and deepness of the lesion using a photons counter. (a) The cut blocks are varnished in the upper surface and right surface, allowing the acid attack in the left surface, perpendicular to the direction of X-ray beam; (b) The cut blocks are varnished in the left surface and right surface, allowing the acid attack in the upper surface, parallel to the direction of X-ray beam.

From these experiments of Pool and Anderson, two important power law are postulated for the dentist research community. First, around the Pool and colleagues experiment and others cited by Anderson Anderson et al. (1998) that argue that "caries progresses as a linear function of $t^{1/2}$". A typical results along this line is the papers of Poole et al. (1981) and Featherstone (1977), and the theoretical justification, see for example van Dijk et al. (1983), is that for a short time period caries is dominated by diffusion, and at least initially, and in a one-dimensional approximation, the concentration of the ions is proportional to $\mathrm{Erf}(x_3/2(Dt)^{1/2})$. On the other hand, many authors, and in particular Anderson and colleagues, provide experimental evidence that caries progresses linearly in t. Therefore, from those two experiments a debate in the literature emerged as *what is the actual rate of caries progression*. This is a paradox for the tooth decay propagation: Is there any power law explaining the real behaviour of the dental caries propagation in the enamel?

Otherwise, the number of experiments in vivo reported by the bibliography are not many, but, from the existing works, particular attention is drawn to the work of Bjorndal and his colleagues Bjrndal and Thylstrup (1995), Bjrndal (2008). The shape of the

propagating lesion was summarized by Kidd and Fejerskov Kidd and Fejerskov (2004). When the lesion starts at the left or right surface of the tooth, it has a triangular shape in the enamel, with a base at enamel surface, and vertex at the enamel-dentin (ED) junction, Figure 1.5(b). Also, another "triangle" is then observed at the dentin, with a base at the ED junction and vertex deep in the dentin, Figure 1.5(a).On the other hand, when the lesion starts from a biofilm at a pit at the central top part of the tooth, it has the shape of a triangle with a vertex at the pit (enamel surface) and a base at the ED junction. So, building a mathematical model in order to reproduce the triangular patterns is a challenge which can help to understand better the propagation of the dental caries.

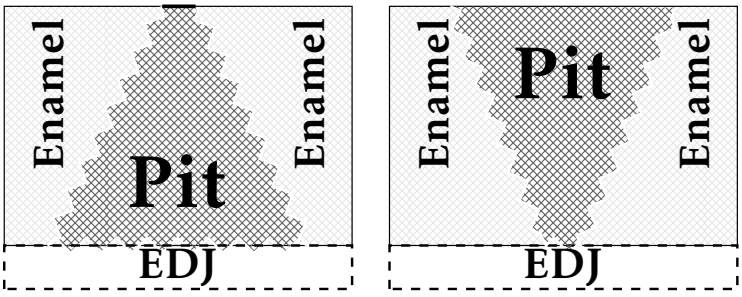

(a) TP1 (b) TP2

Figure 1.5: Diagram showing the triangular patterns developed by the tooth decay propagation in the enamel. (a) Triangular Pattern 1 (TP1). Tooth decay propagation from the top of the tooth to the enamel dentin junction (EDJ). The base of the "triangle" is on the EDJ. (b) Triangular Pattern 2 (TP2). Tooth decay propagation from the left (right) of the tooth surface to the EDJ. The base of the "triangle" is on the enamel surface.

An interesting observation of the propagation of enamel lesions and later on of dentin lesions is provided in Bjrndal and Thylstrup (1995). Some earlier theories claim that the triangle base at the ED junction forms after the lesion's tip reached the junction, and it is caused by a lateral spread of the lesion at the junction. However, Bjorndal et al. point out that the extent of the triangle base at the ED junction is comparable to the extent of the biofilm (triangular base of the lesion) at the enamel surface. From this, and from other observations they conclude that the lesion base at the dentin starts *before* the lesion reached the junction at the enamel. Rather, they speculate that this base at the ED junction is caused directly by the biofilm. This observation has important clinical implications, as it implies that removing the biofilm can arrest the lesion development.

According to the manner in which the bacteria hardly spreads into the tooth before cavities are formed, attention is drawn to other papers by Bjorndal and his colleagues. Notice in particular reference Bjrndal (2008) for clinical significance of this theory.

1.4 Mathematical Models in Dental Caries formation

There is a long history of mathematical models for the initial stages of dental caries, and almost all of them consider appropriate conditions in order to apply Fick's Laws Gray (1962); Holly and Gray (1968); Patel et al. (1987a,b); Wu et al. (1976); Zimmerman (1966a,b,c), etc. Zimmermand's (Zimmerman (1966c)) and Patel's (Patel et al. (1987b)) works in particular will be referred to in order to illustrate the general theories of mathematics applied to the propagation of tooth decay. These models and the others differ in the level of complexity (e.g. the number of compounds) and details of the reaction.

For a better understanding of the results that appear in the following chapters, this chapter will commence with a basic and short background to Fick's Laws before Zimmerman's and Patel's models are described and summarised.

1.4.1 A background of Fick's Laws

The diffusion of chemical species in a solution, porous medium or a combination of them, usually are assumed with the fact that *the flow goes from regions of high concentration to regions of low concentration*, i.e., a gradient of concentration in accordance with Fick's first and second law. From a mathematical viewpoint, the first law in a solution can be modeled of the following way:

Fick's first law: The flux $\mathcal{J}_i$ of chemical specie i is proportional to the concentration gradient

$$\mathcal{J}_i = -D_i \nabla u_i \tag{1.2}$$

where $\nabla = \left(\partial_x, \partial_y, \partial_z\right)$, D_i the diffusion coefficient of specie i, and $\partial_x = \partial/\partial x$ and so on for ∂_y and ∂_z.

However, the Fick's first law is basic for diffusive transport and there is a more fundamental basis for diffusive process, and the explanation appears in the works of Quigley et al. (1987), Daniel and Shackelford (1988) and others. Two important relationships are the so-called Einstein relation for the kinetic theory, connecting the mobility of a particle with the diffusion coefficient $D_i = \mu_i k_B T$, and the Stokes-Einstein relation, for large spherical molecules in a liquid with low Reynolds number $D_i = k_B T/6\pi\eta r_i$, where k_B is Boltzmann's constant, T the the absolute temperature, μ_i is the "mobility" of the particle i, η is the viscosity of the liquid and r_i the radius of the molecules.

In addition, if the concentrations changes with time, we can induce the second Fick's law

Fick's second law (Fourier's Law): Applying the law of conservation of mass to the Fick first law (1.2) *leads to*

$$\partial_t u_i = \nabla \cdot (D_i \nabla u_i) \tag{1.3}$$

where from a general point of view, the diffusion coefficients D_i depend of the spatial coordinates.

1.4.2 The model of Zimmerman

The goal in the model of Zimmerman is studying the behaviour of the solubility of synthetic HAP in chemical solutions controlled with a mathematical model. In order to make more easy the mathematical analysis the following assumptions are taken into account: Diffusion is assumed one-dimensional with a flow parallel to the prisms directions; The enamel is regarded as a granular base (surface) and the Fick's laws are applicable.

In addition, Zimmerman assume that the diffusion in granular base can be considered analytically as a free diffusion with effective diffusion coefficient $D_e = 2\varepsilon D_m/3$ where ε is the porosity of the enamel and D_m the molecular diffusion coefficient of the solute in a particular solvent. Now, using the researches of gases absorption by Wood (1947), the fragmentation of the enamel and the granular total surface area can express of the following way:

$$1 - \varepsilon = \frac{4}{3n\pi r^3} \qquad \text{y} \qquad S = 4\pi n r^2 \tag{1.4}$$

where n is the number of granules for cubic centimeter and r the average diameter of the granules.

On another hand, take into account the main reaction of the solid artificial enamel and the following equilibrium reaction equations in an aqueous medium

$$H_2PO_4^{=} \underset{k_{-2}}{\overset{k_2}{\rightleftharpoons}} H^+ + HPO_4^{=} \qquad H_3PO_4 \underset{k_{-3}}{\overset{k_3}{\rightleftharpoons}} H^+ + H_2PO_4^{=} \qquad HB \underset{k_{-4}}{\overset{k_4}{\rightleftharpoons}} H^+ + B^-, \tag{1.5}$$

Zimmerman get the following system of equation

$$\frac{\partial y_1}{\partial t} = D_1\frac{\partial^2 y_1}{\partial x^2} + 10\frac{S}{\varepsilon}r_1, \qquad \frac{\partial y_2}{\partial t} = D_2\frac{\partial^2 y_2}{\partial x^2} + 6\frac{S}{\varepsilon}r_1 + r_2, \tag{1.6a}$$

$$\frac{\partial y_3}{\partial t} = D_3\frac{\partial^2 y_3}{\partial x^2} - 6\frac{S}{\varepsilon}r_1 + r_2 + r_3 + r_4, \qquad \frac{\partial y_4}{\partial t} = D_4\frac{\partial^2 y_4}{\partial x^2} - r_2 + r_3, \tag{1.6b}$$

$$\frac{\partial y_5}{\partial t} = D_5\frac{\partial^2 y_5}{\partial x^2} - r_3, \qquad \frac{\partial y_6}{\partial t} = D_6\frac{\partial^2 y_6}{\partial x^2} + r_4, \tag{1.6c}$$

$$\frac{\partial y_7}{\partial t} = D_7\frac{\partial^2 y_7}{\partial x^2} - r_4, \tag{1.6d}$$

where $y_1 = [Ca^{++}]$, $y_2 = [HPO_4^{=}]$, $y_3 = [H^+]$, $y_4 = [H_2PO_4^{=}]$, $y_5 = [H_3PO_4]$, $y_6 = [B^-]$, $y_7 = [HB]$ are reactions concentrations and from the equilibrium reaction equations (1.5),

$$r_1 = (k_1 y_3 - k_{-1} y_1 y_2), \qquad r_2 = (k_2 y_4 - k_{-2} y_2 y_3), \tag{1.7a}$$

$$r_3 = (k_3 y_5 - k_{-3} y_3 y_4) \qquad r_4 = (k_4 y_7 - k_{-4} y_3 y_6). \tag{1.7b}$$

The system (1.6) is very difficult to solve analytically and numerically, however, taking into account the fact that coefficient $S/\varepsilon \sim 10^6 \text{cm}^{-1}$ is much faster than the rate of diffusion in the reactions and calculating the derivative with respect to time in the equilibrium equations,

$$K_1 = \frac{y_1 y_2}{y_3}, \quad K_2 = \frac{y_2 y_3}{y_4}, \quad K_3 = \frac{y_3 y_4}{y_5}, \quad K_4 = \frac{y_3 y_6}{y_7}, \tag{1.8}$$

as

$$y_2\frac{\partial y_1}{\partial t} + y_1\frac{\partial y_2}{\partial t} = K_1\frac{\partial y_3}{\partial t}, \qquad y_3\frac{\partial y_2}{\partial t} + y_2\frac{\partial y_3}{\partial t} = K_2\frac{\partial y_4}{\partial t}, \tag{1.9a}$$

$$y_4\frac{\partial y_3}{\partial t} + y_3\frac{\partial y_4}{\partial t} = K_3\frac{\partial y_5}{\partial t}, \qquad y_6\frac{\partial y_3}{\partial t} + y_3\frac{\partial y_6}{\partial t} = K_4\frac{\partial y_7}{\partial t} \tag{1.9b}$$

we can deduce from the substitution of (1.6) into (1.9) the following system of linear equation respect to the reaction rate $\mathbf{Ar} = \mathbf{B}$ where

$$\mathbf{A} = \begin{pmatrix} \frac{S}{\varepsilon}(6(y_1 + K_1) + 10y_2) & K_1 - y_1 & K_1 & K_1 \\ 6\frac{S}{\varepsilon}(y_3 - y_2) & -(y_2 + y_3 + K_2) & K_2 - y_2 & -y_2 \\ -\frac{6S}{\varepsilon}y_4 & y_3 - y_4 & -(y_3 + y_4 + K_3) & -y_4 \\ -\frac{6S}{\varepsilon}y_6 & -y_6 & -y_6 & -(y_3 + y_6 + K_4) \end{pmatrix} \tag{1.10}$$

and

$$\mathbf{B} = \begin{pmatrix} K_2 D_3 \frac{\partial^2 y_1}{\partial x^2} - y_1 D_2 \frac{\partial^2 y_2}{\partial x^2} - y_2 D_1 \frac{\partial^2 y_1}{\partial x^2} \\ K_3 D_4 \frac{\partial^2 y_2}{\partial x^2} - y_2 D_3 \frac{\partial^2 y_3}{\partial x^2} - y_3 D_2 \frac{\partial^2 y_2}{\partial x^2} \\ K_4 D_5 \frac{\partial^2 y_3}{\partial x^2} - y_3 D_4 \frac{\partial^2 y_4}{\partial x^2} - y_4 D_3 \frac{\partial^2 y_3}{\partial x^2} \\ K_4 D_7 \frac{\partial^2 y_7}{\partial x^2} - y_3 D_6 \frac{\partial^2 y_6}{\partial x^2} - y_6 D_3 \frac{\partial^2 y_3}{\partial x^2}, \end{pmatrix}. \tag{1.11}$$

Now, making the calculation $\mathbf{r} = \mathbf{A}^{-1}\mathbf{B}$ and substituting the solution into the initial parabolic system (1.6) we get a parabolic system of the form

$$\frac{\partial y_i}{\partial t} = D_i \frac{\partial y_i}{\partial x^2} + \sum_{j=1}^{7} f_{ij}(y_1, y_2, \ldots, y_7) \frac{\partial y_j}{\partial x^2} \tag{1.12}$$

where some of the functions $f_{ij} = 0$.

Now, after considering some particular boundary conditions and find out a relationship between the porosity and the rate of dissolution,

$$\varepsilon + \tau = 1, \qquad \partial_t \tau = -\frac{S r_1}{\rho} = -\partial_t \varepsilon \Longrightarrow -\partial_t \varepsilon = 4n\pi r^2 \partial_t r \Longrightarrow \partial_t r = \frac{-r_1}{\rho}. \tag{1.13}$$

where τ is the mineral fraction per cc. of enamel, ρ is the density of the enamel in moles/cc, and also, assuming as a consequence of the increase in porosity during the dissolution process, that the fluid that pervades the new space has molecular diffusion coefficients that are the same for all species as the original aqueous organic matrix phase, the remainder of Zimmermen's work is concerned with how to solve the problem from a numeric point of view.

1.4.3 The model of Patel

The goals of Patel's work was to set out a theorical understanding between the dissolution behaviour of HAP and its chemical components in the demineralization process on in vitro experiment with teeth and the numerical simulations of a constructed mathematical model for describe the propagation of dental caries.

Patel, begins the study making different assumptions such as the only transport process occurring in the matrix region is diffusion, the bovine enamel to be an homogeneous single phase of hydroxyapatite crystallites in the form of a porous matrix, for a long time and at sufficient depth in the enamel pores, the solution becomes saturated with respect to hydroxyapatite, the problem is implemented in only one dimension space. In addition, in

accordance with the equation of Levich (1962) the use of the rotating disk system in the in vitro dissolution experiments allow a numerical approximation, $h = 1.612 \cdot D_{aq}^{1/3} \cdot \eta^{1/6} \cdot \omega^{-1/2}$ for of the effective diffusion layer thickness h, where D_{aq} is the diffusivity in the medium, η the kinematic viscosity of the medium, and ω the angular velocity. Taking into account, the assumption for a well-structured geometry, patterned by prism and inter-prism for the dental enamel coupled with the adequate conditions in order to apply Fick's laws are the keys in the carried out study of Patel.

Once the chemical preamble of the problem with $pH = 4.5$ was constructed, they proceed to define the following relation for each enamel matrix element using Fourier's Law plus a reaction term

$$\partial_t C = \partial_x (D(x,t)\partial_x C) + \mathbf{R}_{diss} \tag{1.14}$$

where $D(x,t)$ is the effective diffusivity, $C(x,t)$ is the solution concentration and $\mathbf{R}_{diss}$ (dissolution component) is define as

$$\mathbf{R}_{diss} = k(x,t)\,(C_s - C(x,t)), \tag{1.15}$$

where C, is the equilibrium solubility of hydroxyapatite in the bulk solution and $k(x,t)$ is the first-order surface reaction rate.

The main equation for making the numerical calculation is (1.14), however, according to the Noyes-Nernst's law they take the flux per unit area J/A such as

$$\mathbf{J/A} = \frac{D_{aq}}{h}\,(C_0 - C_h) \tag{1.16}$$

where A is the area of the enamel surface, D_{aq} is the solute diffusivity in the bulk, C_0 and C_h are the concentrations of HAP at the enamel solution interface ($x = 0$) and in the bulk ($x \leqslant -h$), respectively. Beside, as total flux for all times, they conclude to the expression

$$\mathbf{J/A} = \int_0^{+\infty} \partial_t C\, dx + \int_0^{+\infty} \frac{\Delta M(x,t)}{\Delta t}\, dx \tag{1.17}$$

where $M(x,t)$ is the density of HAP as function of space an time and take into account a relationship between the effective diffusion coefficient, the aqueous diffusion coefficient and the total porosity of the enamel $D = D_{aq}\varepsilon(x,t)$ such that

$$\varepsilon = \left(1 - \frac{M(x,t)}{M(x,0)}\right)(1 - \varepsilon_0) + \varepsilon_0, \tag{1.18}$$

where ε_0 is the initial porosity and $M(x,t) = M(x,0) + \sum_0^t \Delta M(x,t)$ with

$$\Delta M(x,t) = \Delta t \cdot \Delta x \cdot k(x,t) \cdot A \cdot (C_s - C). \tag{1.19}$$

In order to finish the theoretical deduction, Patel considered an analytical formulation for the first-order surface reaction rate $k(x,0)\,(M(x,t)/M(x,0))^n$ where n is a crystalline shape factor,

$$M(x,0) = \rho \cdot \Delta x \cdot A \cdot (1 - \varepsilon_0), \tag{1.20}$$

and ρ is the constant initial density of enamel.

Remark 1.4.1. Even when the Patel model has a lot of improving possibilities, also, it has many useful applications, one of them is the consideration by separately of the calculation of dissolution rates for each chemical components, such as Ca^{++} or $HPO_4^{=}$, and from a mathematical theoretic point of view

$$\varepsilon = \left(1 - \frac{M(x,t)}{M(x,0)}\right)(1 - \varepsilon_0) + \varepsilon_0 \to 1 \tag{1.21}$$

when $M(x,t) \to 0$ for $t \to +\infty$ and in consequence

$$D = D_{aq}\varepsilon(x,t) \to D_{aq}, \qquad k(x,t) = k(x,0)\,(M(x,t)/M(x,0))^n \to 0. \tag{1.22}$$

Also, many useful applications? can be taken from the Patel model, such as the existence and the unicity of the solutions.

1.5 Outline of thesis

The goal of this research is to derive a mathematical model for the first part of this process, namely the dissolution of the enamel. The model starts from the local transport equations on the microscopic scale. The local equations are averaged via the method of homogenization to create a macroscopic model. The model proposed in this thesis takes into account key factors such as the anisotropic geometry of the enamel and the time evolution of the microstructure due to demineralization and remineralization.

Chapter 1 provides some background material which includes the motivation for studying tooth decay as well as an elementary description of their structure and functionality.

This chapter also includes a background history of the mathematical models applied to the progression of dental caries.

Enamel has a periodic distribution of crystals into the inter-rod, therefore, in order to consider the geometry of the solid structure, Chapter 2 is dedicated to introducing the basic ideas of the homogenization method and the domain decomposition methods.

The results are presented in Chapter 3 with the microscopic equations. These equations will be homogenized to take into account the evolution of the microgeometry in space and time. An evolution equation for the microstructure is therefore derived. The macroscopic equations involve averaged diffusion coefficients. In addition, the parameters involved in the local enamel dissolution process are considered in some detail. Finally, adding the influence of the outer layer of the enamel to the model, a second model (a version of the first one) is postulated.

Chapter 4 presents a simplified version of the model assuming that the amount of hydrogen ions lost to the reaction is small compared to their total amount and a rectangular geometry that mimic the in vitro experiments. In addition, two examples are provided to describe the method of estimate of the effective diffusion coefficient for two different cell problems. These coefficients are determined by solving certain canonical differential equations. The difficult task of estimating the effective diffusivities in a varying local geometry is also discussed. A number of numerical examples are then presented and contrasted with a number of experiments results.

In Chapter 5 the model used for this research is presented and the underlying assumptions behind it are explained. The equations are solved in a three-dimensional rectangular domain. The model is also upgraded to account for the resilient outer layer of the enamel, and inspect its effect on caries progress. Furthermore, discussion of the important and controversial issue of what is the progression rate of caries solving the equations in a two-dimensional geometry that mimics a realistic tooth shape is provided. In particular consideration is given to the shape of the lesion, in terms of where it starts along the tooth boundary. The chapter finishes with a discussion of the model and the simulations therein.

A summation of the basic ideas of the work will be presented in Chapter 6, which will also reveal the version of general model in general curvilinear coordinates. Finally, a summary of the work from the previous chapters is given in this chapter.

Chapter 7 offers suggestions for future extensions of the model. First, the paradox of Cate in relation to the influence of the fluoride in the process of caries in order to ilustrate

the possible extension of the model is provided. In addition, a possible second extension of the model to the bone remodeling process is suggested.

Finally, in Appendix A, a number of geometrical identities required are derived. Appendix B and Appendix C provide the mathematic frameworks for the numerical solutions of the examples undertaken. An extensive and detailed bibliography is provided at the end of the thesis.

Chapter 2

The Homogenisation and Domain Decomposition methods

The solid structure of the enamel is well organized in a periodic distribution of the crystals into the inter-rod. Therefore, taking into account that all the previous models started directly in the macroscopic level, without considering the geometry of the solid structure, the model will be derived as the final result of the homogenisation method for partial differential equations in order to applying a class of non-trivial numerical methods for simulating the macroscopic model.

One of the key factors for our macroscopic model will be the inclusion of the most outer layer on the top of the enamel, the prismless outer layer Fava (1997). This approach is totally new for the previous models and very relevant for the forecasting of the caries progression into the new experiments outcomes, but, as consequence, the model should be solved numerically in two different domains with a matching interface between the outer layer and the prismatic layer (constituted of hydroxyapatite crystals). The non-trivial numerical methods used for solve this class of problems are called Domain Decomposition Methods. Therefore, in addition, the basic ideas of the Domain Decomposition Methods are described.

In the first section of this chapter the basic idea of the homogenisation method (Bensoussan et al. (2011); Bourgat (1979); Bourgat and Dervieux (1978); Hornung (1997)) are introduced treating a general mode and in section 2 the domain decomposition methods. These methods will be applied in the Chapters 3, 4 and 5.

2.1 Basic procedure of homogenisation method

For the future analysis, a bounded domain $\Omega \subset \mathbb{R}^N$ with smooth boundary $\partial\Omega$ is take into account. Then we starting study the family of boundary-value problems

$$\nabla \cdot (a^\varepsilon(x)\nabla u^\varepsilon(x)) + f(x) = 0 \qquad x \in \Omega \tag{2.1a}$$

$$u(x) = u_D(x) \qquad x \in \partial\Omega \tag{2.1b}$$

where the rapidly oscillating coefficient $a^\varepsilon(x)$ is defined such as $a^\varepsilon(x) := a(x/\varepsilon)$ for all $x \in \Omega$ where the function a is $Y-periodic$ in $\mathbb{R}^N$ with periodicity cell $Y = \left\{y \in \mathbb{R}^N : y \in (0,1)\right\}$ and ε a scale parameter. From the small scale ε arises a natural question: what the solution u^ε does in the limit as $\varepsilon \longrightarrow 0$?

In order to derive the limit problem, we need to ansatz that the unknown function $u^\varepsilon(x)$ can be represented by asymptotic expansions, with respect to ε of the form

$$u^\varepsilon(x) = u_0(x,y) + \varepsilon u_1(x,y) + \varepsilon^2 u_2(x,y) + \dots \tag{2.2}$$

where the coefficient functions $u_i(x,y)$ are Y-periodic with respect to the variable $y = x/\varepsilon$. We say that x is the global variable and that y is the local variable.

Substituting the equation (2.2) into the equations (2.2) we gets

$$\begin{aligned}
&\varepsilon^{-2}\nabla_y \cdot \Big(a(y)\nabla_y u_0(x,y)\Big) + \varepsilon^{-1}\Big(\nabla_y \cdot \Big(a(y)\nabla_y u_1(x,y)\Big) + \nabla_y \cdot (a(y)\nabla_x u_0(x,y)) + a(y)\nabla_x \cdot \nabla_y u_0(x,y)\Big) \\
&+ \varepsilon^0\Big[\nabla_y \cdot \Big(a(y)(\nabla_y u_2(x,y) + \nabla_x u_1(x,y))\Big) + a(y)\Big(\nabla_x \cdot \nabla_y u_1(x,y) + \nabla_x \cdot \nabla_x u_0(x,y)\Big)\Big] \\
&+ \varepsilon(\dots) + \dots + f(x) = 0
\end{aligned} \tag{2.3}$$

where ∇_x and ∇_y are the partial derivatives with respect to x and y respectively and

$$\nabla = \nabla_x + \nabla_y/\varepsilon.$$

By identifying in powers of ε from the equation (2.3) we obtain the following cascade of sub-problems:

$$O(\varepsilon^{-2}) : \nabla_y \cdot \Big(a(y)\nabla_y u_0(x,y)\Big) = 0, \tag{2.4a}$$

$$O(\varepsilon^{-1}) : \nabla_y \cdot \Big(a(y)\nabla_y u_1(x,y)\Big) + \nabla_y \cdot (a(y)\nabla_x u_0(x,y)) + a(y)\nabla_x \cdot \nabla_y u_0(x,y) = 0, \tag{2.4b}$$

$$\begin{aligned}
O(\varepsilon^0) : &\nabla_y \cdot \Big(a(y)(\nabla_y u_2(x,y) + \nabla_x u_1(x,y))\Big) \\
&+ a(y)\nabla_x \cdot \nabla_y u_1(x,y) + a(y)\nabla_x \cdot \nabla_x u_0(x,y) + f(x) = 0,
\end{aligned} \tag{2.4c}$$

Recalling the property of Y-periodicity in the variable y into the equation (2.4a), the independence of the function $u_0(x,y)$ respect to y, i.e., $u_0(x,y) = u_0(x)$ can be proved. Using the independence respect to y for u_0 and the equation (2.4b)

$$\nabla_y \cdot \Big(a(y)\nabla_y u_1(x,y)\Big) = -\nabla_y \cdot (a(y)\nabla_x u_0(x)), \tag{2.5}$$

where we can solve the equation 2.5 expressing the function $u_1(x,y)$ just like a combination of the cell-functions $W_j(y)$

$$u_1(x,y) = \sum_{j=1}^{N} W_j(y)\partial_{x_j} u_0(x) \Longrightarrow \nabla_y u_1(x,y) = \sum_{j=1}^{N} \nabla_y W_j(x,y)\partial_{x_j} u_0(x). \tag{2.6}$$

The next step is to proceed to transforming the terms with ε^0 into the equation 2.6. Therefore, take into account the previous results and integrating this identity over Y we get

$$\int_Y \nabla_y \cdot \Big(a(y)(\nabla_y u_2(x,y) + \nabla_x u_1(x,y))\Big)\, dy + \int_Y a(y)\nabla_x \cdot \nabla_y u_1(x,y)\, dy + \int_Y a(y)\, dy \nabla_x \cdot \nabla_x u_0(x) + f(x) = 0 \tag{2.7}$$

because the volume of Y is 1. Integrating the first term of (2.7) by parts we get

$$\int_Y \nabla_y \cdot \Big(a(y)(\nabla_y u_2(x,y) + \nabla_x u_1(x,y))\Big)\, dy = \int_{\partial Y} \vec{\nu} \cdot \Big(a(y)(\nabla_y u_2(x,y) + \nabla_x u_1(x,y))\Big)\, d\Gamma(y), \tag{2.8}$$

where $\vec{\nu}$ is the normal vector on ∂Y. Once more, as a consequence of the Y-periodicity of the functions $u_1(x,y)$ and $u_2(x,y)$ the integral (2.8) vanishes on the boundary ∂Y.On the other hand, recalling the equation (2.6) we obtain

$$\sum_{i,j=1}^{N} \int_Y a(y)\Big(\partial_{y_i} W_j(y) + \delta_{ij}\Big)\, dy \partial_{x_i}\partial_{x_j} u_0(x) + f(x) = 0, \tag{2.9}$$

where introducing the abbreviation

$$a_{ij} = \int_Y a(y)\Big(\partial_{y_i} W_j(y) + \delta_{ij}\Big)\, dy, \tag{2.10}$$

and suppressing the subindexes for the function u_0 we get a final result

$$\sum_{i,j=1}^{N} a_{ij}\partial_{x_i}\partial_{x_j}u(x) + f(x) = 0. \tag{2.11}$$

Therefore, using the tensor $A = (a_{ij})_{i,j}$, we sum up and get the following statement.

Proposition 2.1.1. The homogenisation of the problem (2.1) is given by

$$\nabla \cdot (A\nabla u(x)) + f(x) = 0 \qquad x \in \Omega \tag{2.12a}$$

$$u(x) = u_D(x) \qquad x \in \partial\Omega \tag{2.12b}$$

It has to be emphasized that the coefficient in the equation (2.10) are in general, not diagonal. In other words, we have derived an equation that describes an anisotropic medium. However, in general, the tensor is symmetric and positive definite. In addition, without any difficulty we can generalize and consider the coefficient $a : \Omega \times Y \to \mathbb{R}$ that depend on the *slow* variable $x \in \Omega$ and are periodic with respect to the fast variable $y \in Y$, i.e., the homogenized tensor is a function of x and y.

2.1.1 Periodic media with obstacles

Now, as a more complicated problem, we assume that the medium in which we have to study our problem has a periodic arrangement of obstacles (see Figure 2.1(a)). Hence, we in the standard periodicity cell Y, there is a regular obstacle $\mathcal{B} \subset\subset Y$ with a piecewise smooth boundary Γ, as we depicted in Figure 2.1(b). The remainder domain is denoted by $\mathcal{A} = Y \setminus \mathcal{B}$ (see Figure 2.1(b)) and also, this standard geometry is repeated periodically over $\mathbb{R}^N$.

In addition, the geometric structure within the fixed domain Ω is obtained by intersecting the ε-multiple of this periodic geometry with Ω, i.e.,

$$\mathcal{A}^\varepsilon = \Omega \cap (\varepsilon\mathcal{A}) \qquad \text{and} \qquad \gamma^\varepsilon = \Omega \cap (\varepsilon\Gamma).$$

There is many difficult techniques that we can avoid if we assume that $\partial\Omega \cap \varepsilon\Gamma = \emptyset$ (see Figure 2.1(a)). in this case, we are interesting in study the diffusion process that take place

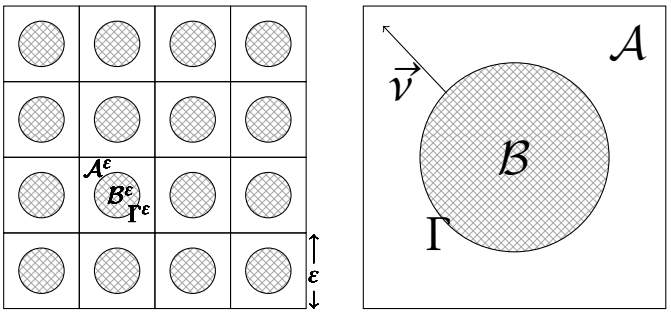

(a) Periodic medium (b) Standard micro cell

Figure 2.1: Examples of periodic medium and its standard micro-cell.

in the remainder domain $\mathcal{A}^\varepsilon$, namely, the following simple boundary-value problem

$$\nabla \cdot (a^\varepsilon(x)\nabla u^\varepsilon(x)) + f(x) = 0 \qquad x \in \mathcal{A}^\varepsilon \tag{2.13a}$$

$$\vec{\nu} \cdot a^\varepsilon(x)\nabla u^\varepsilon(x) = 0 \qquad x \in \Gamma^\varepsilon \tag{2.13b}$$

$$u(x) = u_D(x) \qquad x \in \partial\Omega \tag{2.13c}$$

where $\vec{\nu}$ is the normal vector on Γ^ε and $a^\varepsilon(x) = a(x/\varepsilon)$ is assumed Y-periodic. The zero flux condition on Γ^ε is used to model the obstacles as impermeable, therefore, the problem (2.12) can be looked at as a generalization of the problem (2.1), from the previous section if we introduce a characteristic function of $\mathcal{A}$ and changing the factor $a^\varepsilon(x)$ by $(\chi^\varepsilon(x)a^\varepsilon(x))$ into the equation (2.12) where

$$\chi(x) = \begin{cases} 1, & x \in \mathcal{A}, \\ 0, & x \in \mathcal{B}, \end{cases}$$

and define $\chi^\varepsilon(x) = \chi^\varepsilon(x/\varepsilon)$. Hence, we can apply with the same analysis applied in the section above for the problem (2.1), emphasizing the difference in the cell problems in consequence of the added flux boundary condition, i.e., now the cell problem are written in order to determine Y-periodic functions $W_j(y)$ such that

$$\begin{aligned} \nabla_y \cdot \Big(a(y)\nabla W_j(y)\Big) &= -\nabla_y \cdot \Big(a(y)\vec{e}_j\Big), & x \in \mathcal{A}, \\ \vec{\nu} \cdot \nabla_y W_j(y) &= -\vec{\nu} \cdot \vec{e}_j, & y \in \Gamma, \end{aligned} \tag{2.14}$$

where the the tensor $A = (a_{ij})_{i,j}$ should be defined by

$$a_{ij} = \Big(a(\nabla W_j + \vec{e}_j), \vec{e}_i\Big)_{\mathcal{A}} \tag{2.15}$$

arriving to a analogous result that the homogenisation of problem (2.12) is the problem (2.11).

Remark 2.1.2. One of the more complicated aspects, when we need to solve a problem having applied the homogeneization method it's related with the solutions of the cell problem, because, the function $W_j(y)$ are uniquely defined only up to an additive constants, therefore, we need to solve a numerical problem not trivial . In Appendix B we point out a way to solve numerically the cell problem using the software FreeFem++, starting from the weak formulation of the problem.

2.2 Domain decomposition methods

Domain decomposition methods are designed to allow the effective numerical solution of partial differential equations on parallel computer architectures. They comprise a relatively new field of study, but have already found important applications in many branches of physics and engineering.

Some of the motivations for the use of these methods include:

1. Potential for efficient parallelization through the use of data locality.
2. Ability to deal with PDEs on complicated physical geometries.
3. Ability to deal with PDEs that exhibit different behavior on different parts of the domain (heterogeneous operators).
4. Auperior convergence properties of the iterative method even on sequential machines.

Basically the methods can be classified into two categories: The overlapping methods and the non-overlapping methods. In overlapping domain decomposition methods, the subdomains share a thin layer with their neighbors. The Schwarz alternating method and the additive Schwarz method, for example, are two popular overlapping domain decomposition approaches. Otherwise, in non-overlapping methods, adjacent subdomains only share a $d-1$ dimensional part of the computational domain, the so-called interface. Several approaches like finite element tearing and interconnect or the Balancing domain decomposition exist and are used widely.

2.2.1 Schwarz's methods

The method was developed by Hermann Amandus Schwarz in 1869 and not as a domain decomposition method, because in those days the mathematicians solved mathematical problems with simple geometries, but they had a clear idea of how to solve problems get involved the overlap of these simple geometries. The idea of Schwarz was using the solution for simple geometries separately in order to knowing the solution in a overlapping geometry.

In order to describe the basics ideas of the domain decompositions methods, we are going to consider the classical Poisson problem:

$$\begin{cases} -\Delta u = f, & \text{in } \Omega; \\ u = 0, & \text{in } \partial\Omega, \end{cases} \tag{2.16}$$

where Ω is a $d-$dimensional domain ($d = 2, 3$) with a Lipschitz boundary $\partial\Omega$, f is a given function of $L^2(\Omega)$ and $\Delta = \sum_i^d \partial^2_{x_i^2}$ is the Laplace operator.

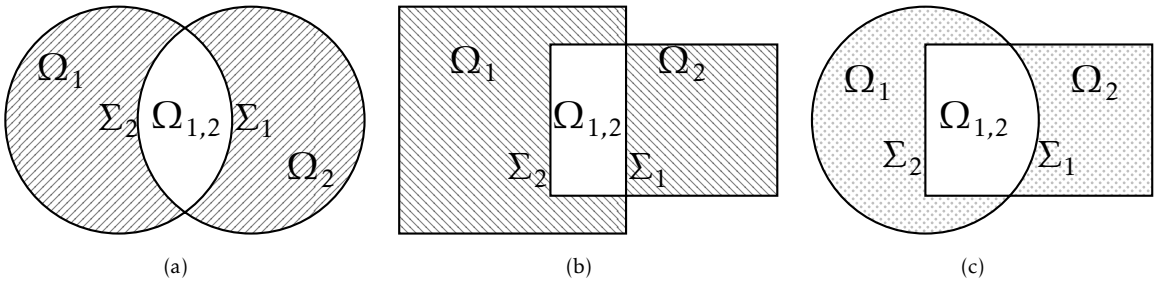

Figure 2.2: Three examples of domains with overlapping partitions

Let's consider that Ω is partitioned into two overlapping subdomains, i.e., $\Omega = \Omega_1 \cup \Omega_2$ where Ω_1 and Ω_2 are the two overlaping subdomains and $\Sigma_1 = \partial\Omega_1 \cap \Omega_2$, $\Sigma_2 = \partial\Omega_2 \cap \Omega_1$, $\Omega_{1,2} = \Omega_1 \cap \Omega_2$ (see Figure 2.2). In addition, let's u^0 be an initialisation function defined in Ω and vanishing on $\partial\Omega$, and set $u_2^0 := u^0$ into Ω_2. In addition, defining the sequences u_1^{n+1} and u_2^{n+1} for $n \geqslant 0$ finding the solution to each problem correspondingly:

$$\begin{cases} -\Delta u_1^{n+1} = f, & \text{in } \Omega_1; \\ u_1^{n+1} = 0, & \text{in } \partial\Omega_1 \cap \partial\Omega, \\ u_1^{n+1} = u_2^n, & \text{in } \Sigma_1; \end{cases} \tag{2.17a}$$

$$\begin{cases} -\Delta u_2^{n+1} = f, & \text{in } \Omega_2; \\ u_2^{n+1} = 0, & \text{in } \partial\Omega_2 \cap \partial\Omega, \\ u_2^{n+1} = u_1^{n+1}, & \text{in } \Sigma_2; \end{cases} \tag{2.17b}$$

This means that we need to use the solution of problem 2.17a restricted to Σ_2 as boundary condition for problem 2.17b. This approach is called multiplicative Schwarz method.

On the other hand, the problem 2.17a-2.17b is not closed, because, a natural question comes up. What happens with the convergence of the solution of problem 2.17a-2.17b and the problem 2.16? In other words, we need to providing some mild assumptions on the subdomains Ω_1 and Ω_2 in order to ensure the convergence of problem 2.17a-2.17b to the solution u of problem 2.16.

Applying the maximum principle we can set out the following the estimates

$$\|u_{|\Omega_1} - u_1^{n+1}\|_{L^\infty(\Omega_1)} \leqslant C_1^n C_2^n \|u - u^0\|_{L^\infty(\Sigma_1)} \tag{2.18a}$$

$$\|u_{|\Omega_2} - u_2^{n+1}\|_{L^\infty(\Omega_2)} \leqslant C_1^{n+1} C_2^n \|u - u^0\|_{L^\infty(\Sigma_2)} \tag{2.18b}$$

where the error reduction constants $C_1, C_2 \in (0,1)$ can be quite close to one if the overlapping region $\Omega_{1,2}$ is thin (see Quarteroni and Valli (1999)).

In order to write the weak formulation of the decomposition method we consider

$$H_0^1(\Omega_i) = \{v \in H_0^1(\Omega) : v|_{\Omega \setminus \overline{\Omega}_i} = 0\} \tag{2.19}$$

for $i = 1, 2$ and the classical bilinear form $a(u,v) = \int_\Omega \nabla u \cdot \nabla v \, dx$, $f(v) = \int_\Omega f v \, dx$. Therefore, given $u^0 \in H_0^1(\Omega)$, solve

$$\begin{cases} z_1 \in H_0^1(\Omega_1) \\ a(z_1, v_1) = f(v_1) - a(u^n, v_1), \quad \forall v_1 \in H_0^1(\Omega_1); \\ u_1^{n+1/2} = u^n + \widetilde{z}_1 \in H_0^1(\Omega), \end{cases} \tag{2.20a}$$

$$\begin{cases} z_2 \in H_0^1(\Omega_2) \\ a(z_2, v_2) = f(v_2) - a\left(u^{n+1/2}, v_2\right), \quad \forall v_2 \in H_0^1(\Omega_2); \\ u_1^{n+1} = u^{n+1/2} + \widetilde{z}_2 \in H_0^1(\Omega), \end{cases} \tag{2.20b}$$

where $\widetilde{z_i}$ denotes the extension of z_i by 0 in $\Omega \setminus \Omega_i$.

On the other hand, we can obtain the additive method of Schwarz modifying the multiplicative method, such that the calculations for each step in each subdomain are done of parallel way, without that the information of the first one intercepts in the second one. For example, having set $w_1^0 := u_{|\Omega_1}^0$ and $w_2^0 := u_{|\Omega_2}^0$ we can make the two steps independent

of each other by solving

$$\begin{cases} -\Delta w_1^{n+1} = f, & \text{in } \Omega_1; \\ w_1^{n+1} = 0, & \text{in } \partial\Omega_1 \cap \partial\Omega, \\ w_1^{n+1} = w_2^n, & \text{in } \Sigma_1; \end{cases} \tag{2.21a}$$

$$\begin{cases} -\Delta w_2^{n+1} = f, & \text{in } \Omega_2; \\ w_2^{n+1} = 0, & \text{in } \partial\Omega_2 \cap \partial\Omega, \\ w_2^{n+1} = w_1^n, & \text{in } \Sigma_2; \end{cases} \tag{2.21b}$$

Similarly, we can set out the variational formulation for the problem 2.21a-2.21b

$$\begin{cases} Z_1 \in H_0^1(\Omega_1) \\ a(Z_1, v_1) = f_{\Omega_1}(v_1) - a(w^n, v_1), \quad \forall v_1 \in H_0^1(\Omega_1); \end{cases} \tag{2.22a}$$

$$\begin{cases} Z_2 \in H_0^1(\Omega_2) \\ a(Z_2, v_2) = f_{\Omega_2}(v_2) - a(w^n, v_2), \quad \forall v_2 \in H_0^1(\Omega_2); \end{cases} \tag{2.22b}$$

such that $w^{n+1} = w^n + \sum_i^2 \widetilde{Z}_i$ and having set $w^0 = u^0$.

The convergence of this method in general needs some additional hypotheses, but if it converges, the number of necessary iterations to converge will be the double than the method multiplicative.

The additive Schwarz method is sequential, but, on the other hand, the multiplicative Schwarz method can be run in parallel but has a remarkable part in the algorithm and its implementation. In addition, the convergence of the multiplicative Schwarz method is not optimal in this formulation, but, there are some approaches that optimize its convergence. We can find the generalisation of the Schwarz method to the case of when Ω is partitioned into $m > 2$ subdomains in the bibliographies Mathew (2008); Quarteroni and Valli (1999).

2.2.2 The Framework of Steklov-Poincaré

Considering again the Poisson problem 2.16, but, now, let Ω_1, Ω_2 denote a non-overlapping decomposition of Ω, as in Figure 2.3, with interface $\Sigma = \overline{\Omega}_1 \cap \overline{\Omega}_2$ separating the two subdomains and $\Sigma_i = \partial\Omega_i \cap \Omega$. Let $\mathbf{n}_i(x)$ denote the unit outward normal vector to $\partial\Omega_i$ at the point $x \in \Sigma$.

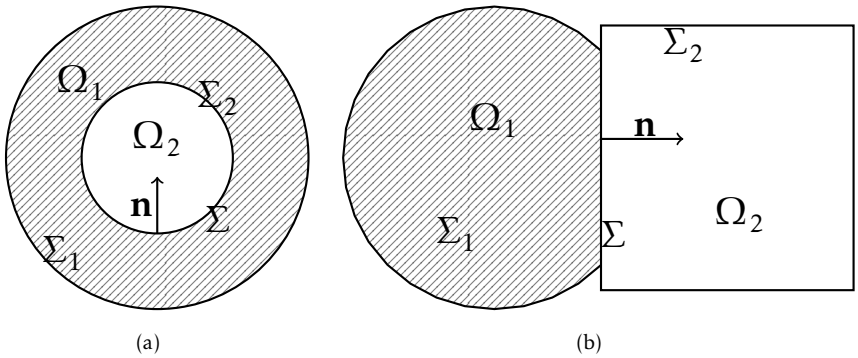

Figure 2.3: Two examples of domains with no-overlapping partitions

Suppose u is a smooth solution to problem 2.16 and $u_i = u$ on Ω_i. By construction, we get

$$\begin{cases} -\Delta u_1 = f, & \text{in } \Omega_1; \\ u_1 = 0, & \text{in } \Sigma_1, \end{cases} \tag{2.23a}$$

$$\begin{cases} -\Delta u_2 = f, & \text{in } \Omega_2; \\ u_2 = 0, & \text{in } \Sigma_2, \end{cases} \tag{2.23b}$$

and by continuity of u or as consequence of the trace theorem, we obtain that $u_1 = u_2$ on Σ. On the other hand, employing the weak formulation of (2.23), and expressing each integral on Ω as a sum of integrals on Ω_1 and Ω_2, we get

$$\sum_{i=1}^{2} a_i(u_i, v) = \sum_{i=1}^{2} f_{\Omega_i}(v), \tag{2.24}$$

for $v \in C_0^\infty(\Omega)$ where

$$a_i(u_i, v) = \int_{\Omega_i} \nabla u_i \cdot \nabla v \, dx \qquad \text{and} \qquad f_{\Omega_i}(v) = \int_{\Omega_i} f v \, dx. \tag{2.25}$$

Now, if we chose v not identically zero on Σ and with compact support in Ω, then integration by parts yields:

$$\sum_{i=1}^{2} -\int_{\Omega_i} \Delta u_i v \, dx - \sum_{i=1}^{2} \int_{\Sigma} \mathbf{n}_i \cdot \nabla u_i v \, dS_x = \sum_{i=1}^{2} \int_{\Omega_i} f v \, dx. \tag{2.26}$$

Using the equations (2.23), it follows that:

$$\sum_{i=1}^{2} \int_{\Sigma} \mathbf{n}_i \cdot \nabla u_i v \, dS_x = 0, \qquad \forall v \in C_0^{\infty}(\Omega), \tag{2.27}$$

and consequently $\mathbf{n}_1 \cdot \nabla u_1 = -\mathbf{n}_2 \cdot \nabla u_2$. The converse result can be verified analogously.

Summarizing the results, we derived the following couple of *transmission conditions* on the interface Σ

$$u_1 = u_2, \qquad \text{on } \Sigma, \tag{2.28a}$$

$$\mathbf{n}_1 \cdot \nabla u_1 = -\mathbf{n}_2 \cdot \nabla u_2, \qquad \text{on } \Sigma, \tag{2.28b}$$

The first condition requires the subdomain solutions u_1 and u_2 to match on Σ, while the second condition requires the local fluxes $\mathbf{n}_1 \cdot \nabla u_1$ and $\mathbf{n}_2 \cdot \nabla u_2$ associated with u_1 and u_2 to also match on Σ.

Finally, combining the conditions (2.28) with the elliptic equation on each subdomain, yields the following formulation equivalent to (2.16):

$$\begin{cases} -\Delta u_i = f, & \text{in } \Omega_i; \\ u_i = 0, & \text{in } \Sigma_i, \\ u_1 = u_2, & \text{in } \Sigma, \\ \mathbf{n}_1 \cdot \nabla u_1 = \mathbf{n}_1 \cdot \nabla u_2, & \text{in } \Sigma, \end{cases} \tag{2.29a}$$

where $\mathbf{n}_1 = -\mathbf{n}_2$ on Σ and $i = 1, 2$. Then, the following result will hold

$$\begin{aligned} u_1 &= u, \quad \text{on } \overline{\Omega}_1, \\ u_2 &= u, \quad \text{on } \overline{\Omega}_2. \end{aligned} \tag{2.30}$$

2.2.3 The method of Dirichlet-Neumann

There are various iterative methods for solving the Steklov-Poincaré system (2.29), such as the *Dirichlet-Neumann method*, the Neumann-Neumann method, the *Robin-Robin method* and others. We are going to describe the algorithm of the first two methods mentioned.

Let μ^0 (where $\mu^0 \equiv u_2^0$ on Σ) denote a starting guess and $0 < \theta < 1$ denote a relaxation parameter required to ensure convergence Mathew (2008); Quarteroni and Valli (1999) The steps 2-4 require the solution of an elliptic equation in Ω with Dirichlet conditions on Σ_1 and Σ and the local fluxes may not match on Σ. In addition, the steps 5-7 require

Algorithm 1 Dirichlet-Neumann

1: **for** $k = 0, 1, \ldots$ until convergence **do**
2: $\quad -\Delta u_i^{k+1} = f$ in Ω_i; ▷ $i = 1, 2$
3: $\quad u_i^{k+1} = 0$ on Σ_i; ▷ $i = 1, 2$
4: $\quad u_1^{k+1} = \mu^k$ on Σ; ▷ Interface condition I
5: $\quad \mathbf{n}_2 \cdot \nabla u_2^{k+1} = \mathbf{n}_2 \cdot \nabla u_1^{k+1}$ on Σ; ▷ Flux interface condition with $\mathbf{n}_2 = -\mathbf{n}_1$
6: $\quad \mu^{k+1} = \theta u_{2|\Sigma}^{k+1} + (1-\theta)\mu^k$; ▷ Update of μ^{k+1}
7: **end for**
8: Output: (u_1^k, u_2^k)

the solution of an elliptic equation in Ω_2 with Dirichlet conditions on Σ_2 and Neumann conditions on Σ, but, on the contrary u_2^{k+1} may not match u_1^{k+1} on Σ.

For the weak formulation of the iterative algorithm of Dirichlet-Neumann, we consider the space

$$V_i = \{v_i \in H^1(\Omega_i) : v_i = 0 \,\text{in}\, \partial\Omega \cap \partial\Omega_i\}, \qquad V_i^0 = H_0^1(\Omega_i) \tag{2.31a}$$

$$B = H_{00}^{1/2}(\Sigma) = \{\eta \in H^{1/2}(\Sigma) : \eta = v_{|\Sigma} \,\text{for suitable}\, v \in H_0^1(\Omega),\} \tag{2.31b}$$

where $H^{1/2}(\Sigma)$ is the trace space of $H^1(\Omega)$ on the boundary Σ and also, we will denote by Λ_i any possible continuous operator from B to V_i^0 that satisfies $(\Lambda_i \eta)_{|\Sigma} = \eta$. Any such operator which can be proved to exist, will be called an extension operator from $H_{00}^{1/2}$ to $H_0^1(\Omega_i)$.

Now, the weak formulation of the Dirichlet-Neumann algorithm can be set out as follow: find $u_i^{k+1} \in V_i$ such that

$$\begin{cases} a_i\left(u_i^{k+1}, v_i\right) = f_{\Omega_i}(v_i), & \forall v_i \in V_i^0; \\ u_1^{k+1} = \mu^k, & \text{in } \Sigma, \\ \sum_{i=1}^2 a_i\left(u_i^{k+1}, \Lambda_i \beta\right) = \sum_{i=1}^2 f_{\Omega_i}(\Lambda_i \beta), & \forall \beta \in B, \end{cases} \tag{2.32}$$

where Λ_i denotes any possible extension operator from B to V_i^0 and $a_i(\cdot,\cdot)$, f_{Ω_i} have been introduced in (2.25).

2.2.4 The method of Neumann-Neumann

Another iterative method for solving the system (2.29) is the so-called Neumann-Neumann method. Considering an initial given datum μ^0, a relaxation parameter $0 < \theta < 1$ and two positive averaging coefficients α_1, α_2 the Neumann-Neumann algorithm has the following form.

Algorithm 2 Neumann-Neumann

for $k = 0, 1, \ldots$ until convergence **do**
  $-\Delta u_i^{k+1} = f$ in Ω_i; ▷ $i = 1, 2$
  $u_i^{k+1} = 0$ on Σ_i; ▷ $i = 1, 2$
  $u_i^{k+1} = \mu^k$ on Σ; ▷ $i = 1, 2$
  $-\Delta \phi_i^{k+1} = 0$ in Ω_i; ▷ $i = 1, 2$
  $\phi_i^{k+1} = 0$ on Σ_i; ▷ $i = 1, 2$
  $\mathbf{n}_1 \cdot \nabla \phi_2^{k+1} = \mathbf{n}_1 \cdot \nabla u_1^{k+1} - \mathbf{n}_1 \cdot \nabla u_2^{k+1}$ on Σ; ▷ Flux interface condition with $\mathbf{n}_2 = -\mathbf{n}_1$
  $\mu^{k+1} = \mu^k - \theta\left(\alpha_1 \phi_{1|\Sigma}^{k+1} - \alpha_2 \phi_{2|\Sigma}^{k+1}\right)$; ▷ Update of μ^{k+1}
end for
Output: (u_1^k, u_2^k)

Carrying on with the same notation of the method of Dirichlet-Neumann, the weak formulation of the Neumann-Neumann method reads:find $u_i^{k+1}, \phi_i^{k+1} \in V_i$ such that

$$\begin{cases} a_i\left(u_i^{k+1}, v_i\right) = f_{\Omega_i}(v_i), & \forall v_i \in V_i^0; \\ u_i^{k+1} = \mu^k, & \text{in } \Sigma, \\ a_i\left(\phi_i^{k+1}, v_i\right) = 0, & \forall v_i \in V_i^0; \\ a_i\left(\phi_i^{k+1}, \Lambda_i \beta\right) = (-1)^i \left(\sum_{i=1}^2 f_{\Omega_i}(\Lambda_i \beta) - \sum_{i=1}^2 a_i\left(u_i^{k+1}, \Lambda_i \beta\right)\right), & \forall \beta \in B, \end{cases} \tag{2.33a}$$

for $i = 1, 2$. The proof of the convergence of this algorithm can be found in Mathew (2008); Quarteroni and Valli (1999).

2.2.5 The method of Lions

Over the year 1990 P. L. Lions carried on a relevant improvement of the additive Schwarz method replacing the Dirichlet interface conditions by Robin interface conditions, see Lions (1990); Quarteroni and Valli (1999). Let μ be a positive number and given an initial guess u_i^0, the modified algorithm reads: The explanation of the Lions's method can be

Algorithm 3 Neumann-Neumann

for $k = 0, 1, \ldots$ until convergence **do**
  $-\Delta u_i^{k+1} = f$ in Ω_i; ▷ $i = 1, 2$
  $u_i^{k+1} = 0$ on Σ_i; ▷ $i = 1, 2$
  $\left(\mathbf{n}_1 \cdot \nabla - (-1)^i \mu\right) u_i^{k+1} = \left(\mathbf{n}_1 \cdot \nabla + (-1)^j \mu\right) u_j^k$ on Σ; ▷ $i, j = 1, 2$, $i \neq j$, $\mathbf{n}_2 = -\mathbf{n}_1$
end for
Output: (u_1^k, u_2^k)

deduced writing its variational formulation. In addition, the proof of the convergence of this scheme can be found in Lions (1990); Quarteroni and Valli (1999).

Chapter 3

The model of Fábregas & Rubinstein

In order to derive a general formulation, we start our model from the microscopic geometry, with the goal of deriving macroscopic equations. In this process we highlight the importance of the anisotropy of the local enamel geometry, that implies anisotropic diffusion matrix for the different compounds. On the other hand, we shall replace the reaction term (1.1) with a simpler model:

$$\mathrm{HAP} + 8\,\mathrm{H} \underset{k_{-1}}{\overset{k_1}{\rightleftharpoons}} 10\mathrm{c} \tag{3.1}$$

where we use the notations H and c to denote the hydrogen and calcium concentration of the equation (1.1). This means that we take into account separately the reaction and diffusion for each of the components of the right hand side of equation (1.1), and we will start by consider the calcium concentration, later on we could consider the others components in the right side of equation (1.1) as an extensions of the model.

In the first section of this chapter, we will obtain the main equations applying a no-trivial variation of the homogenization method. Additionally, in the last section we upgrade the model to account for the resilient outer layer of the enamel.

3.1 Local model

We describe a simple model that incorporates some of the basic mechanisms outlined above. The model is only for the formation of the lesion and not formation of cavities. Moreover, in this first study we consider only lesion formation in enamel.

We assume that the biofilm generates hydrogen ions at a given rate. A typical time scale for this is an hour or two following food consumption, since the secretion of the acid takes place after meals.

We consider the enamel to occupy half space ($x_3 > 0, -\infty < x_1,\ x_2 < \infty$). The line $x_3 = 0$ is the tooth edge. We assume that the biofilm, i.e. source of acid, occupies a smaller domain $x_3 = 0, -\delta < x_1,\ x_2 < \delta$. The concentration of H^+ ions is denoted by $H(x,t)$, where $x = (x_1, x_2, x_3)$. There are several processes taking place in the tooth. One is the diffusion and reaction of H^+ ions. A second is diffusion and reaction of the various compounds on the right hand side of equation (1.1). For simplicity we consider here only the calcium ions Ca^{2+}, and we denote its concentration $c(x,t)$. The description above of the enamel surface and the underlying reactions implies that the diffusion process is macroscopically anisotropic. In fact, we expect caries to be controlled by two general principles. One is that the diffusion coefficients depend on the porosity of the solid, and this, in turn is affected by the enamel density. The second is that diffusion is faster *along* the rods than *across* them. To make the work easier to read we describe in detail the diffusion and reaction of c, and then homogenize the equation for it. The equation for H can be analyzed and averaged in a similar manner.

The local length scale for the underlying process will be denoted by us l. Because of the radius of the enamel prisms and the typical distance between them we set $l = 1\ \mu m$. To obtain proper nondimensional variables it is useful to write an ad-hoc one dimensional model (Bollet-Quivogne et al. (2005); Patel et al. (1987a,b)) consisting of a single reaction diffusion system:

$$\partial_t c = D\partial^2_{x_3} c + R(c_s - c). \tag{3.2}$$

Here D is a diffusion coefficient and R is a reaction rate. The parameter c_s is the equilibrium value of the reaction, determined by the acidity, i.e. H, at any given point. We use the notation ∂_t for differentiating c with respect to t.

There is a great diversity of estimates for D and R in the literature. We choose here parameters following mostly the papers Bollet-Quivogne et al. (2005) and van Dijk et al. (1983). We thus set $D = 10^2\ \mu m^2/s$, $R = 10^{-2}\ 1/s$, and $c_s = 2{\cdot}10^{-3}\ g/cm^3$, which corresponds to acidity of about pH =4 Bollet-Quivogne et al. (2005).

The values of D and R define naturally a length scale

$$\lambda \sim (D/R)^{1/2} \sim 100\ \mu m. \tag{3.3}$$

This is the length scale where the diffusion and reaction are balanced. For example, consider equation (3.2) in the semi infinite interval $x_3 > 0$, with initial conditions $c(x_3, 0) = c_s$. We assume that c approaches c_s for large values of x_3. Assume further that the boundary condition at $x_3 = 0$ is $c = c_s$, except for bursts of larger $c(0,t)$ of short duration, resulting from a reduction in pH following a meal. In these short bursts a reaction takes place according to equation (3.2). The penetration length of the acidity is thus λ. We point out, though, that there is another length scale associated with caries progression. It is given by $\lambda_b = (Dt_m)^{1/2}$, where t_m is a typical time scale for sugar intake by the biofilm after a meal. Roughly, one can assume $t_m \sim 0.5h.$ and therefore $\lambda_b \sim 400\mu m$.

We point out, though, that the diffusion coefficient D is not fixed in time, since the melting of the enamel increases the size of the pores, and thus increases D. Another point that should be taken into account is that the reaction term (the second term on the right hand side of equation (3.2)) depends not just on c but rather on the difference $c_s - c$. When comparing the reaction term with the diffusion term we assumed that the difference $c_s - c$ is of the same order as c itself. However, when c is near c_s, the reaction term is practically smaller, and then the penetration length λ is longer. Finally we recall that c_s is determined by the acidity as will be written explicitly below. We thus need to solve for both c and H.

3.1.1 Homogenization of the microscopic equations

We assume that the enamel portion of the tooth consists of a volume E occupied by the rods and an inter-rod volume that we denote by $\mathcal{V}$. The ions and enamel matrix solute diffuse in the inter-rod domain $\mathcal{V}$, and might react when they reach the rod boundaries ∂E. We therefore write a diffusion equation for the concentration $c(x_1, x_2, x_3, t)$ in $\mathcal{V}$ and appropriate flux condition at the interface ∂E. Since the enamel melts under the reaction with the H^+ ions, we must take into account the time variation of $\partial E(t)$. We thus write the following equations for the diffusion of c and the reaction on ∂E:

$$\partial_t c = D\Delta c, \qquad x \in \mathcal{V}, \tag{3.4a}$$

$$D\partial_n c = R_0(c_s - c) - \bar{v}_n c, \qquad x \in \partial E. \tag{3.4b}$$

We use here $\bar{v}_n$ to denote the normal velocity of the rod boundary ∂E. The parameter R_0 denotes the reaction rate at the boundary ∂E, and we neglect diffusion inside the prism. Also, we use throughout the thesis the symbol Δ for the three-dimensional Laplacian, ∇ denoted the gradient operator, and the notation ∂_x or ∂_t stands for partial differentiation.

We scale the length by λ: $x' = x/\lambda$, and time by $1/R$: $t' = Rt$. In what follows we shall omit the primes to simplify the notation. Before writing down the scaled equations we describe our model for the microstructure geometry. As noted above the local scale of the prism, which we denoted by l, is much smaller than λ. We thus define the small parameter $\varepsilon = l/\lambda$. We assume that E consists of many elongated prisms (rods) whose thickness is of $O(l)$. The prisms main axis and also their cross section shape varies slowly on the λ - scale. To distinguish between the two length scales we introduce local variables $y_1 = x_1/\varepsilon$, $y_2 = x_2/\varepsilon$. Because of the layered form of the prisms we assume that the geometry is essentially periodic in the y_1, y_2 variables. However we do allow for geometry variations also on the global (x_1, x_2, x_3) scale since different parts of the enamel react at different rates, determined by variations in c.

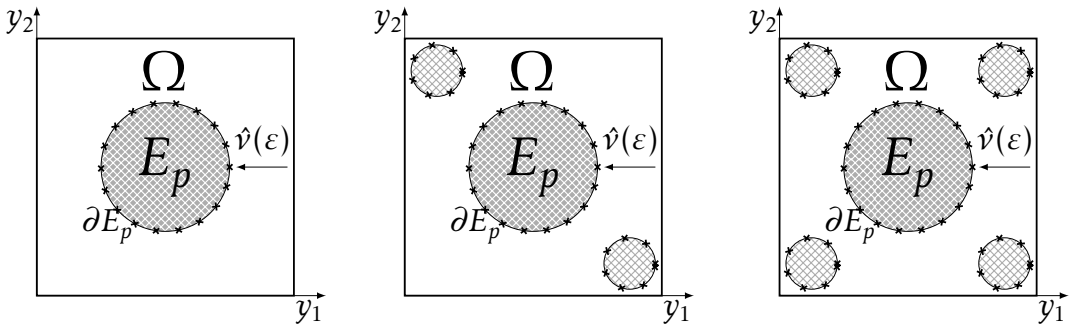

Figure 3.1: Examples for the periodic cell cross sections: (a) Local periodic cell containing one prism, (b) Local periodic cell containing 3 prisms, (c) Local periodic cell containing 5 prisms.

We denote the inter-rod domain in a single cell, i.e. a single period, by Ω and the enamel cross section in a single cell is denoted by E_p. See Figure 3.1 for a sketch of simple two cases of a cells containing 1 prism (Figure 3.1(a)), and 5 prisms (Figure 3.1(c)) with circular cross sections. The patterns depicted in Figure 1 are typical to prisms cross section Dumont (1995, 1996); Maas and Dumont. (1999). It is useful to express the assumptions above on the separation of scales by writing the boundary ∂E_p of the enamel surface via an implicit function

$$\partial E_p : \{(x_1, x_2, x_3, y_1, y_2, t) | \, F(x_1, x_2, x_3, y_1, y_2, t) = 0\}. \tag{3.5}$$

We also need an expression for the normal vector $\hat{n}(\varepsilon)$ to ∂E_p in terms of F. In fact, we need to retain only the first two terms in the ε expansion of $\hat{n}$. A straightforward calculation

(see the Appendix) gives

$$\hat{n}(\varepsilon) = \hat{\nu} + \varepsilon\Big((\hat{\tau}\cdot\nabla_2^x F)/G_F\ \hat{\tau} + \hat{k}\partial_{x_3}F/G_F\Big), \tag{3.6}$$

where we introduced the notation $\hat{\nu}$ for the two-dimensional normal to ∂E_p, i.e.

$$\hat{\nu} = \nabla_2^y F/G_F, \quad G_F = |\nabla_2^y F|. \tag{3.7}$$

Here $\hat{\tau}$ denotes the unit two-dimensional tangent vector to ∂E_p, and $\hat{k}$ is a unit vector in the x_3 direction. Also, here and in what follows we use ∇_2^y and Δ_2^y to denote the gradient and Laplacian operators in the two dimensional space (y_1, y_2). Similarly, we use ∇_2^x and Δ_2^x to denote the gradient and Laplacian operators in the two dimensional space (x_1, x_2).

The motion of the boundary of the prism ∂E_p varies on the l local scale. Therefore we write

$$\bar{v}_n = Rl\, v_n, \tag{3.8}$$

so that v_n is the nondimensional boundary normal velocity. To complete the scaling we normalize the concentration c by a representative value $\bar{c}$ of the equilibrium value c_s, i.e. $c' = c/\bar{c}$.

We are now at a position to write the nondimensional version of equations (3.4a)-(3.4b):

$$\partial_t c = \Delta c, \qquad x \in \mathcal{V}, \tag{3.9a}$$

$$\partial_n c = (\lambda R_0/D)(c_s - c) - (Rl\lambda/D)\, v_n c, \qquad x \in \partial E. \tag{3.9b}$$

Because of the elongated shape of the rods, where the long axis extends essentially in the x_3 direction, we expect the solution to vary rapidly in the x_1, x_2 variables. Following the convention in homogenization theory, we thus seek a solution of the form $c(x_1, x_2, x_3, y_1, y_2, t)$. We assume that to leading order $c_s = c_s(x_1, x_2, x_3, t)$. Later on we shall justify this assumption. Since on the present length and time scales we expect an averaged equation with balanced diffusion and reaction, we also make the assumption that $\lambda R_0/D = \varepsilon R_1$, with $R_1 = O(1)$. Therefore, the boundary condition (3.9b) becomes

$$\partial_\nu c = \varepsilon\Big(R_1(c_s - c) - v_\nu c - (\partial_{x_3}c)\partial_{x_3}F/G_F - (\hat{\tau}\cdot\nabla_2^x F)/G_F\ \hat{\tau}\cdot(\nabla_2^x c + 1/\varepsilon\ \nabla_2^y c)\Big), \tag{3.10}$$

where v_ν is the projection of the normal velocity of the boundary on the (x_1, x_2) plane. We use everywhere ∂_ν to denote the normal derivative in the (x_1, x_2) plane, and ∂_n to denote

the normal derivative in the (x_1, x_2, x_3) space.

Now, is time to apply the homogenization method as shown above, therefore, we need to to expand c in terms of the small parameter ε like an asymptotic expansion

$$c(x_1, x_2, x_3, y_1, y_2, t) = c^0 + \varepsilon c^1 + \varepsilon^2 c^2 + \dots \ , \ c^i = c^i(x_1, x_2, x_3, y_1, y_2, t). \tag{3.11}$$

Upon substituting this expansion into equation (3.9a) and the boundary condition (3.10), we obtain a cascade of equations at different orders of ε. At the leading order we obtain

$$\Delta_2^y c^0 = 0, \qquad y \in \Omega, \tag{3.12a}$$

$$\hat{\nu} \cdot \nabla_2^y c^0 = 0, \qquad y \in \partial E_p. \tag{3.12b}$$

It is easy to verify that equations (3.12a)-(3.12b) imply that c^0 is independent of the local scale y, i.e. $c^0 = c^0(x_1, x_2, x_3, t)$.

At the next order we obtain the following equations for c^1:

$$\Delta_2^y c^1 = 0, \qquad y \in \Omega, \tag{3.13a}$$

$$\hat{\nu} \cdot \nabla_2^y c^1 = -\hat{\nu} \cdot \nabla_2^x c^0, \qquad y \in \partial E_p, \tag{3.13b}$$

where the terms containing the $y-$derivatives of c^0 vanish due to the its independence of y. We thus express c^1 in the form

$$c^1(x_1, x_2, x_3, y_1, y_2, t) = W^1(x_1, x_2, x_3, y_1, y_2, t)\partial_{x_1} c^0 + W^2(x_1, x_2, x_3, y_1, y_2, t)\partial_{x_2} c^0. \tag{3.14}$$

The *cell functions* W^i solve a *cell problem* (see Appendix B) of the form

$$\Delta_2^y W^i = 0, \qquad y \in \Omega, \tag{3.15a}$$

$$\hat{\nu} \cdot \nabla_2^y W^i = -\hat{\nu}_i, \qquad y \in \partial E_p, \tag{3.15b}$$

with periodic boundary condition on the outer boundary of cell Ω. Here $\hat{\nu}_i$ denotes the i-th component of ν_i. Notice that the cell problems are implicitly parameterized by (x_1, x_2, x_3, t) since ∂E_p depends on these variables.

Proceeding to the next level in the expansion we find

$$\partial_t c^0 = \partial^2_{x_3} c^0 + \Delta_2^x c^0 + \Delta_2^y c^2 + \nabla_2^y \cdot \nabla_2^x c^1 + \nabla_2^x \cdot \nabla_2^y c^1, \qquad y \in \Omega, \tag{3.16a}$$

$$\hat{\nu} \cdot \nabla_2^y c^2 = -\hat{\nu} \cdot \nabla_2^x c^1 + R_1(c_s - c^0) - v_\nu c^0 - (\partial_{x_3} c^0)\partial_{x_3} F/G_F - (\hat{\tau} \cdot \nabla_2^x F)/G_F \; \hat{\tau} \cdot \left(\nabla_2^x c^0 + \nabla_2^y c^1\right), \qquad y \in \partial E_p. \tag{3.16b}$$

We integrate equation (3.16a) over the cell Ω, and write

$$|\Omega|\partial_t c^0 = |\Omega|\partial^2_{x_3} c^0 + \int_\Omega \nabla_2^x \cdot (\nabla_2^y c^1 + \nabla_2^x c^0)\, dy + \int_\Omega \nabla_2^y \cdot (\nabla_2^y c^2 + \nabla_2^x c^1)\, dy = |\Omega|\partial^2_{x_3} c^0 + J_1 + J_2. \tag{3.17}$$

The integral J_2 on the right hand side is transformed into a boundary term, where we use the periodicity of the c^1 and c^2 on the outer boundary of Ω, the boundary condition (3.16b), and the fact that c^0 does not depend upon y:

$$J_2 = |\partial E_p| R_1(c_s - c^0) - \left(\int_{\partial E_p} v_\nu\right) c^0 - \left(\int_{\partial E_p} \partial_{x_3} F/G_F\right) \partial_{x_3} c^0 - \int_{\partial E_p} (\hat{\tau} \cdot \nabla_2^x F)/G_F \; \hat{\tau} \cdot (\nabla_2^x c^0 + \nabla_2^y c^1). \tag{3.18}$$

To compute the first integral J_1 in equation (3.17) we use the following formula that we prove in the Appendix

$$J_1 = \nabla_2^x \cdot \int_\Omega (\nabla_2^y c^1 + \nabla_2^x c^0)\, dy + \int_{\partial E_p} \nabla_2^x F/G_F \cdot (\nabla_2^y c^1 + \nabla_2^x c^0). \tag{3.19}$$

The normal ($\hat{\nu}$) component of $(\nabla_2^y c^1 + \nabla_2^x c^0)$ vanishes on ∂E_p in light of equation (3.34). The tangential component of this term integrated in the second term on the right hand side of equation (3.19) cancels with the last term on the right hand side of equation (3.18). Next we define the 2×2 matrix

$$\bar{D}_{ij} = |\Omega|\delta_{ij} + \int_\Omega \partial_{y_i} W^j \, dy, \tag{3.20}$$

where the function $W^j(y)$ are defined in equations (3.15a)-(3.15b), and we denote δ_{ij} the Kronecker delta function. This notation enables us to express the first term on the right hand side of equation (3.19) in the form $\sum_{i=1}^2 \partial_{x_i}\left(\bar{D}_{ij}\partial_{x_j}\right) c^0$. The computations of J_1 and J_2

and the definition (3.20) enable us to rewrite equation (3.17) in the form

$$|\Omega|\partial_t c^0 = |\Omega|\partial^2_{x_3} c^0 + \sum_{i=1}^{2} \partial_{x_i}\left(\bar{D}_{ij}\partial_{x_j}\right)c^0 + |\partial E_p| R_1(c_s - c^0) - \left(\int_{\partial E_p} v_\nu\right)c^0 - \left(\int_{\partial E_p} \partial_{x_3} F/G_F\right)\partial_{x_3} c^0. \quad (3.21)$$

Equation (3.21) is the averaged (homogenized) equation for the evolution of c^0. To simplify it, and to recognize it as a conservation law, we make use of two geometric identities that are proved in the Appendix:

$$\int_{\partial E_p} v_\nu = \partial_t |\Omega|, \quad \int_{\partial E_p} \partial_{x_3} F/G_F = -\partial_{x_3}|\Omega|. \quad (3.22)$$

We now apply identities (3.22) to rewrite equation (3.21) in the form

$$\partial_t\left(|\Omega|c^0\right) = \partial_{x_3}\left(|\Omega|\partial_{x_3} c^0\right) + \sum_{i=1}^{2} \partial_{x_i}\left(\bar{D}_{ij}\partial_{x_j}\right)c^0 + |\partial E_p| R_1(c_s - c^0). \quad (3.23)$$

Notice that we wrote the derivatives of c^0 with respect to x_3 and with respect to (x_1, x_2) separately to emphasize the symmetry breaking induced by the prism geometry.

Equation (3.23) is not closed, since the enamel E_p melts and therefore both $|\partial E_p|$ and $|\Omega|$ change in time and space. In addition, the effective diffusion tensor $\bar{D}$ depends upon the concentration c^0. This issue will be addressed in section 4. We also need to determine the solubility term c_s. In our model we assume a linear relation of the form $c_s = \gamma H$. We point out that this is an approximation aimed at simplifying the model. As a partial justification for it, we refer to the reaction equation (1.1). At equilibrium the concentration c_s is proportional to $H^{4/5}$, so the linear model is a reasonable approximation. We also point out that the dependency of initial caries progress on the pH level is known to be smooth Shellis and Wilson (2004), which gives further support to the approximation we use here.

We need also to evaluate the macroscopic equation for H. However, the hydrogen ions diffuse and react in the same geometry as the calcium ions. Therefore, applying the same homogenization procedure that was performed in this section also to H, we get

$$\partial_t\left(|\Omega|H\right) = d_H\left(\partial_{x_3}\left(|\Omega|\partial_{x_3} H\right) + \sum_{i=1}^{2} \partial_{x_i}\left(\bar{D}_{ij}\partial_{x_j}\right)H\right) - |\partial E_p| R_1(c_s - c), \quad (3.24)$$

where d_H is the ratio of the local diffusion coefficients of the hydrogen ions and the calcium ions.

We can write the following proposition in order to summarizing the results of the final equations for the evolution of the hydrogen's and calcium's ions omitting the 0 superscript for convenience in the form:

Proposition 3.1. *The propagation of the macroscopic process of dental caries is governed by the following system of evolution equations, i.e., the homogenization of the problem* (3.9a)-(3.9b) *is given by*

$$\partial_t(|\Omega|c) = \partial_{x_3}\left(|\Omega|\partial_{x_3}c\right) + \sum_{i=1}^{2}\partial_{x_i}\left(\bar{D}_{ij}\partial_{x_j}\right)c + |\partial E_p|R_1(\gamma H - c), \tag{3.25a}$$

$$\partial_t(|\Omega|H) = d_H\left(\partial_{x_3}\left(|\Omega|\partial_{x_3}H\right) + \sum_{i=1}^{2}\partial_{x_i}\left(\bar{D}_{ij}\partial_{x_j}\right)H\right) - |\partial E_p|R_1(\gamma H - c). \tag{3.25b}$$

taking into account that $c_s = \gamma H$.

In Chapters 4 and 5 we shall address the question of initial and boundary conditions for these two equations.

3.1.2 Enamel dissolution

In this section we couple the effective reaction diffusion equation to the enamel dissolution process. The diffusion and reaction are described by equations (3.25).

To close the system of equations for the evolution of c and H we need to couple equations (3.25a) and (3.25b) to the evolution of the microstructure. Clearly the time derivative of $|E_p|$ must be proportional to the reaction rate, the difference $c_s - c$ and $|E_p|$ itself. In this work we assume that the enamel prisms cross sections are essentially circular Dumont (1995, 1996); Maas and Dumont. (1999), and therefore are characterized by a single function, namely their radius which we denote by $\rho(x,t)$. Recall that we used the length λ as a length unit and $1/R$ as a time unit. Also, the cell area $|\Omega|$ and the prism boundary $|\partial E_p|$ are computed on the local y scale (l), and therefore they are both $O(1)$ objects.

Our goal is to derive an equation for the enamel dissolution. This equation is needed to close our model. For this purpose we shall concentrate on the global reaction term in equation (3.25a)

$$\partial_t(|\Omega|c) \sim R_1|\partial E_p|(c_s - c). \tag{3.26}$$

To understand the order of magnitude of the different parameters involved in the enamel melting model we find it useful to return momentarily to dimensional units. We use here 1h for the time variable and $1\mu m$ for the length variable. The dimensional reaction rate will be denoted by $\tilde{R}_1$. In light of the enamel basic symmetry we concentrate on a two dimensional slice of the enamel. The concentration c is expressed in units of mol/μm^2. The reaction model (1.1) relates the number of hydroxyapatite molecules to the number of calcium ions. Denote the number of calcium ions in Ω (per 1cm in the x_3 coordinate) by N^c, and similarly the number of hydroxyapatite molecules in E_p (per 1cm in the x_3 direction) is denoted N^e. Since the reaction dissolution is confined to ∂E_p we write

$$\partial_t N^e = -0.1\partial_t N^c. \tag{3.27}$$

The reaction relation (3.26) can be written as

$$\partial_t N^e \sim -0.1\tilde{R}_1|\partial E_p|(c_s - c). \tag{3.28}$$

To convert this result to the rate of change of E_p itself we need to compute the molar concentration of hydroxyapatite. This can be computed from the known value of the molar mass of this molecule (500 g/mol) and its known density (3000 g/Liter). Thus the molar concentration of enamel is

$$\kappa^e = 6 \text{ mol/Liter} = 6 \cdot 10^{-11} \frac{\text{mol}}{\mu m^2\, cm}. \tag{3.29}$$

Using the formula $\kappa^e = N^e/|E_p|$, and since κ^e is constant in time, we obtain

$$\partial_t |E_p| = -0.1|\partial E_p| \frac{\tilde{R}_1}{\kappa^e}(c_s - c). \tag{3.30}$$

A precise melting equation requires an evolution equation not just for the area $|E_p|$ but also for the prisms shape. In general this involves a complex moving boundary problem. However, since the concentration c varies slowly on the scale of individual prisms we propose a simplified model. For example, we assume that initially E_p is a disc, and this shape does not change appreciably as the prism melts. Thus the function $E_p(x,t)$ is characterized by a single parameter, namely the radius $\rho(x,t)$ of the prism. Therefore, we can express both the surface area $|\partial E_p|$ and the area $|\Omega|$ using ρ. The evolution of ρ is easily obtained form equation (3.30). Denoting the cell, including the prism, by $\bar{\Omega}$, we write

$|\Omega| = |\bar{\Omega}| - \pi\rho^2$, $|\partial E_p| = 2\pi\rho$. It follows that ρ evolves according to

$$\partial_t \rho = -0.1 \frac{\tilde{R}_1}{\kappa^e}(c_s - c) = -\frac{\tilde{R}_1}{60}(c_s - c), \tag{3.31}$$

where in the last term we express the concentrations c_s and c in units of mol/Liter. Similarly, we can construct a more complex local prism geometry, such as a collection of discs of different radii at every cell, where each of the discs evolves by equation (3.31). Finally we return to nondimensional units and rewrite this equation in a scaled form:

$$\partial_t \rho = -\frac{R_1}{60}\gamma(H - q), \tag{3.32}$$

where we scaled c by γ in the form $c = \gamma q$, and therefore, the scaled concentration q satisfies the following proposition

Proposition 3.2. *The propagation of the macroscopic process of dental caries is governed by the following system of evolution equations, i.e., the homogenization of the problem* (3.9a)-(3.9b) *is given by*

$$\partial_t(|\Omega| q) = \partial_{x_3}\left(|\Omega|\partial_{x_3} q\right) + \sum_{i=1}^{2} \partial_{x_i}\left(\bar{D}_{ij}\partial_{x_j}\right) q + |\partial E_p| R_1 (H - q), \tag{3.33a}$$

$$\partial_t(|\Omega| H) = d_H\left(\partial_{x_3}\left(|\Omega|\partial_{x_3} H\right) + \sum_{i=1}^{2} \partial_{x_i}\left(\bar{D}_{ij}\partial_{x_j}\right) H\right) - |\partial E_p| R_1 \gamma (H - q), \tag{3.33b}$$

$$\partial_t \rho = -b R_1 \gamma (H - q) \tag{3.33c}$$

where d_H is the ratio of the local diffusion coefficients of the hydrogen ions and the calcium ions and b is related to the molar concentration.

In addition, the diffusion tensor $\bar{D}$ is computed from equations (3.15a)-(3.15b) and the integral (3.20). In the Appendix A we describe a methodology in order to calculate the diffusion coefficient and its approximate curve.

3.2 The sound outer layer of enamel

The model above can be simplified under the mild approximation $d_H \sim 1$. Then, a single distribution function $w := H - c/\gamma$ can be defined and the model takes the form

$$\partial_t (|\Omega| w) = \partial_{x_3} \left(|\Omega| \partial_{x_3} w \right) + \sum_{i=1}^{2} \partial_{x_i} \left(\bar{D}_{ij} \partial_{x_j} \right) w - (1+\gamma) |\partial E_p| R_1 w, \tag{3.34}$$

together with the equation for the evolution of ρ:

$$\partial_t \rho = -b\gamma R_1 w. \tag{3.35}$$

So far we looked at bulk enamel. However, the outer layer of the tooth consists of a thin layer of hydroxyapatite molecules that are not organized in prisms, but in a much denser and disordered pattern. In addition this layer is known to be resistant to dissolution relative to bulk enamel. It is termed 'relative sound enamel layer' by Holly and Gray Holly and Gray (1968) and 'prismless enamel layer' by Ripa et al. Ripa et al. (1966) and by others. To incorporate this very important feature of tooth microgeometry into our equations, and following the histological studies of Ripa et al. (1966), we model this layer as a medium with a homogeneous and isotropic diffusion tensor, where the single diffusion coefficient is much smaller than the diffusion coefficients in bulk enamel. Also, since this outer layer is quite thin, and also more resistant to melting, we shall neglect the enamel dissolution altogether in this layer. Therefore we replace in this layer the reaction-diffusion equation (3.34) by the equation

$$\partial_t w = \nabla (D_r \nabla w). \tag{3.36}$$

The thickness of the outer layer, that we denote here ξ is reported to be in the range of $15 - 40$ μm Ripa et al. (1966), Fava (1997), Holly and Gray (1968). For the purpose of our simulation below we take the layer to be of size 30 μm, which is about 0.3 in the nondimensional length unit scaled by λ.

We could not find in the literature direct estimates for the diffusion coefficient D_r in the prismless layer. However, the experiments of Anderson et al. Anderson et al. (1998) give some indication for the magnitude of D_r. The authors report on a delay in the initiation of the enamel dissolution curve (Figure 4 in their paper). The delay is approximately $10h - 20h$. If we attribute this delay to the prismless outer layer, then using the estimate $D_r \sim \xi^2/T$, and taking $T = 10h$, and $\xi = 30\mu m$, we obtain $D_r \sim 3 \cdot 10^{-2} \mu^2/s$. To conform with the equations for bulk enamel that are written down in the nondimensional units introduced

at the begining of Section 2, we denote the nondimensional diffusion coefficient by d_r, which is the ratio between D_r and the main diffusion coefficient in bulk enamel that we took earlier to be approximately $10^2\mu^2 m/s$; we thus obtain $d_r \sim 1/3000$.

3.2.1 The model

Our model consists now of equation (4.6) in the prismless layer, and the model (3.34) or (3.16b) in the bulk enamel. However, these models involve very different diffusion coefficients. Therefore, it is useful to rescale the time variable in all the equations through $t = t'/d_r$. Then, the left hand side of equation (3.34) (or (3.16b)) can be neglected. We write the augmented model, that includes the prismless layer, in a rectangular geometry, and to simplify the notation we omit the prime over the new time variable. The model thus consists of the following two equations:

$$\partial_t(|\Omega|w) = \sum_{i=1}^{3} \partial_{x_i}\left(|\Omega|\partial_{x_i} w\right), \qquad 0 < x_3 < \xi, \tag{3.37a}$$

$$0 = \partial_{x_3}\left(|\Omega|\partial_{x_3} w\right) + \sum_{i=1}^{2} \partial_{x_i}\left(\bar{D}_{ij}\partial_{x_j} w\right) - (1+\gamma)|\partial E_p| R_1 w, \qquad x_3 > \xi. \tag{3.37b}$$

Notice that in the prismless layer the geometry, i.e. Ω, is fixed; we introduced it into equation (3.37a) in order to compare the diffusion coefficients of the two equations. The solution w, as well as its flux are continuous across the interface $x_3 = \xi$. In addition to equations (3.37a)-(3.37b) we need to follow the evolution of ρ, though only in the bulk enamel $x_3 > \xi$. In the new time scale this equation reads:

$$\partial_t \rho = -\frac{b\gamma R_1}{d_r} w. \tag{3.38}$$

Physically, the model means that the reaction-diffusion process in the bulk enamel is *slaved* by the boundary behavior of the prismless enamel, in the sense that it is always at equilibrium with the data of w at the boundary between the prismless strip and the bulk enamel. Also, while the basic time unit for the earlier model (3.34) was about $20s$, the time scale for the upgraded model (3.37a) - (3.37b) is about $16h$.

Chapter 4

A two-dimensional approach for the initial progress of caries

In this Chapter we consider the numerical implementation of the model derived in Chapter 2. In particular we are going to study our model in a domain with rectangular geometry in order to mimic the in vitro experiments. Hence, the implementation of our model in a rectangular domain, allow to make the comparison between our results and the goals or laws derived by the experimental scientific community from chemical results.

In the first section we present the assumptions in order to simplify the model and the rectangular domain. The second section is dedicated to the simulations, starting with the computation of the effective diffusion tensor and later on with the proposed examples. The last section is assigned for the discussion of the proposed examples and a summary of the results.

4.1 Geometry and assumptions

The evolution equations for c (or q) and H are solved in a finite domain. Also, for simplicity we restrict the examples to two spatial dimensions. The anisotropy of the diffusion process is already manifested in this case. We thus consider in all the examples below the domain to be

$$V = \{-1 < x_1 < 1,\ \ 0 < x_3 < 3\}.$$

Paying attention at first Chapter 1 to the Anderson's experiments 1.4, we can appreciate the similarity the selected domain Figure 4.1.

In addition, as consequence of the estimates from the preceding section for c_s at pH=4 we get $\gamma \sim 20$.

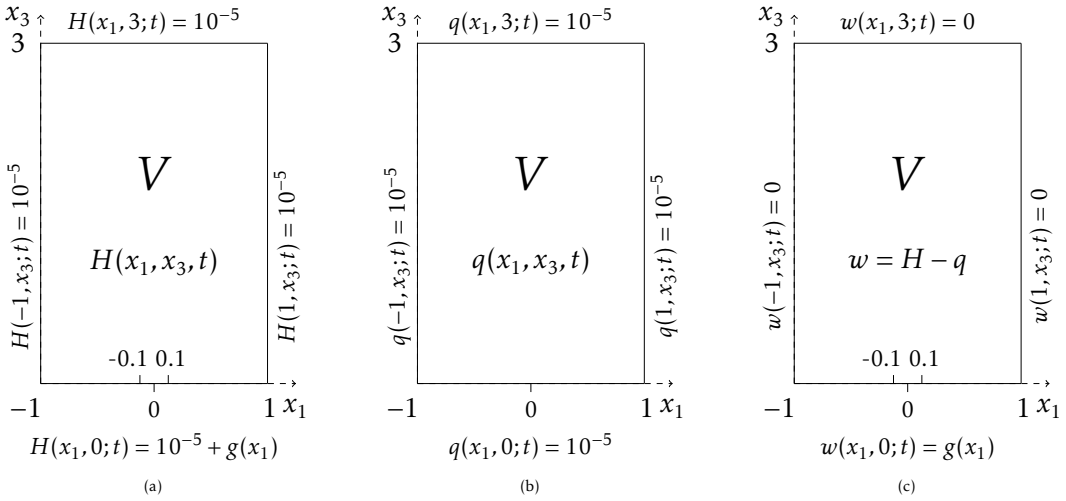

Figure 4.1: Domain $V=\{-1<x_1<1,\ \ 0<x_3<3\}$ such that $g(x_1)=9\cdot 10^{-5}A(0.1-|x_1|)$ or $g(x_1)=10^{-4}\cos(\pi x_1/2)$.

As a further simplification we also assume that the amount of hydrogen ions lost to the reaction is small compared to their total amount, and therefore we neglect the reaction term in the equation (3.33b). In addition, we assume that the diffusivities of the hydrogen and calcium ions are essentially the same, i.e., the ratio of the local diffusion coefficients of the hydrogen ions and the calcium ions $d_H=1$. Hence, from the Proposition 3.2 and equation (3.32) we can write the system of equations

$$\partial_t(|\Omega|q)=\partial_{x_3}\left(|\Omega|\partial_{x_3}q\right)+\sum_{i=1}^{2}\partial_{x_i}\left(\bar{D}_{ij}\partial_{x_j}\right)q+|\partial E_p|R_1(H-q), \tag{4.1a}$$

$$\partial_t(|\Omega|H)=\partial_{x_3}\left(|\Omega|\partial_{x_3}H\right)+\sum_{i=1}^{2}\partial_{x_i}\left(\bar{D}_{ij}\partial_{x_j}\right)H, \tag{4.1b}$$

$$\partial_t\rho=-\frac{R_1}{60}\gamma(H-q). \tag{4.1c}$$

where $|\Omega|=4-\pi\rho^2$ and $|\partial E_p|=2\pi\rho$.

4.2 Simulations.

The more difficult point in order to solve the system equation (4.1), is the computation of the effective diffusion tensor $\bar{D}$. Since the local cell geometry varies as a function of x and t, we must solve the cell problem (3.15a)-(3.15b) and then compute the integral (3.20) for each local value of $\rho(x,t)$. Therefore, we star the calculations solving the cell problem numerically, in other words, we need to find this tensor at each grid point (in

space and time). Later on, we can proceed to solve the system equation (4.1) applying the Crank-Nicolson method.

4.2.1 Diffusion coefficient

We are going to examine several interpolation models in order to calculate the diffusion coefficient $\bar{D}$. This requires solving the cell problem (3.15a)-(3.15b). This is a hard problem even under the simplification that E_p is characterized by a single disc Figure 3.1(a). We thus propose a method to overcome this problem. The idea is to compute *a priori* the tensor $\bar{D}$ as a function of the radius ρ for a finite set of values $(\rho_1, \rho_2, .., \rho_n)$. Then, at each point $\rho(x,t)$ we interpolate $\bar{D}(\rho(x,t))$ from the precomputed set of $\bar{D}$. In the Appendix A we describe the finite scheme and the numerical approach.

Example 1: First, we demonstrate this idea for the simple case where the cell consists of the 2×2 square, and E_p is a disc of radius ρ at its center, as depicted in Figure 3.1(a). Symmetry implies that in this case $\bar{D}$ is of the form $\bar{D} = dI$ where $d(\rho)$ is an effective diffusion coefficient (EDC), and I is the 2×2 identity matrix. Solving the cell problem for this geometry starting on $\rho = 0.1$ with step 0.1 and bi-periodic boundary condition over the boundary of Ω, gives the 4 particular simulations Figure 4.2 with its corresponding diffusion coefficients curve $d(\rho)$ as depicted in the dotted line in Figure 4.3.

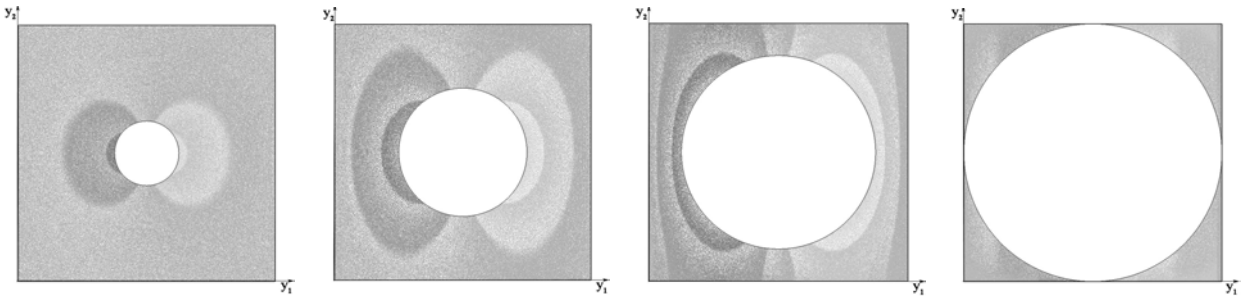

(a) $\rho(x,t) = 0.25$ (b) $\rho(x,t) = 0.5$ (c) $\rho(x,t) = 0.75$ (d) $\rho(x,t) = 1.0$

Figure 4.2: Numeric solutions of cell problem into Ω, Figure 3.1(a) for different values of the radius $\rho(x,t)$ and number of finite elements in order to calculate the diffusion matrix $\bar{D}$.

Example 2: As another example we consider the cell (again a 2×2 square) with E_p consisting of 5 discs, see Figure 3.1(c). One large disc of radius ρ_1 at the center, and 4 smaller discs of radius $\rho_2 = 0.1$ at near the 4 corners. In this geometry one can get to higher relative enamel volume fraction than in the previous case. We computed the effective tensor $\bar{D}$

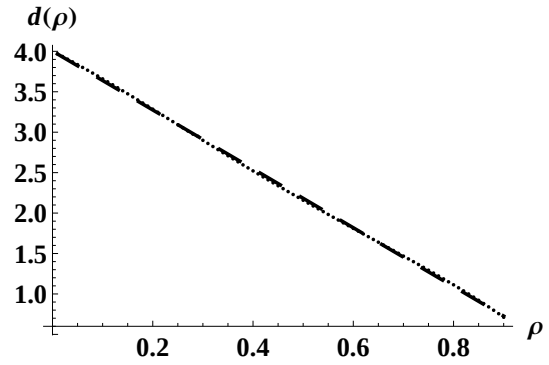

Figure 4.3: The effective diffusion coefficient $\bar{D}(\rho)$ for the Example 1, geometry of Figure 3.1(a) as a function of the local geometry (dotted line) compared with approximations of it given by $\bar{D}(\rho) = 4 - 3.64\rho$.

for this geometry starting on $\rho_1 = 0.1$ with step 0.1, gives the 4 particular simulations Figure 4.4 with its corresponding diffusion coefficients curve $d(\rho_1)$ as depicted in the dotted line in Figure 4.5.

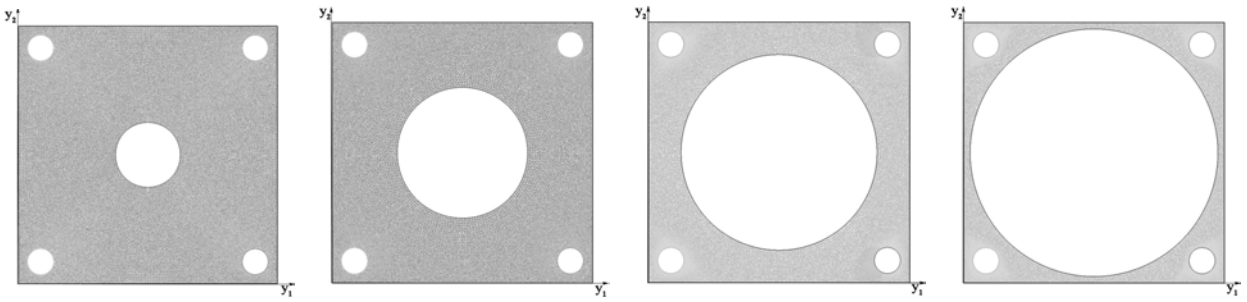

(a) $\rho(x,t) = 0.25$ (b) $\rho(x,t) = 0.5$ (c) $\rho(x,t) = 0.75$ (d) $\rho(x,t) = 0.95$

Figure 4.4: Numeric solutions of cell problem into Ω, Figure 3.1(c) for different values of the radius $\rho_1(x,t)$ and number of finite elements in order to calculate the diffusion matrix $\bar{D}$

4.2.2 System simulations

Once an analytical expression for the diffusion coefficient was calculated, we can proceed to solve the system of equation (4.1) by the Crank-Nicolson method. One special feature is that we need to update at each time step the geometric functions $|\Omega(x,t)|$ and $|\partial E_p(x,t)|$. As explained above, this can be done by updating at each time step the radius function $\rho(x,t)$.

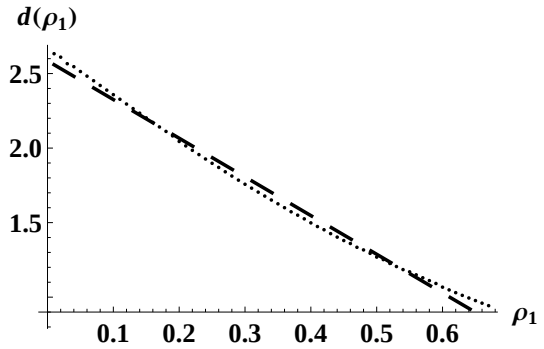

Figure 4.5: The effective diffusion coefficient $\bar{D}(\rho_1)$ for the Example 2, geometry of Figure 3.1(c) as a function of the local geometry (dotted line) compared with approximations of it given by $\bar{D}(\rho_1) = 2.6 - 2.6\rho_1$.

4.2.2.1 Example 1:

Our first test is carried out for the reaction diffusion alone, neglecting the effect of changes in the enamel geometry. This is certainly justified for short time periods. The cell consists of a single disc of radius ρ. Symmetry implies that in this case the effective diffusion tensor $\bar{D}$ is diagonal, and therefore the suppression of the x_2 variable does not have a serious effect on the problem. For this geometry we computed the effective horizontal diffusion coefficient for $\rho = 0.9$ and found $\bar{D} = 0.72$.

We solve for the specific scenario where the system is at equilibrium, and then is disturbed by a burst of acidity (low pH) for a certain time period. To fix ideas, we assume that $H = 10^{-5}$ at all the boundaries except at the top of the tooth ($x_3 = 0$ in our convention). For the time period, $0 < t < T = 72$ we simulate the burst of low pH by setting the boundary condition $H(x_1, 0; t) = 10^{-5} + 9 \cdot 10^{-5} A(0.1 - |x_1|)$, where $A(\xi)$ is the Heaviside function.

Given H, and neglecting the change in Ω and $|\partial E_p|$ we solve equation (4.1b). We set the boundary condition $q = 10^{-5}$ over the entire boundary. While this is a reasonable condition on the lateral boundaries, and also deep inside the tooth, it is not so obvious at the tooth edge $x_3 = 0$. However, we point out that this condition stabilizes q in the sense that it acts to inhibit demineralization. This is consistent with the physiology of the tooth, where there is an external thin layer near the surface that is resilient to demineralization. The initial condition is set to be $q \equiv 10^{-5}$.

Because of the similarity of the equations and boundary conditions for H and q, we can simplify the calculations by defining the difference function $w(x,t) = H - q$. Thus, w solves

$$\partial_t (|\Omega| w) = \partial_{x_3} \left(|\Omega| \partial_{x_3} w \right) + \partial_{x_1} \left(d \, \partial_{x_1} \right) w - |\partial E_p| R_1 w, \tag{4.2}$$

with the appropriate boundary conditions set above. Upon solving for q and H (or for

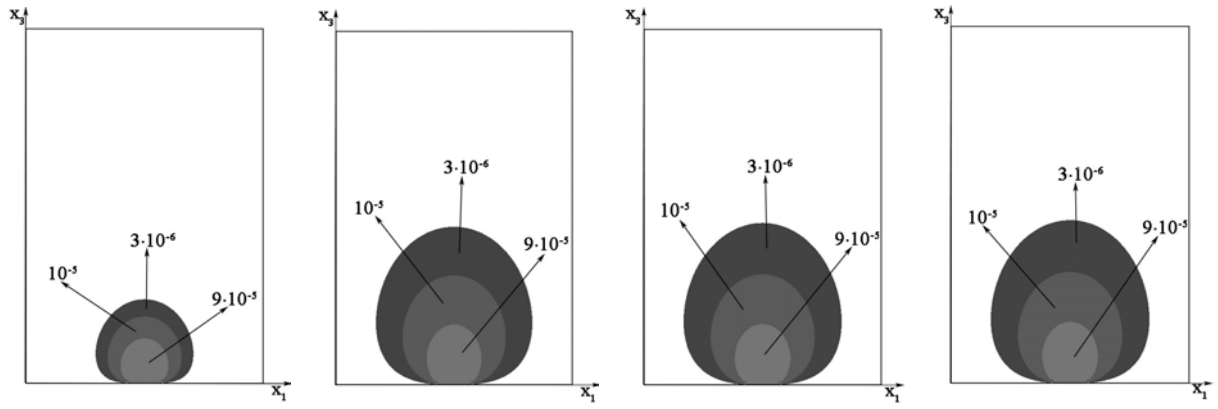

(a) t=0.05 (b) t=0.5 (c) t=1.0 (d) t=72

Figure 4.6: Snapshots of the progression of tooth decay described by fixed level sets of w for the Example 1, where we have taken into account a small time like starting point for the first three simulations (a)-(c).

w), we can compute the evolution of $\rho(x,t)$ according to equation (B.2). Recall that in this example, while we compute $\rho(x,t)$ we do not change the geometry. Since the change in ρ is small in this time interval, we express ρ in the form $\rho = \rho_0 + 10^{-4}\rho_1(x,t)$, where ρ_0 is the original (constant) value of ρ. Therefore $\rho_1(x,t)$ solves the equation

$$\partial_t \rho_1 = -\frac{10^4 R_1}{60}\gamma(H-q) = -\frac{10^3 R_1}{6}\gamma w. \tag{4.3}$$

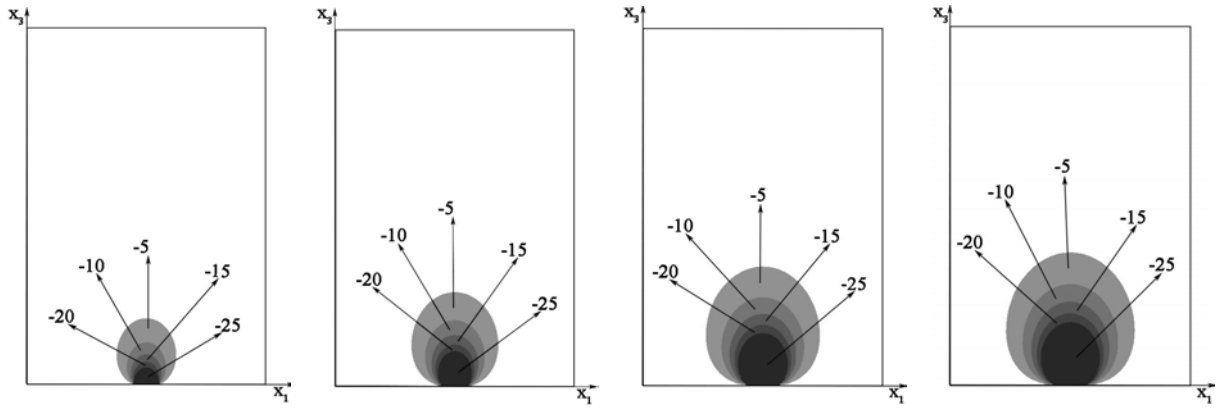

(a) t=18 (b) t=36 (c) t=56 (d) t=72

Figure 4.7: Snapshots of the progression of tooth decay described by fixed level sets of ρ_1 for the Example 1.

In our simulations we used the values $R_1 = 1$, and $\gamma = 200$; although the value for γ is larger than our estimate above, this choice does not affect the qualitative nature of the results, and helps accelerate the dissolution simulation.

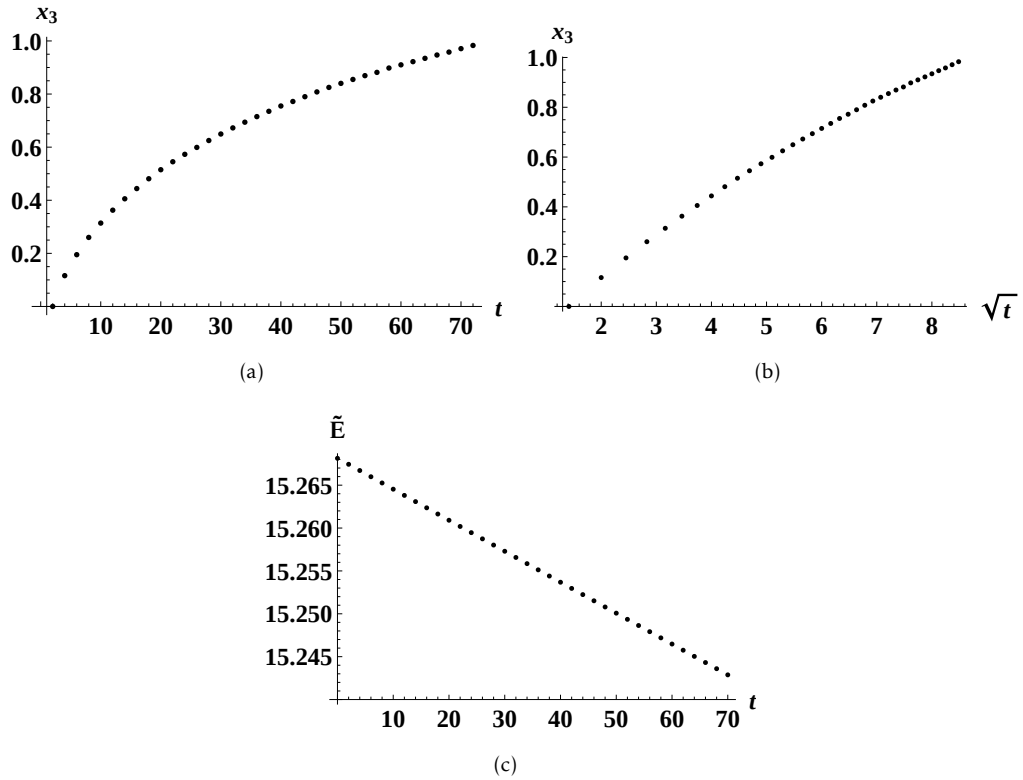

Figure 4.8: Progression of caries for the first boundary condition of Example 1: (a) Motion of the tip of a level set of ρ_1, (b) Motion of the same level set as a function of $t^{1/2}$, (c) The evolution of the total enamel volume $\tilde{E}(t)$

The progression of caries, as calculated in this example, is presented in Figure 4.6,Figure 4.7 and Figure 4.8. In Figure 4.6 the level sets of the solution w are depicted in order to show the short period of time in which the solution arrives to the steady state. In addition, Figure 4.7 describes the progression of the fixed level sets of ρ_1. On the other hand, and as the main result in Figure 4.8(a) we draw the tip of the level set $\rho_1 = -15$ (see Figure 4.7) as a function of t. In Figure 4.8(b) we draw the same level set tip, but now as a function of $t^{1/2}$. Figure 4.8(c) depicts the total enamel volume $\tilde{E}$, i.e. the integral of $|E_p|$ over the entire domain, as a function of t. We chose these specific graphs in order to compare our model, at least qualitatively, with well-known experiments. There is a debate in the literature as to what is the actual rate of caries progression. Anderson et al. Anderson et al. (1998) cite a number of authors that argue that caries progresses as a linear function of $t^{1/2}$. A typical result along this line is the paper of Poole et al. Poole et al. (1981). On the other

hand, many authors, and in particular Anderson himself, provide experimental evidence that caries progresses linearly in t.

We argue that the progression rate depends on how one defines it. This can be seen from the present example. When the total enamel volume lost to reaction is computed, which corresponds to the decline in $\tilde{E} = \pi \int \rho^2$ in our case, the progression is linear. This follows directly from our equations. Consider first the evolution of ρ (B.2). The evolution of $\tilde{E}$ is proportional to the integral of $\rho \partial_t \rho$. From equation (B.2) this, in turn, is proportional to the integral of ρw. Since the evolution of w, which is determined by equation (B.2), stabilizes in a few hours (see Figure 4.6), the integral of ρw is proportional to the total flux of w (a conclusion that is simply the law of mass conservation). However, since the evolution of ρ is slow on the relevant time scale, the flux is approximately constant in time, and therefore the evolution of $\tilde{E}$ is linear in time. This argument is indeed manifested in Figure 4.8(c).

A number of authors, including for example Poole et al. (1981) and Featherstone (1977), claim that the progression of caries is proportional to $t^{1/2}$. The theoretical justification, see for example van Dijk et al. (1983), is that for a short time period caries is dominated by diffusion, and at least initially, and in a one-dimensional approximation, the concentration of the ions is proportional to $\mathrm{Erf}(x_3/2(Dt)^{1/2})$. However, with the observed value of the diffusion coefficient D, and the typical scaling for caries, this description is only valid for a couple of hours at most. Therefore it cannot be used for experiments like those in reference Poole et al. (1981), for example, where the enamel was exposed to large acidity for days.

The authors in references Poole et al. (1981) and Featherstone (1977) (and similar publications) visually inspected the lesion, and deduced the progression from this inspection. This is similar to following the tip of a specific value of ρ, as depicted in Figure 4.8(a). It is tempting to associate this curve with some power law. For instance, we drew in Figure 4.8(b) the motion of the level set as a function of $t^{1/2}$. This curve looks approximately linear. However, selecting a power law can be misleading. We draw attention to the recent analysis of Stumpf and Porter Stumpf and Porter (2012). They showed that power law expressions empirical studies is often unjustified. To demonstrate this point in the present context, we performed another numerical test, where we replaced the boundary condition above for H and q by the boundary condition (for their difference)

$$w(x_1, 0, t) = 10^{-4} \cos(\pi x_1/2). \tag{4.4}$$

The advantage of selecting this boundary condition is that after a short time period

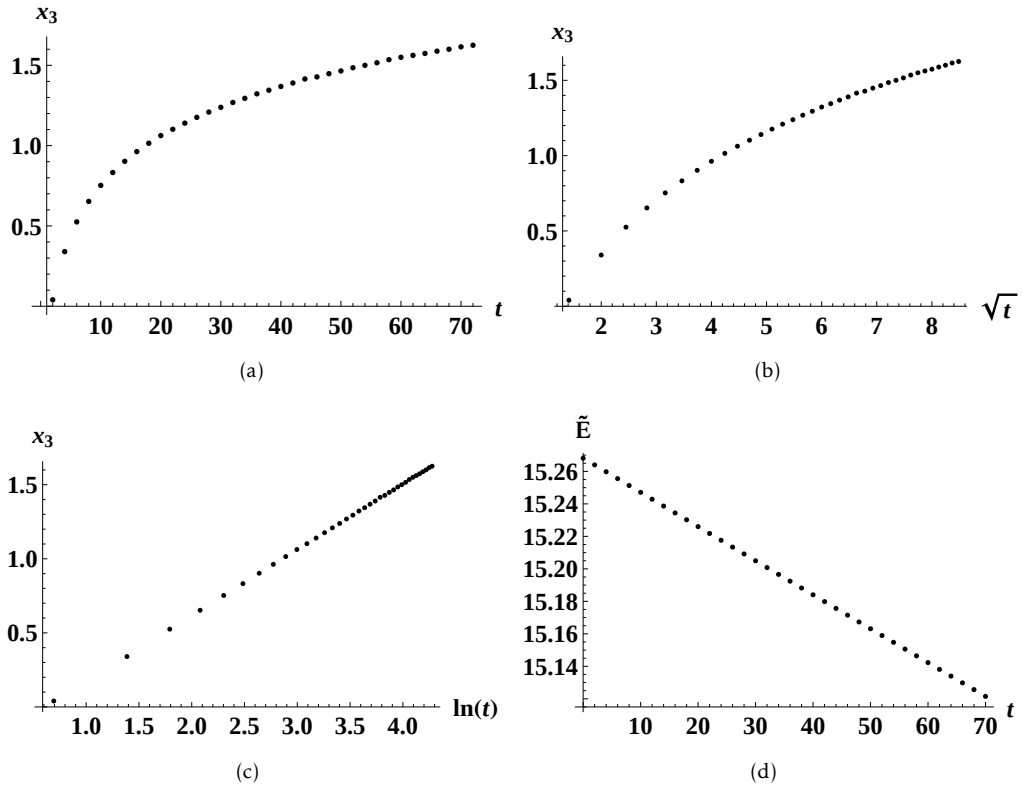

Figure 4.9: Progression of caries for the boundary condition $v(x_1, 0, t) = 10^{-4}\cos(\pi x_1/2)$: (a) Motion of the tip of a level set of ρ_1, (b) Motion of the tip of the same level set as a function of $t^{1/2}$, (c) Motion of the tip of the same level set as a function of $\ln t$; It is seen that the progression is dominated by the reaction term, and it slower than the in the case of pure diffusion, (d) The evolution of the total enamel volume $\tilde{E}(t)$.

the function w reaches a steady state ((see Figure 4.6)) that can be solved explicitly. For the specific parameters in this example we have that in the steady state w solves $\partial^2_{x_3} w + \partial^2_{x_1} w/2 - 3.87w = 0$. Thus, approximately we have

$$w \sim 10^{-4}\cos(\pi x_1/2)e^{-2.25x_3}. \tag{4.5}$$

The equation for ρ then implies that level sets of ρ evolve (for $t > 1$, say) approximately according to

$$x_3(t) = 0.44\ln t + C, \tag{4.6}$$

for some constant C. Indeed the computed curve of $x_3(t)$ is shown in Figure 4.9(a), and the linear dependency of $x_3(t)$ on $\ln t$ is clearly observed in Figure 4.9(c), with the predicted slope.

4.2.2.2 Example 2:

We compare here two simulations. We use the same geometry as in Example 1, with boundary condition $q = 10^{-5}$ over the entire boundary and initial condition $q \equiv 10^{-5}$. Also, we assume that $H = 10^{-5}$ at all the boundaries except at the top of the tooth. We solve for the time period, $0 < t < T = 264$ (11 days), and the boundary conditions at $x_3 = 0$ are given by $H(x_1, 0; t) = 10^{-5} + 5 \cdot 10^{-4} A(0.1 - |x_1|)$, which simulates relatively low pH.

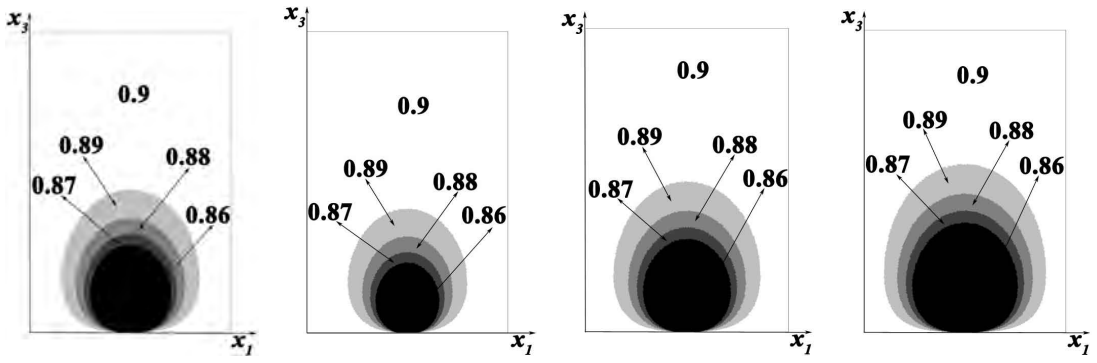

(a) $t = 264$ (b) $t = 120$ (c) $t = 192$ (d) $t = 264$

Figure 4.10: (a) Level sets of $\rho(x, t = 264)$ for the boundary conditions of Example 2, neglecting the evolution of the geometry and of $\bar{D}$. (b)-(d) Level sets of $\rho(x, t)$ for three values of t for the boundary conditions of Example 2. Here the evolution of the geometry and of $\bar{D}$ was taken into account.

In the first simulation (Figure 4.10(a)) we fixed the geometry for the diffusion-reaction, i.e. ρ at its initial value $\rho = 0.9$. We compute $\rho(x_1, x_3, t)$ as in Example 1 above, and draw the level sets of $\rho(x_1, x_3, 264)$. In the second simulation we update $\rho(x_1, x_3, t)$ throughout the evolution of v. We draw for comparison the level set at $\rho(x_1, x_3 120)$, (Figure 4.10(b)), $\rho(x, 192)$ (Figure 4.10(c)), and $\rho(x_1, x_3, 264)$ (Figure 4.10(d)). Since the enamel melts appreciably in this long time interval, ρ decreases and thus $\bar{D}$, which is now a function of space and time increases. As a result, a faster progression of caries can be appreciated in Figure 4.10(d) than in Figure 4.10(a).

4.3 Discussion

We made a number of assumptions along the model derivation. We assumed that the domain has a rectangular shape, where the outer layer of the tooth is given by the plane $x_3 = 0$. The enamel prisms were assumed to have their long axis essentially along the x_3 direction. While this rectangular geometry is of course not accurate for an actual tooth, it

can serve well for a first model. We consider below an extension of the model that removes this assumption.

We demonstrated the model in a few examples, where we concentrated on two issues. One is the effect of the anisotropy and of the melting. This is best seen in Example 2 in the preceding section. Caries is seen to propagate faster along the "easy" x_3 axis, than in the orthogonal direction. The effect of dissolution is observed by comparing Figure 4.10(a) to Figure 4.10(d). In both cases the equations were solved for a long period of time under conditions of low pH. However, in the first case we neglected the change in the geometry, and in the second case we updated the geometry, and also the diffusion coefficient. Indeed in the second case caries propagated faster also in the horizontal direction.

Another goal of our numerical simulation was to consider the question of progression rate of caries. A number of conflicting theories appear in the literature Anderson et al. (1998), Poole et al. (1981). We demonstrated in the preceding section that the progression rate depends on the way it is defined. We also pointed out that the use of power law can be misleading Stumpf and Porter (2012).

Chapter 5

A three-dimensional approach for the initial progress of caries

As mentioned above, the model consists of two conservation equations for the concentration of the calcium $c(x_1, x_2, x_3, t)$, hydrogen ions $H(x_1, x_2, x_3, t)$ and the local radius of the prism $\rho(x_1, x_2, x_3, t)$. Although a comprehensive system of equations should be written down in a general curvilinear coordinates that fit the global geometry, we find it more useful to write them down first for a rectangular domain, where the x_3 axis is oriented along the prism long axis. Later we shall formulate the model in a domain with spherical or circular symmetry that resembles a tooth shape.

In the next sections we shall present the model and the underlying assumptions behind it. In Section 1 we solve the equations in a three-dimensional rectangular domain and we inspect the effect of the resilient outer layer of the enamel on caries progress on the model upgraded. In Section 2 we solve the equations in a two-dimensional geometry that mimics a realistic tooth shape. In particular we discuss there the important and controversial issue of what is the progression rate of caries. We also consider there the shape of the lesion, depending on where it starts along the tooth boundary. Finally we discuss the model and the simulations.

5.1 Progression in a rectangular geometry

Recalling Proposition 3.1 in a domain with rectangular symmetry, where assuming that the prism are essentially periodically arranged in the cross section orthogonal to the long axis, and normalizing the period length to $2l$, we have $|\Omega| = 4 - \pi\rho^2$, and $|\partial E_p| = 2\pi\rho$. Additionally, we computed $\bar{D}$ for many representative values of ρ, and found out that, except

for the limit of extremely packed prism, $\bar{D}$ can be approximated by a linear function of ρ: $\bar{D}(\rho) \sim (4-3.64\rho)I_d$, where I_d is the 2×2 identity matrix. We note that this simple formula does not hold when ρ is near 1, i.e. at highly packed prism configuration. At extreme values of ρ a separate calculation should be done, solving in full the local equations that govern $\bar{D}$.

The model still contains three parameters: R_1 is determined by the local reaction rate, γ is determined by the precise model for the equilibrium concentration c_s, and b is related to the molar concentration of the hydroxyapatite crystals. However, we prefer at this point to leave R_1, γ, b as free parameters that can later on be adjusted either from theoretical considerations or by fitting the model to observations. Finally, the factor d_H is the ratio of the local diffusion coefficients of the hydrogen ions and the calcium ions.

5.1.1 Models with and without the prismless layer

To compare the models with and without the prismless layer we solve both cases in the rectangular geometry V with $L_1 = 1$, $L_2 = 3$, $\xi = 0.3$, i.e.,

$$V = \{|x_1|, |x_2| < 1, 0 < x_3 < 3\}.$$

In particular our goal is to understand the rate of caries progress. Before presenting specific simulations we point out that the model above can be simplified if we approximate the factor d_H by 1. Under this approximation we can define the function $w := H - c/\gamma$. The model then becomes

$$\partial_t(|\Omega|w) = \partial_{x_3}\left(|\Omega|\partial_{x_3}w\right) + \sum_{i=1}^{2}\partial_{x_i}\left(\bar{D}_{ij}\partial_{x_j}\right)w - (1+\gamma)|\partial E_p|R_1 w, \tag{5.1}$$

together with the equation for the evolution of ρ:

$$\partial_t\rho = -b\gamma R_1 w. \tag{5.2}$$

Example 1: In our numerical simulation we assume the boundary condition $w = 0$ at all the boundaries, except for the square $\Sigma:\ x_3 = 0,\ |x_1|, |x_2| < 0.1$, where we apply the boundary condition $w = 10^{-4}$. These boundary conditions simulate a burst of low pH at the outer tooth surface, and we expect the activity of the hydrogen ions to start the caries process. We use the following parameters in the simulations: $R_1 = 1$, $\gamma = 1$, $b = 3$. The initial conditions are $w = 0$, $\rho = 0.9$.

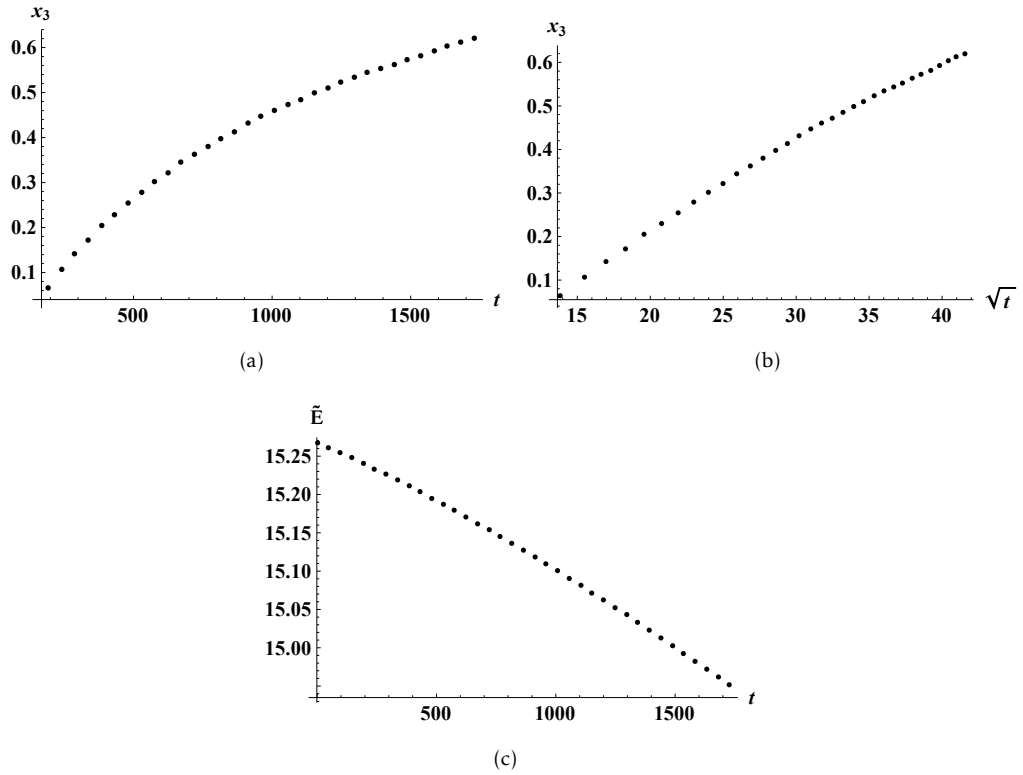

Figure 5.1: Progression of the fixed level set $\rho = 0.86$: (a) Motion of the tip of a level set of ρ, denoted $x_3(t)$, (b) Motion of the same level set as a function of $t^{1/2}$, (c) The evolution of the total enamel volume $\tilde{E}(t)$

Results: We present the progression of caries in two ways. First, we follow the tip of a certain level set of ρ. This mimics a visual inspection of the lesion. An alternative (but not equivalent) way is to follow the total amount of enamel. This is the same as measuring the amount of calcium ions leaving the tooth. The motion of the tip $x_3(t)$ of the level set $\rho = 0.86$ is depicted in Figure 5.1(a). Recall that the basic time unit is 20 s, so the curve follows a period of about 10 h. The total amount of enamel, determined by the total volume $\tilde{E}$ is depicted in Figure 5.1(c). A number of authors argue that in light of the importance of the diffusion transport process, and since the distance covered by a Brownian particle is proportional to $\sqrt{dt}$, where d is a diffusion coefficient, then caries should propagate at rate proportional to $\sqrt{t}$. Therefore, we depict in Figure 5.1(b) the motion of the tip x_3 as a function of $\sqrt{t}$. The curve seems not far from linear, but, as we argue below, this shape is misleading.

5.1.2 The sound outer layer of enamel

We simulate two physiological setups using the model presented in Chapter 3

$$\partial_t(|\Omega|w) = \sum_{i=1}^{3} \partial_{x_i}\left(|\Omega|\partial_{x_i} w\right), \qquad 0 < x_3 < \xi, \tag{5.3a}$$

$$0 = \partial_{x_3}\left(|\Omega|\partial_{x_3} w\right) + \sum_{i=1}^{2} \partial_{x_i}\left(\bar{D}_{ij}\partial_{x_j} w\right) - (1+\gamma)|\partial E_p| R_1 w, \qquad x_3 > \xi, \tag{5.3b}$$

$$\partial_t \rho = -\frac{b\gamma R_1}{d_r} w. \tag{5.3c}$$

Numerical solution of the system (5.3) is not trivial due to the change in nature of the equations at the boundary $x_3 = \xi$. We use here the method of domain decomposition with no overlapping (see for example Quarteroni and Valli (1999), Lions (1990)).

Example 2: The same geometry as in Example 1 above is applied here. The prismless enamel domain is defined as $x_3 < \xi$. We set as before equilibrium boundary condition $w = 0$ at all boundaries except at the tooth surface $\Sigma:\ x_3 = 0$, $|x_1|, |x_2| < 0.1$. There we set $w(x_1, x_3 = 0, t) = \alpha(t)10^{-4}$, where $\alpha(t) = 1$ for $0 < t < 0.1$, $0.5 < t < 0.7$, and $\alpha(t) = 0$ for other values of t. This boundary condition mimics two localized bursts of low pH, say, following two meals separated by a dimensional time interval of about $6h$.

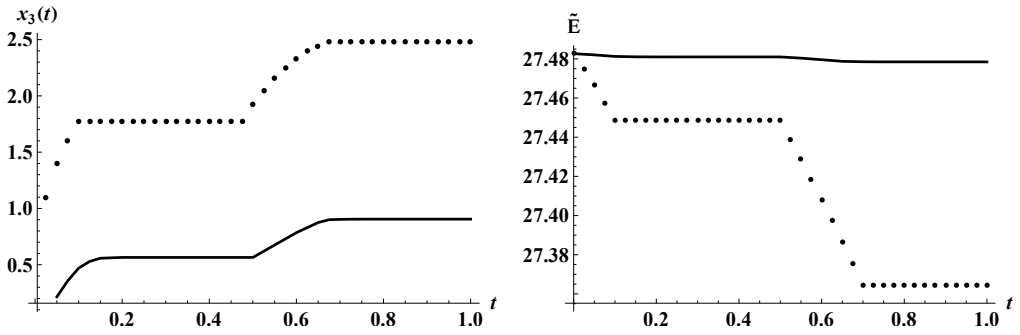

Figure 5.2: The influence of the prismless layer on the evolution of a caries lesion, as simulated in Example 2. (a) Progression of the tip of the level set of ρ (solid curve) of model (5.3), and the the tip of the same level set (dotted curve) for the model (5.3b)-(5.3c); (b) The evolution of the total enamel volume $\tilde{E}(t)$ for the models (5.3) (solid curve) and (5.3b)-(5.3c) (dotted curve).

Results: In Figure 5.2 we draw the evolution of the tip of level set $\rho = 0.898$. For comparison we draw this level set (solid line) together with the evolution of the same level set

when there is no prismless outer layer (dotted line). The powerful effect of the prismless layer and its rule in slowing sown caries evolution is clearly seen in the figure.

In the next simulation the geometry is similar to Example 2, but the boundary conditions now mimic a burst of localized low pH, say following meals, followed by a period of elevated pH that gives rise to remineralization.

Example 3: We use the same geometry as in Example 2 above, with the prismless enamel domain defined as $x_3 < \xi$. We set as before equilibrium boundary condition $w = 0$ at all boundaries except at the tooth surface $x_3 = 0$. There we set $w(x_1, x_3 = 0, t) = 10^{-4}$ on Σ for $0 < t < 0.2$, then $w(x_1, x_3 = 0, t) = -10^{-5}$ for $0.2 < t < 0.4$ and finally $w(x_1, x_3 = 0, t) = 0$ for $0.4 < t < 0.5$ to complete the cycle of about $8h$.

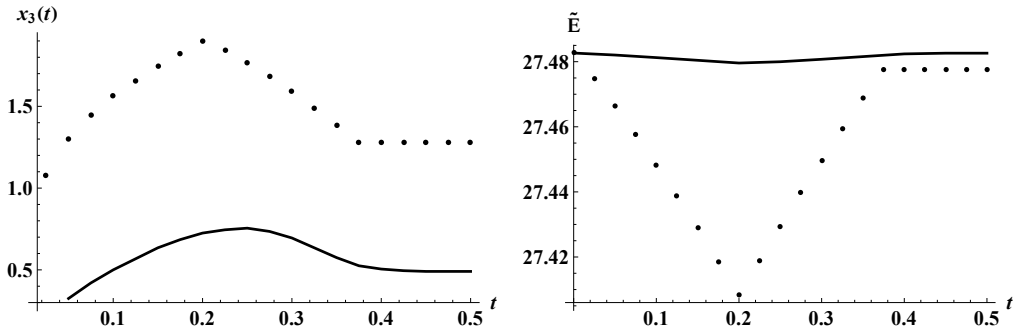

Figure 5.3: Progression of dental caries with and without the influence of the outer layer for the Example 3. (a) Progression of the tip of the level set of ρ (solid curve) of model (5.3), and the the tip of the same level set (dotted curve) for the model (5.3b)-(5.3c); (b) The evolution of the total enamel volume $\tilde{E}(t)$ for the models (5.3) (solid curve) and (5.3b)-(5.3c) (dotted curve).

Results: In Figure 5.3 we draw the evolution of the tip of level set $\rho = 0.898$ (solid line), compared with the evolution of the same level set when there is no prismless outer layer (dotted line). The effect of the prismless layer is transparent. We also notice that on the scale where the graph is drawn, there seems to be a delay in the initiation of the caries evolution due to the outer layer.

5.2 Simulations in a circular geometry

To simulate the model in a more realistic geometry, as sketched in Figure 5.4, we need in principle to construct a global system of curvilinear coordinates, and write the model in these coordinates. However, the formulation can be greatly simplified if we consider that

caries is, at least initially, a local process, and moreover, caries typically starts either near the occlusal surface or near the approximal surface (dotted regions in Figure 5.4). In both cases, we can work locally in a spherical geometry. To solve in a spherical geometry we rewrite the model equation for $w = H - c/\gamma$:

$$\partial_t(|\Omega|w) = \frac{1}{r^2}\partial_r\left(|\Omega|r^2\partial_r w\right) + \frac{1}{r^2\sin\theta}\partial_\theta\left(\bar{D}\sin\theta\partial_\theta\right)w + \frac{1}{r^2\sin^2\theta}\partial_\phi\left(\bar{D}\partial_\phi\right)w - (1+\gamma)|\partial E_p|R_1 w. \quad (5.4)$$

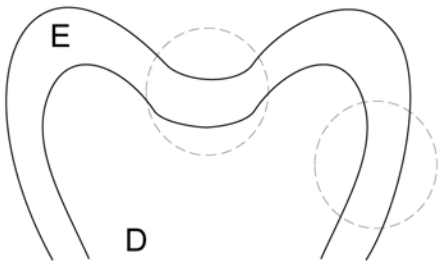

Figure 5.4: A sketch of realistic tooth geometry

As a further simplification, and also as another example of the model in a curvilinear geometry, we interpret the drawing in Figure 5.4 as a 2D sketch, and solve the equation in a polar coordinate framework. The equation for w takes the form

$$\partial_t(|\Omega|w) = \frac{1}{r}\partial_r(r|\Omega|\partial_r w) + \frac{1}{r^2}\partial_\theta\left(\bar{D}\partial_\theta\right)w - (1+\gamma)|\partial E_p|R_1 w. \quad (5.5)$$

We solve equation (5.5), together with the equation for ρ and using the formula for $|\Omega|$ and $|\partial E_p|$ in two setups. In both cases the geometry is an angular sector; see the sketch in Figure 5.4, Figure 5.5 and Figure 5.9.

$$G = \{(r,\theta) : r_1 < r < r_2, |\theta| < \beta\}. \quad (5.6)$$

Example 4: The purpose of this example is to simulate caries progress when it starts at an *occlusal surface*. The geometry is depicted in Figure 5.5. The boundary conditions are $w = 0$ at all the boundaries, except at the sector on Γ_1 defined by $\Gamma_s = \{(r,\theta)|\, r = r_1, |\theta| < \theta_0\}$, where $w(r_1,\theta,t) = \cdot 10^{-4}$. We use the parameters $r_1 = 1$, $r_2 = 3$, $\beta = \pi/4$, $\theta_0 = \pi/30$, $b\gamma = 3$ and $R_1 = 1$.

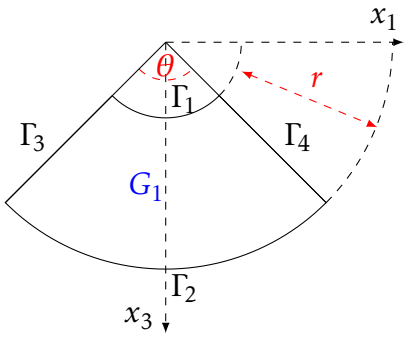

Figure 5.5: A sketch of circular sector describing the local region near an occlusal surface for the Example 4.

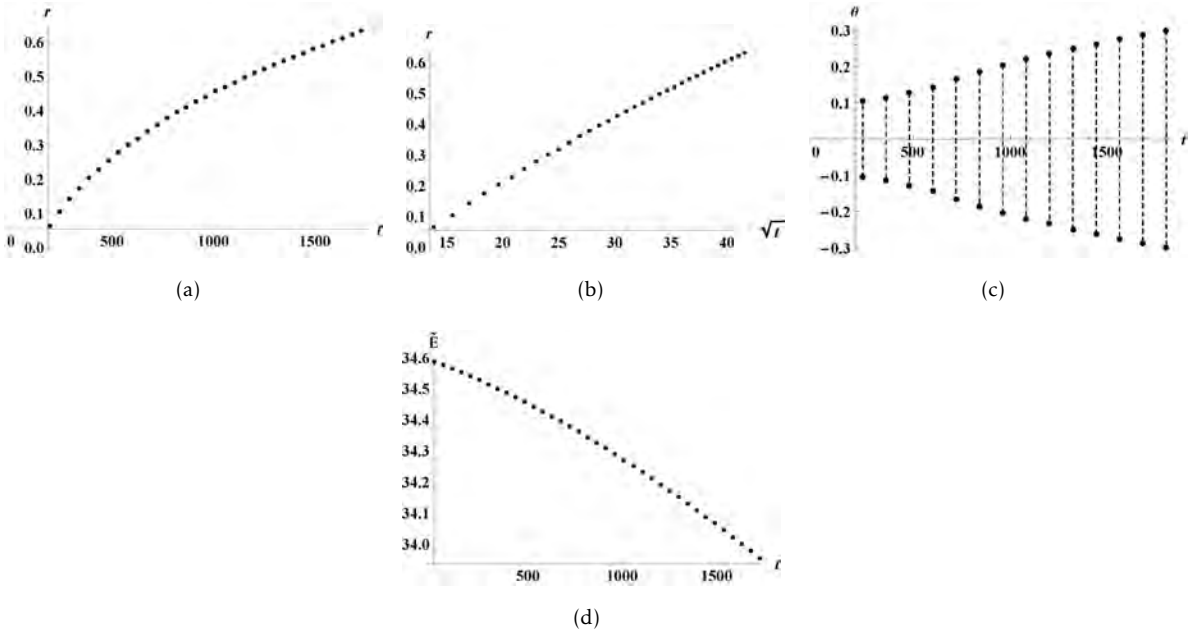

Figure 5.6: Progression of the tip of the level set $\rho = 0.86$ for the Example 4: (a) Motion of the tip of a level set. (b) Motion of the same level set as a function of $t^{1/2}$,(c) Width of the positive curve of the level set 0.86 in the angular θ direction, (d) The evolution of the total enamel volume $\tilde{E}(t)$.

Results: Just as in the previous example, we follow the motion $r(t)$ of the tip of a level set of ρ, as an indication of a visible lesion (Figure 5.6(a)), as well as the total amount of enamel $\tilde{E}$ (Figure 5.6(d)). The tip's evolution is also drawn as a function of $\sqrt{t}$ to examine the importance of the diffusion process in the caries progress. We also draw in Figure 5.6(c) the boundary of a given level set $\theta(t)$. These curves exhibit in a clear way the triangular shape of caries lesion that expands from a small area at an occlusal surface. In Figure 5.7 we draw a few snapshots of level sets of ρ at different times. Again, the triangular nature of the growing lesion is evident.

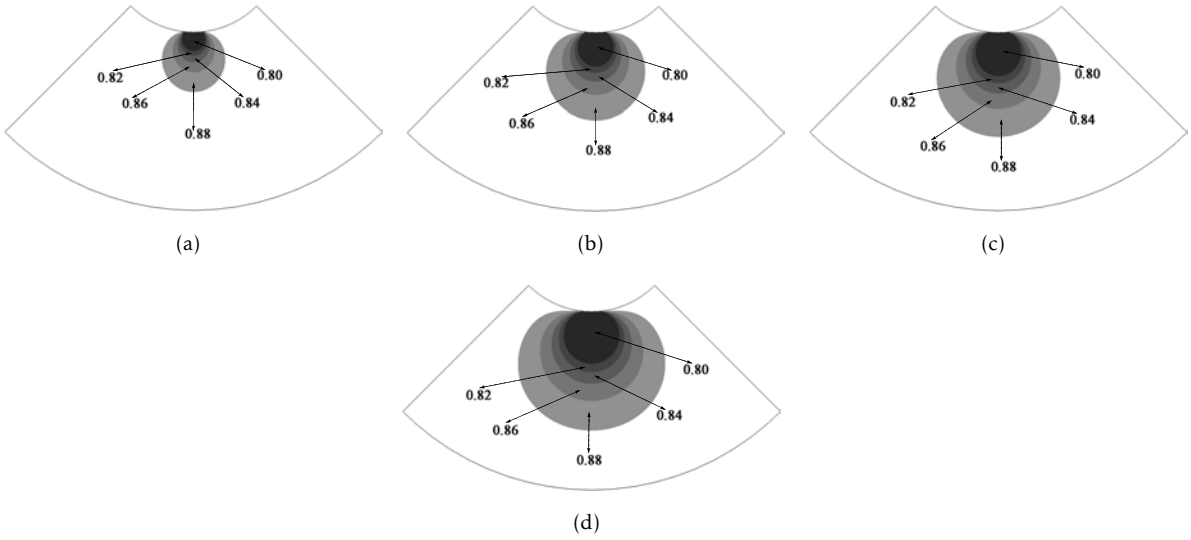

Figure 5.7: Four snapshots of the tooth decay progression calculated for the Example 4, described by level sets of $\rho(r,\theta,t)$ in the domain G_1: (a) t=960, (b) t=1800, (d) t=2400 ,(d) t=3000.

Example 5: There is a debate in the literature as to what is the actual rate of caries progression. Anderson et al. Anderson et al. (1998) cite a number of authors who argue that caries progresses as a linear function of $\sqrt{t}$. A typical result along this line is the paper of Poole et al. Poole et al. (1981). On the other hand, some authors, and in particular Anderson himself, provide experimental evidence that caries progresses linearly in t. The main argument in favor of the $\sqrt{t}$ progression rate is that caries is dominated by the diffusion of the hydrogen ions, and as is well-known, a particle undergoing Brownian motion propagates at this rate; alternatively, the diffusion equation has a similarity solution as a function of $x/\sqrt{t}$. However, this argument ignores the effect of the reaction term. Moreover, Stumpf and Porter (2012) recently warned against a tendency in life sciences to associate observations with power laws.

Indeed the curves depicted in Figure 5.1(b) and Figure 5.6(b) are not convincing that the lesion propagates at a rate proportional to $\sqrt{t}$. Also, we point our that if we measure caries progression not by the propagation of a level set of the enamel density, but by the total amount of enamel removed from the tooth, then the progression looks linear in t; see Figures 5.1(c) and 5.6(d).

To demonstrate the danger in such power laws, we simulated an additional example, where the evolution of the tip of a level set of ρ can be solved analytically. We use the same model and geometry as in Example 4 above, except that the boundary condition on the curve Γ_1 (defined by $r = r_1$) is now $w(r_1,\theta,t) = 10^{-4}\cos(2\theta)$. In light of the relatively slow enamel dissolution process we solve the equation for w at a fixed geometry where $\rho =$

0.98. At this extreme value of ρ we cannot use anymore the linear formula for $\bar{D}$. Instead we evaluated the effective diffusion coefficient by solving the cell problem introduced in the Chapter 4, the Appendix B, Fabregas and Rubinstein (2013) and found $\bar{D} = 0.25$. In addition we used the parameters $R_1 = 1/3$, $\gamma = 3$, $b = 1/3$.

For these choice of parameters the equations for w and ρ are approximately

$$\partial_t w = \frac{1}{r}\partial_r (r\partial_r w) + \frac{1}{4r^2}\partial^2_{\theta\theta} w - 4w, \quad \partial_t \rho = -w. \tag{5.7}$$

The function w reaches a steady state that can be solved explicitly:

$$w = 10^{-4}\frac{K_1(2r)}{K_1(2)}\cos(2\theta), \tag{5.8}$$

where K_1 is the modified Bessel functions of the second kind. It is convenient to define $\rho = \rho_0 + 10^{-4}\rho_1$ where for the parameters we used $\partial_t \rho_1 = -10^4 w$. Substituting the expression given by w in the equation (5.8) into the equation $\partial_t \rho_1 = -10^4 w$ and solving for ρ_1 at the tip, that as for $\theta = 0$, we obtain

$$\rho_1(r, 0, t) = -\frac{K_1(2r)}{K_1(2)}t. \tag{5.9}$$

It follows that the tip of the level set $\rho_1 = 10$ is given by the relation $t(r) = \frac{K_1(2)}{K_1(2r)}10$.

Results: We use the formula for $t(r)$ to draw the theoretical inverse curve $r(t)$ in Figure 5.8(c). This curve can now be compared to the numerical solution $r(t)$ given in Figure 5.8(a), and the curve $r(\sqrt{t})$ depicted in Figure 5.8(b). It is clear from these curves that the $\sqrt{t}$ is not a correct power law.

Example 6: A sketch of the local coordinate frame is depicted in Figure 5.9. The boundary conditions are $w = 0$ at all the boundaries, except at the sector on Γ_2 defined by $\Gamma_s = \{(r, \theta) | r = r_2, |\theta| < \theta_0\}$, where $w(r_2, \theta, t) = 10^{-4}$. We use the parameters $r_1 = 1$, $r_2 = 3$, $\beta = \pi/4$, $\theta_0 = \pi/30$, $b\gamma = 3$ and $R_1 = 1$.

Results: Similarly to Examples 1 and 2 above we follow the caries progress by drawing (Figure 5.10(a)) the function $r(t)$ the tip of the level set $\rho = 0.86$, and (Figure 5.10(c)) the function $\tilde{E}(t)$ which is the total volume of enamel. In Figure 5.10(b) we draw the width of a given level set. An inverted triangular shape, can be observed at this graph, although it is not as transparent as the triangular shape of a lesion starting from an occlusal surface (Figure 5.6(c)).

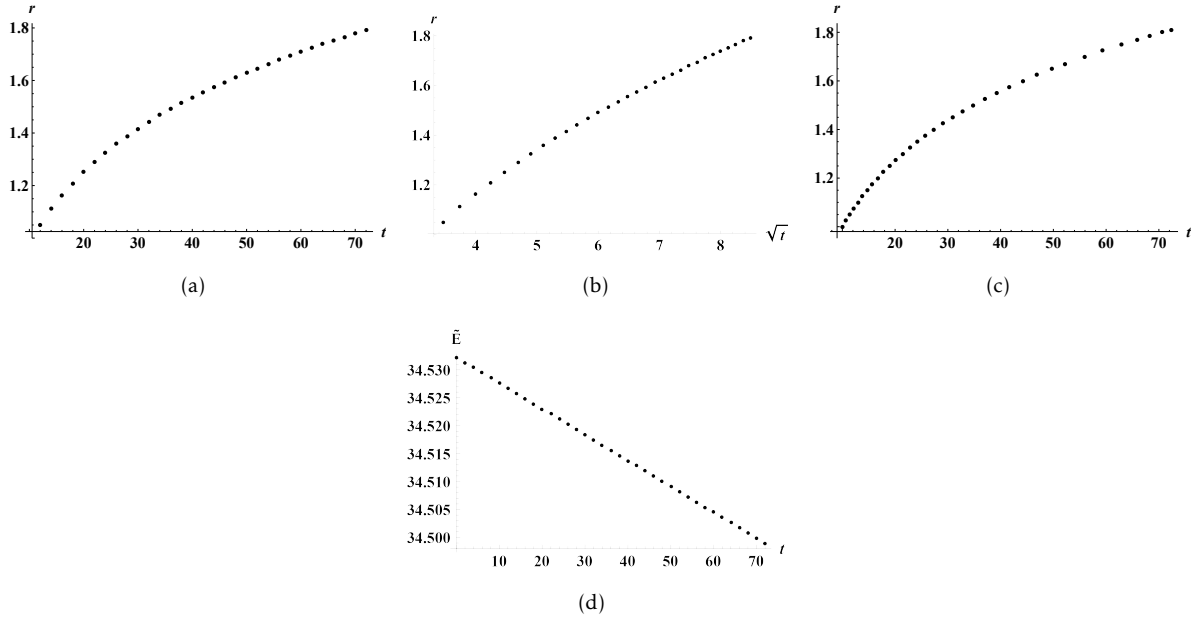

Figure 5.8: Progression of the tip of a level set $\rho_1 = -10$: (a) Motion of the tip of a level set. (b) Motion of the same level set as a function of $t^{1/2}$,(c) The theoretical curve for the motion of the level set tip, (d) The evolution of the total enamel volume $\tilde{E}(t)$.

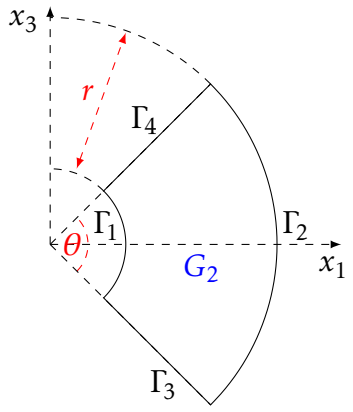

Figure 5.9: A sketch of circular sector describing the local region near an approximal surface for the Example 6.

5.3 Discussion

A three dimensional model for the initial evolution of dental caries was presented. The model takes into account the diffusion of two main compounds, the hydrogen ions and the calcium ions, and the reaction at the surface of the enamel prisms.

We first simulated the equations in a rectangular geometry, where system (5.3) is considerably simpler. In addition, we showed how our basic model can be augmented to include the outer prismless layer of enamel. The extended equations model this layer as

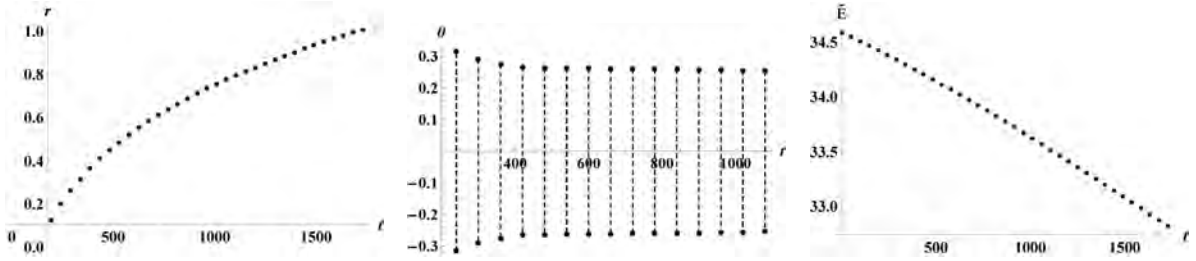

(a) (b) (c)

Figure 5.10: Progression of the tip and "positive curvature of the tooth" (width) of fixed level set $\rho = 0.86$ corresponding to the Example 6: (a) Motion of the tip of a level set of ρ, (b) Width of the level set 0.86, (c) The evolution of the total enamel volume $\tilde{E}(t)$.

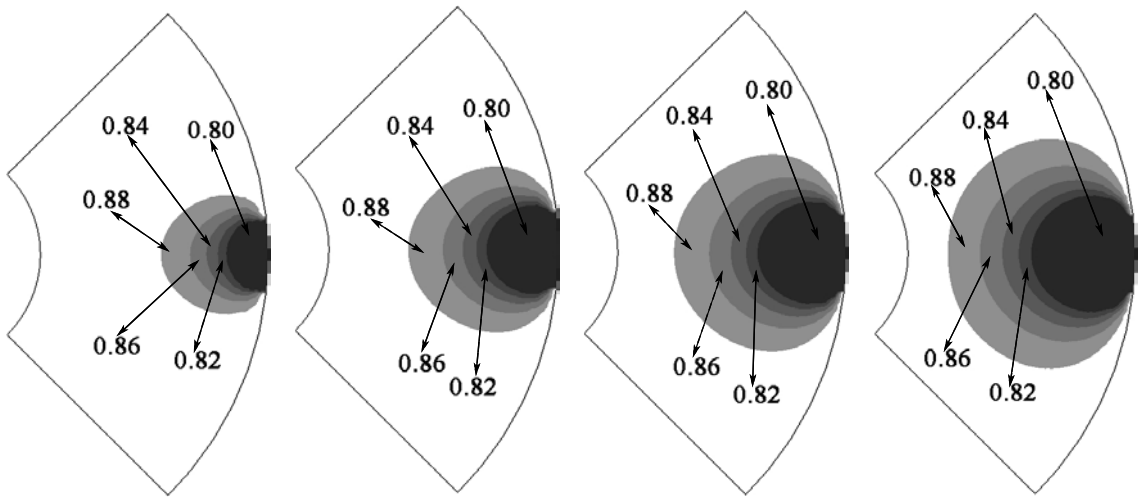

(a) (b) (c) (d)

Figure 5.11: Four snapshots of the tooth decay progression for the Example 4, described by level sets of $\rho(r, \theta, t)$ on the domain G_2.

a thin domain with isotropic diffusion matrix that is resistive to dissolution relating to bulk enamel. The presence of even a very thin such layer is shown to considerably reduce the progress of caries. In addition this model explains qualitatively graph 4 of reference Anderson et al. (1998).

We then presented two simulations in a circular (spherical) geometry, that is adequate for most initial forms of caries. In our simulations we emphasized two alternative ways of quantifying caries evolution: First by visual inspection, that we model by following a level set of the prism density distribution, and second by measuring the total volume of enamel. The simulations performed above in circular geometry model caries progress near an occlusal surface and near an approximal surface. In both cases our model captures the well-known triangular shape of the global caries lesion. Additionally, one more time,

but, in a realistic geometry, we showed that the $t^{1/2}$ power law, proposed by a number of authors, is questionable. In fact, no clear power law can be written down, which gives support to the view expressed recently in Stumpf and Porter (2012).

We point out that modeling the progress of caries by following c, H and ρ enables direct correlation of the model with experiments. The importance of the hydrogen ions concentration H is evident. The concentration of the calcium ions c is useful since measuring the flux of the calcium ions leaving the tooth is a good indication of the amount of dissolved enamel. Another criterion for caries is the formation of observable lesions, and this can be correlated with the value of ρ.

Chapter 6

Conclusions

A new model for the initial progression of dental caries lesions has been presented. Started from a model for the microscopic geometry. The local reaction diffusion equations are homogenized, while taking into account the change of the geometry in space and time because of the dissolution of the enamel. The global macroscopic equations include features such as anisotropic diffusion, resulting from the local geometry, an effective reaction term, and an equation for the evolution of the geometry. The equations are nonlinear due to the mutual coupling of the reaction-diffusion and the geometry.

Enamel dissolves into a number of substances. In order to simplify the present model, we followed just one of them, say Ca^{2+} ions. Thus, our model consists of equations for the evolution of the hydrogen and calcium ions under different external (acidity) conditions. We further assumed for simplicity that the equilibrium density of the calcium ions is proportional to the concentration of the hydrogen ions. A more elaborate model that takes into account all the dissolved components, more precise balance equations, and more precise diffusion coefficients, can be derived along similar lines.

Since the microgeometry of the enamel is inherently anisotropic, and since the its main axes depend on the tooth boundary, the equations should in general be written down in curvilinear coordinates. In a general tooth geometry we define orthogonal curvilinear coordinates where each point is given as $\mathbf{q}(y_1, y_2, y_3)$, such that the prism long axis is aligned along the y_3 coordinate. The metric coefficients are defined by $h_i = |\partial_{y_i}\mathbf{q}|$. It is also convenient to define the diagonal matrix D whose diagonal is $(d(\rho), d(\rho), |\Omega|)$. In this general coordinate system our 3D reduced model is

$$\partial_t(|\Omega|w) = \frac{1}{h_1 h_2 h_3}\sum_i \partial_{y_i}\left(\frac{h_1 h_2 h_3}{h_i^2} D_{ii}\partial_{y_i} w\right) - (1+\gamma)|\partial E_p| R_1 w, \tag{6.1}$$

together with the equation for the evolution of ρ:

$$\partial_t \rho = -b\gamma R_1 w. \tag{6.2}$$

A brief summary of our work is given below. In Chapter 1, we reviewed the mathematical models of Zimmerman's a and Patel's for the progression of the tooth decay. These models are in one-dimensional space and thus the anisotropy plays no role, but, they are the initial inspiration of this work. The models differ in the level of complexity and details of the reaction. Chapter 2 studied the basic procedure of the homogenization method for partial differential equations and the domain decomposition methods. In the case of the homogenization method, we described the basic procedure and the procedure for a periodic medium with obstacles. On the other hand, we examined the methods additive and multiplicative of Schwarz for overlapping domains and in addition for the no-overlapping domains we presented a family of iterative methods, namely, the Dirichlet-Neumann method, the Neumann-Neumann method and Lions's method in order to solve the framework of Steklov-Poincaré. The Chapter 3 starts describing the values of the parameters gotten from in vitro or in vivo experiments in order to fixing the proper nondimensional variables. In consequence, setting out the local model and applying the homogenization method, we can deduce the macroscopic model taking into account the inclusion of a changing geometry and an anisotropic diffusion. Later on, was deduced a relationship between the macroscopic model and the evolution microstructure in order, in other words, we coupled the effective reaction diffusion equation to the enamel dissolution process. Finally, we added the outer layer of enamel to the model getting a new version of the model. Chapter 4 and Chapter 5 have implemented a number of simulations for illustrate the procedure to calculate the anisotropic diffusion; bring some light to the results exposed by Anderson et al. (1998); Bollet-Quivogne et al. (2005) and Poole et al. (1981) in its experiments about the existence of a power law for the progression of dental caries; verifying and explaining the powerful influence of the outer layer of enamel and finally, confirming the conjecture proposed by Bjrndal and Thylstrup (1995) about the triangular pattern of shape for the in vivo tooth decay propagation.

The model presented here still contains a few undetermined parameters, such as b, R_1 and γ. They can be estimated by matching the model to experiments. Then the model can be used to predict outcomes of new experiments, and in general for *in silico* tests of different aspects of dental caries.

Chapter 7

Future approaches

There are a number of ways in which the model can be further extended. One is to improve the understanding of boundary conditions. Another extension, is to consider separate reaction diffusion equation for the different compounds in the reaction. Furthermore, adding compounds such as fluoride to the model will enable applying the model to study medical treatments for arresting caries. We are indeed working on upgrading our model in these directions.

On the other hand, and just recalling the family of hard tissues in the human body anatomy, the tooth is one of the hardest tissue of the human body and is included in the family of human bones. Therefore, the question is: Can we extend the model of Fabregas and Rubinstein (2013) to other processes of de/remineralization, for example, bone remodeling process?

7.1 Cate's fluoride paradox

At the present time, in the in vitro remineralization direction the work of Cate's 97 ten Cate (1997) is consider one of the most important experiments. Cate's 97 analyzes many experiments on fluoride effect.

One idea was that fluoride reacts with the dissolved components of hydroxyapatite to create fluorapatite (see Figure 7.1), and that fluorapatite is resistant to caries and therefore this prevents caries formation.

This idea was refuted in the experiments where shark tooth, that are made fully of fluorapatite are subjected to the same pH conditions as human tooth, and compared also to human tooth treated with fluoride rinse. The experiments showed the mineral loss of the shark tooth was smaller than the human tooth by about a factor of 2, but a human

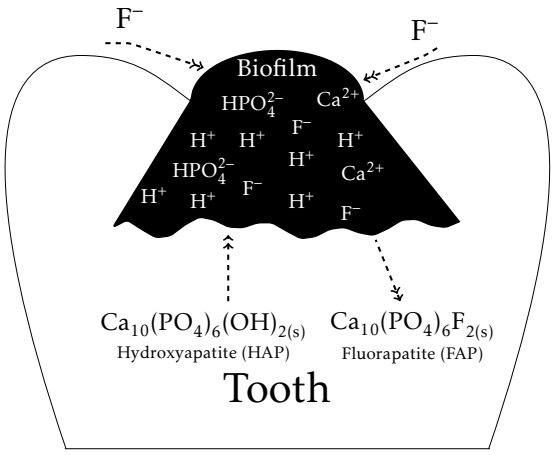

Figure 7.1: A sketch of the demineralization process adding the fluoride.

tooth rinsed with some fluoride had even smaller amount of loss. Therefore, the mere presence of fluorapatite is not the cause for the reduction of caries by fluoride.

A reasonable theory suggested by Cate is: Assume typical pH conditions, say pH about 5. Then hydroxyapatite is dissolved (but fluorapatite not). The calcium of phosphate thus released react with the small amount of fluoride supplied, say by rinse and toothpaste. They create fluorapatite. This has two effects: First, the dissolved minerals are not lost (by diffusion out of the tooth) as would have happened if they would not have reacted. Second, stable hard fluorapatite is created, and this is a replacement to hydroxyapatite.

In our opinion this theory means that fluoride has three effects:

1. First, it prevent mineral loss. This means that it is relevant to demineralization.
2. It also creates new crystals, and in this way it acts as some sort of remineralization.
3. Fluorapatite is more resilient to caries as the shark's data shows in Cate's 97, ten Cate (1997).

Furthermore, adding compounds such as fluoride to the model will enable applying the model to study medical treatments for arresting caries. Therefore, the most interesting challenge for our model should be the study of the progression of caries when the fluoride is adding into the reaction equation.

7.2 Bone-remodeling

Bone remodeling is the process executed by cells called osteoclast and osteoblast necessary for the bone growth. This process is divided into two sub-process called as bone resorption

where the hard tissue is removed from the skeleton and ossification where a new hard tissue is formed (see Figure 7.2).

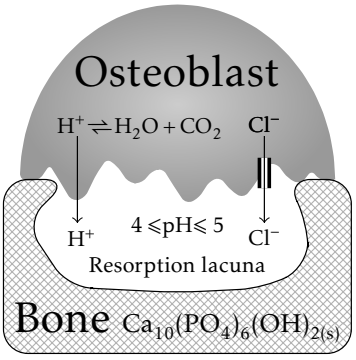

Figure 7.2: A sketch of the bone resorption process.

There is a long history of mathematical models applied to the bone-remodeling process (see Herrero and López (2005); Martin (1994); Rouhi and Herzog (2007); Silva and Ulm (2002)), but, just a few of them take into account a molecular point of view as starting point Martin (1994); Rouhi and Herzog (2007); Silva and Ulm (2002).

There is few papers with the explicit stoichiometric chemical equations describing the resorption-ossification process, but, definitely it is well known the fact of releasing various products such as calcium (Ca_2^+), phosphoric acid (H_3PO_4), etc., from dissolved osseous matrix. This leads to a reaction of the solid (mineral) enamel according to Rouhi and Herzog (2007); Silva and Ulm (2002)

$$\underset{\text{Hydroxyapatite}}{Ca_{10}(PO_4)_6(OH)_{2(s)}} + 2\,H^+_{(aq)} \underset{k_{-1}}{\overset{k_1}{\rightleftharpoons}} 10\,Ca^{2+}_{(aq)} + 6\,PO^{3-}_{4(aq)} + 2\,H_2O_{(l)} \tag{7.1}$$

In addition, with the opposite function, the osteblasts mediate in the synthesization of a new osseous matrix which is added to the pre-existing, i.e., reversing the reaction (7.1).

The processes of bone remodeling and tooth decay have different origin, but, both physiological process share the same first sub-process of demineralization in a solution under a specificity *pH* low, independently of the agents that mediate (Osteoclast, bacteria, etc) Ehrlich and Pokrovsky (2008). Therefore, putting particular attention to the work of Martin (1994) and the structure of the osseous matrix, a possible extension of the model of Fabregas and Rubinstein (2013) can be assembled.

Appendix A

Proof of some geometric formulae

We prove in this appendix some of the geometric formula we used earlier in deriving the averaged equation of the concentration c.

To prove formula (3.6) for the normal $\hat{n}$ we recall that F changes along the x_3-axis slower than along the x_1, x_2-axes. Thus, we write

$$\hat{n} = \alpha\left(\partial_{y_1}F + \varepsilon\partial_{x_1}F, \partial_{y_2}F + \varepsilon\partial_{x_2}F, \varepsilon\partial_{x_3}F\right),$$

where α is a factor chosen so $\hat{n}$ has unit norm. Retaining terms up to $O(\varepsilon)$ we obtain

$$\alpha = 1/G_F\left(1 - \varepsilon\nabla_2^y F \cdot \nabla_2^x F/G_F^2\right),$$

where G_F was defined in equation (3.7). Therefore, recalling the notation $\hat{\nu}$ for a unit vector to the boundary in the two dimensional cross section, we can write

$$\hat{n} = \hat{\nu} + \varepsilon/G_F\left(\nabla_2^x F - \hat{\nu}(\hat{\nu}\cdot\nabla_2^x F) + \hat{k}F_{x_3}\right).$$

Formula (3.6) follows from the last identity.

To prove the first formula of (3.22) we observe that the volume of Ω is $|\Omega| = 1 - |E_p|$, can also be written as as

$$|\Omega| = (1 - \int_{cell}\chi_{E_p}\,dy),$$

where χ_{E_p} is the characteristic function of E_p. We then notice the relation $\partial_t\chi_{E_p} = \delta(x - \partial E_p)v_\nu$. Substituting the last relation into the equation

$$\partial_t|\Omega| = -\int_{cell}\partial_t\chi_{E_p}\,dy \tag{A.1}$$

leads to the first formula of (3.22).

The second identity of equation (3.22) and identity (3.19) follow from the following general argument: Let θ be any of the arguments (x_1, x_2, x_3) of the function F introduced in equation (3.5). To emphasize that we concentrate on this argument we write

$$\partial E_p(\theta) : \{F(y_1, y_2, \theta) = 0\}.$$

We now show that

$$\frac{\partial}{\partial \theta}|E_p| = -\int_{\partial E_p} \partial_\theta F / G_F. \tag{A.2}$$

To find the change in the area of E_p as we vary the parameter θ we need to find the area of ring between $E_p(\theta)$ and $E_p(\theta + d\theta)$. To find the thickness of the ring we move a distance δ along the normal ν in the (y_1, y_2) plane. To determine δ we expand the relation $F(y_1 + \delta \partial_{y_1} F/G_F, y_2 + \delta \partial_{y_2} F/G_F, \theta + d\theta) = 0$. Using also $F(y_1, y_2, \theta) = 0$ we obtain $\delta = -\partial_\theta F d\theta / G_F$. Therefore $d\delta/d\theta = -\partial_\theta F/G_F$. This proves (A.2)

The same arguments that were used above to prove identity (A.2) can be applied to prove the more general identity

$$\nabla_2^x \int_\Omega g \, dy = \int_\Omega \nabla_2^x g \, dy - \int_{\partial E_p} (\nabla_2^x F/G_F)\, g, \tag{A.3}$$

for any (smooth) function $g(x_1, x_2, x_3, y_1, y_2)$. This identity was used in section 3 to derive formula (3.19).

Appendix B

Numerical schemes and Domain Decomposition Algorithm

In this Chapter we write the abstract weak (variational) formulation used for solving the system in rectangular coordinates (4.1) and spherical coordinates (5.5) applying the finite element method.

First, we find the solution to the so-called cell-problem. As second and third analysis, we carry out the methodology in order to transform the general systems in cartesian coordinates (4.1) and polar coordinates (5.5) in a full discrete schemes, i.e., in matrix form. In addition, we show up how good they are the proposed solutions analysing the L^2-error between the proposed solutions (4.5) and (5.8) with an exponential decay and the each corresponding numerical solution.

On the other hand, to present the finite element method in a general formulation, we need to use function spaces, particularly, we will denote to $\mathcal{V}_0$, $\mathcal{V}_\Omega$, $\mathcal{V}_V$, $\mathcal{V}_G$ as Sobolev spaces, where $\Omega, V, G \subset \mathbb{R}^2$ are bounded domains. In correspondence with each Sobolev space, we consider the inner products

$$\langle u, \varphi \rangle_\Omega = \int_\Omega u(y)\varphi(y)\, dy, \qquad \langle u, \varphi \rangle_V = \int_V u(x)\varphi(x)\, dx, \tag{B.1a}$$

$$\langle u, \varphi \rangle_G = \int_G u(r,\theta)\varphi(r,\theta)\, r\, dr\, d\theta, \tag{B.1b}$$

where $x = (x_1, x_2, x_3)$, (r, θ) are the macroscopic coordinates and $y = (y_1, y_2)$ are the microscopic coordinates, taking into account the polar transformation $x_1 = r\cos(\theta)$ and $x_3 = r\sin(\theta)$, and the Jacobian r into the inner product.

B.0.1 Numerical solution for the cell problem

To solve the homogenized model proposal in Proposition 3.2, and subsequently the examples of the Chapters above, first, the effective diffusion matrix $\bar{D}$ needs to be calculated as is explain in Chapter 4, Section 4.2.1,

$$\bar{D}_{ij} = |\Omega|\delta_{ij} + \int_{\Omega} W^j_{y_i}\, dy, \tag{B.2}$$

but, this required finding the *cell functions* W^i solving the well-known *cell problem*

$$\Delta_2^y W^i = 0, \quad y \in \Omega, \tag{B.3a}$$

$$\hat{\nu} \cdot \nabla_2^y W^i = -\hat{\nu}_i, \quad y \in \partial E_p, \tag{B.3b}$$

with periodic boundary conditions or bi-periodic boundary conditions on the outer boundary of cell Ω where $\hat{\nu}_i$ denotes the i-th component of ν_i.

The numerical solution of the cell problem has been pursued by many authors Bensoussan et al. (2011); Bourgat (1979); Bourgat and Dervieux (1978); Hornung (1997); Keller (1963), etc, and the main numerical difficulty is the periodic boundary condition, because, frequently the periodic boundary conditions are not available in usual numerical codes. One alternative, is to consider appropriate symmetry conditions, in order to replace the periodic boundary condition by a simpler combination of Dirichlet and Neumann conditions or considering the so-called *Bloch wave method* Conca et al. (2001, 2002). Fortunately for us, we considered the programming language FreeFem++ Hecht et al. (2012) which has a comfortable environment for adding the periodic boundary conditions.

Additionally, for our cell problem the shape of the enamel E_p evolves in space and time, therefore, we need to solve the cell problem for each time iteration and at all space points (on the x scale). To simplify this task, and since the local prism changes slowly in space on its local y scale, we assume that the enamel motion is averaged, in the sense that the dissolution reaction is approximately uniform over the prism's boundary. This implies that the boundary ∂E_p moves normal to itself, and therefore the shape E_p forms a one-dimensional family of domains. The matrix $\bar{D}$ can be computed for a number of representative shapes from this family, and then the value of $\bar{D}$ for an actual shape can be determined by interpolation from the computed family. Multiplying (B.3) by a test function φ, integrating by part and considering the Neumann boundary condition, we get

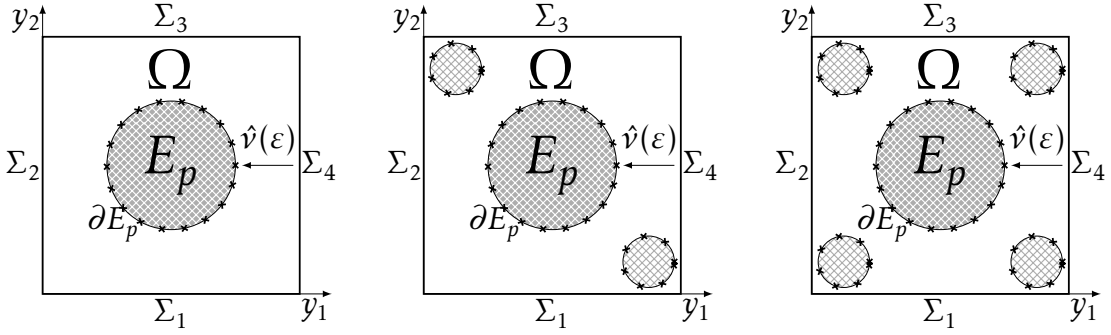

Figure B.1: Examples for the periodic cell cross sections: (a) Local periodic cell containing one prism, (b) Local periodic cell containing 3 prisms, (c) Local periodic cell containing 5 prisms.

the variational formulation for (B.3): Find

$$W^i \in \mathcal{V}_\Omega := \left\{ \varphi \in H^1(\Omega) : \varphi|_{\Sigma_1} = \varphi|_{\Sigma_3} \text{ and } \varphi|_{\Sigma_2} = \varphi|_{\Sigma_4} \right\}, \tag{B.4}$$

such that

$$\left\langle \nabla_2^y W^i, \nabla_2^y \varphi \right\rangle_\Omega + \int_{\partial E_p} \hat{v}_i \, \varphi \, d\partial E_p = 0, \tag{B.5}$$

where Σ_i for $i = 1, 2, 3, 4$ are the boundaries of the cell.

Now, writing W^i as a linear combination of the basis $\{\varphi_s\}_s^N$ and discretizing the test space setting out $\varphi = \varphi_j$ we arrive to the following scheme

Proposition B.1. *The numerical scheme for the equation* (B.5) *can be set out in a matrix form*

$$\mathbf{A}\hat{W}^i + \mathbf{B} = 0 \tag{B.6}$$

where the square matrix of order $N \times N$ $\mathbf{A}$, $\mathbf{B}$ *and the vectors* $\hat{W}^i$ *has the expressions*

$$\mathbf{A} = \left\langle \nabla_2^y \varphi_s, \nabla_2^y \varphi_j \right\rangle_\Omega, \quad \mathbf{B} = \int_{\partial E_p} \hat{v}_s \, \varphi_j \, d\partial E_p, \quad \hat{W}^i = \left\{ W_1^i, \ldots, W_N^i \right\}$$

for $s, j = 1, \ldots, N$ *and* $i = 1, 2$.

B.0.2 Scheme in Cartesian Coordinates

Calculated an analytical approximation for the effective diffusion coefficient $\bar{D}(\rho) = d(\rho)I$, we can proceed to solving the equation (B.2) into the domain

$$V = \left\{(x_1, x_3) \in \mathbb{R}^2 : |x_1| < 1, 1 < x_3 < 3\right\}, \tag{B.7}$$

see Figure B.2, and boundaries

$$\Gamma_1 = \{x \in \mathbb{R}^2 : |x_1| < 1\, x_3 = 0\}, \quad \Gamma_2 = \{x \in \mathbb{R}^2 : x_1 = 1, 0 < x_3 < 3\}, \tag{B.8}$$

$$\Gamma_3 = \{x \in \mathbb{R}^2 : |x_1| < 1\, x_3 = 3\}, \quad \Gamma_4 = \{x \in \mathbb{R}^2 : x_1 = -1, 0 < x_3 < 3\}, \tag{B.9}$$

see Figure B.2. Additionally, take into account that the functions $|\Omega| = |\bar{\Omega}| - \pi\rho$, $\bar{D} = a_1 - a_2\rho$, $|\partial E_p| = 2\pi\rho$ are sufficiently good with a_1, a_2, R_1 not negative constants and $b \neq 0$, we can rewrite the equations (B.2) and (B.2) in a better form in order to apply the finite element method

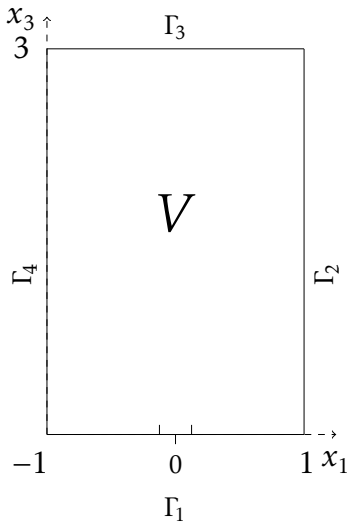

Figure B.2: The domain V where the homogenized equations are solved and definition of the boundary geometries Γ_1, Γ_2, Γ_3 and Γ_4.

$$|\Omega|\partial_t w = \partial_{x_1}\left(d\partial_{x_1} w\right) + \partial_{x_3}\left(|\Omega|\partial_{x_3} w\right) + |\partial E_p|(bw - R_1)\, w, \qquad \text{in } V \times (0,T) \tag{B.10a}$$

$$\partial_t \rho = bw, \qquad \text{in } V \times (0,T) \tag{B.10b}$$

$$w|_{\Gamma_1} = g(x_1), \quad w|_{\Gamma_{2,3,4}} = 0 \qquad \text{in } (0,T) \tag{B.10c}$$

$$w(x,0) = w_0(x), \qquad \text{in } V \tag{B.10d}$$

$$\rho(x,0) = \rho_0(x) \qquad \text{in } V \tag{B.10e}$$

where $T = \mathcal{O}(1)$.

Multiplying (B.10a), (B.10b), (B.10d) and (B.10e) by a test function $\varphi \in \mathcal{V}_0$ where

$$\mathcal{V}_0 := \left\{ \varphi \in H^1(V) : \varphi|_{\Gamma_i} = 0 \right\}, \tag{B.11}$$

for all $i = 1, \ldots, 4$ and then integrating over the domain V leads to a variational formulation. Additionally, integrating by parts the equations (B.10a), (B.10b) and using the boundary conditions, the problem (B.10) can be written in the variational form: Find $w : (0, T) \to \mathcal{V}_V$ such that

$$\langle |\Omega| \partial_t w, \varphi \rangle + \langle \nabla w, \nabla \varphi \rangle = F(\rho, w), \qquad \forall \varphi \in \mathcal{V}_0, t \in (0, T) \tag{B.12a}$$

$$\langle \partial_t \rho, \varphi \rangle = \langle bw, \varphi \rangle, \qquad \forall \varphi \in \mathcal{V}_0, t \in (0, T) \tag{B.12b}$$

$$\langle w(x, 0), \varphi \rangle = \langle w_0(x), \varphi \rangle, \qquad \forall \varphi \in \mathcal{V}_0 \tag{B.12c}$$

$$\langle \rho(x, 0), \varphi \rangle = \langle \rho_0(x), \varphi \rangle \qquad \forall \varphi \in \mathcal{V}_0 \tag{B.12d}$$

where $F(\rho, w) = \left\langle |\partial E_p| (bw - R_1) w, \varphi \right\rangle$ and $\nabla = \bar{D}^{1/2} \partial_{x_1} \hat{e}_1 + |\Omega|^{1/2} \partial_{x_3} \hat{e}_3$ denotes the gradient of the scalar field w treating x_1 and x_3 as ordinary cartesian coordinates and defining

$$\mathcal{V}_V := \left\{ \varphi \in H^1(V) : \varphi|_{\Gamma_1} = g(x_1) \text{in}, L^2(V) \right\} \tag{B.13}$$

as a Sobolev sub-space.

Let $\mathcal{V}_V^h$ be a finite element subspace of $\mathcal{V}_V$ and replacing $\mathcal{V}_V$ in (B.12) by $\mathcal{V}_V^h$, we have the finite element method: Find $w_h : (0, T] \longrightarrow \mathcal{V}_V^h$ such that

$$\langle |\Omega|_h \partial_t w_h, \varphi \rangle + \langle \nabla_h w_h, \nabla_h \varphi \rangle = F(\rho_h, w_h), \qquad \forall \varphi \in \mathcal{V}_0^h, t \in (0, T) \tag{B.14a}$$

$$\langle \partial_t \rho, \varphi \rangle = \langle bw, \varphi \rangle, \qquad \forall \varphi \in \mathcal{V}_0^h, t \in (0, T), \tag{B.14b}$$

$$\langle w(\cdot, 0), \varphi \rangle = \langle w_0, \varphi \rangle, \qquad \forall \varphi \in \mathcal{V}_0^h, \tag{B.14c}$$

$$\langle \rho(\cdot, 0), \varphi \langle = \langle \rho_0, \varphi \rangle \qquad \forall \varphi \in \mathcal{V}_0^h, \tag{B.14d}$$

where

$$\nabla_h = |\Omega|_h^{1/2} \partial_{x_3} \hat{e}_3 + \bar{D}_h^{1/2} \partial_{x_1} \hat{e}_1, \qquad F(\rho_h, w_h) = \left\langle |\partial E_p|_h (bw_h - R_1) w_h, \varphi \right\rangle, \tag{B.15}$$

with

$$|\Omega|_h = |\bar{\Omega}| - \pi \rho_h^2, \quad |\partial E_p|_h = 2\pi \rho_h, \quad \bar{D}_h = a_1 - a_2 \rho_h. \tag{B.16}$$

The system (B.14) are discretized in space, but continuous in time. Hence, if $\{\varphi_i(\hat{x})\}_i^N$ is a base of the vectorial space $\mathcal{V}_h^0$ we can expressing w_h, ρ_h as

$$w_h = \sum_{i=1}^{N} w_i(t)\varphi_i(\hat{x}), \qquad \rho_h = \sum_{i=1}^{N} \rho_i(t)\varphi_i(\hat{x}). \tag{B.17}$$

Therefore, for $j = 1,\dots,N$, we take $\varphi = \varphi_j$ in (B.14) and utilize (B.17) to see that, for $t \in (0,T)$

$$\mathbf{B}(\hat{\rho})\frac{d\hat{w}}{dt} + \mathbf{A}(\hat{\rho})\hat{w} = \mathbf{F}(\hat{\rho},\hat{w}), \qquad t \in (0,T), \tag{B.18a}$$

$$\mathbf{M}\frac{d\hat{\rho}}{dt} = b\mathbf{M}\hat{w}, \qquad t \in (0,T), \tag{B.18b}$$

$$\mathbf{M}\hat{w}(0) = \hat{w}_0, \tag{B.18c}$$

$$\mathbf{M}\hat{\rho}(0) = \hat{\rho}_0 \tag{B.18d}$$

where the $N \times N$ matrices $\mathbf{M}$, $\mathbf{A}$, $\mathbf{B}$, $\mathbf{F}$ and the vectors $\hat{w}$, $\hat{\rho}$, $\hat{w}_0$ and $\hat{\rho}_0$ using the equations (B.16) are

$$\mathbf{M} = \langle \varphi_i, \varphi_j \rangle, \qquad \mathbf{B} = \left\langle \left(4 - \pi \left(\sum_{s=1}^{N} \rho_s \varphi_s \right)^2 \right) \varphi_i, \varphi_j \right\rangle, \tag{B.19a}$$

$$\mathbf{A} = \langle \nabla_h \varphi_i, \nabla_h \varphi_j \rangle, \quad \mathbf{F}(\hat{\rho},\hat{w}) = 2\pi \left\langle \left(\sum_{s=1}^{N} \rho_s \varphi_s \right) \left(b \left(\sum_{s=1}^{N} w_s \varphi_s \right) - R_1 \right) \varphi_i, \varphi_j \right\rangle w_i, \tag{B.19b}$$

$$\hat{w} = (w_1, w_2, \dots, w_N)^T, \quad \hat{\rho} = (\rho_1, \rho_2, \dots, \rho_N)^T, \quad \hat{w}_0 = (w_0, \varphi_j), \quad \hat{\rho}_0 = (\rho_0, \varphi_j) \tag{B.19c}$$

with

$$\nabla_h = \left(a_1 - a_2 \sum_{i=1}^{N} \rho_i \varphi_i \right)^{1/2} \partial_{x_1} \hat{e}_1 + \left(|\bar{\Omega}| - \pi \left(\sum_{i=1}^{N} \rho_i \varphi_i \right)^2 \right)^{1/2} \partial_{x_3} \hat{e}_3 \tag{B.20}$$

for $i, j, s = 1, 2, \dots, N$.

At the last analysis, we are going to transform the matrix formulation (B.18) to a full-discreet problem considering $n+1$ points equispaced $t_k = k\tau$, where $k = 0, \dots, n$, $\tau = T/n$ and $n \in \mathbb{N}$. First, for each index k and $k+1$ we approximate the temporary derivative of w in the points (t_k) and (t_{k+1}) for an incremental average between the finite-difference progressive and regressive quotient, e.g., writing the system (B.18) in the instants t_k and t_{k+1}, using the notation $\hat{w}^k = \hat{w}(t_k)$, $\hat{w}^{k+1} = \hat{w}(t_{k+1})$ and $\mathbf{B}^k = \mathbf{B}(\hat{\rho}^k)$, $\mathbf{B}^{k+1} = \mathbf{B}(\hat{\rho}^{k+1})$, $\mathbf{A}^k = \mathbf{A}(\hat{\rho}^k)$, etc.,

and considering the finite difference operators δ_t and δ_t^ϑ which are introduce through the definitions

$$\delta_t(z) = z^{k+1} - z^k \quad \text{and} \quad \delta_t^\vartheta(z) = \vartheta z^{k+1} + (1-\vartheta)z^k = \vartheta\delta_t(z) + z^k \tag{B.21}$$

in order to simplify the representation of the schemes, we obtain the corresponding finite-difference progressive quotient approximation

$$\mathbf{B}^k\delta_t(\hat{w}) + \tau\mathbf{A}^k\hat{w}^k = \tau\mathbf{F}^k, \tag{B.22a}$$

$$\mathbf{M}\delta_t(\hat{\rho}) = b\tau\mathbf{M}\hat{w}^k. \tag{B.22b}$$

On the other hand, the finite-difference regressive approximation has the following expression

$$\mathbf{B}^{k+1}\delta_t(\hat{w}) + \tau\mathbf{A}^{k+1}\hat{w}^{k+1} = \tau\mathbf{F}^{k+1}, \tag{B.23a}$$

$$\mathbf{M}\delta_t(\hat{\rho}) = b\tau\mathbf{M}\hat{w}^{k+1}. \tag{B.23b}$$

Now, multiplying the system (B.22) by $(1-\vartheta)$ and (B.23) by ϑ for fixing $\vartheta \in [0,1]$ and adding both systems we get:

Proposition B.2. *The discrete scheme associated to the equations - can be set out in the following form*

$$\delta_t^\vartheta(\mathbf{B})\,\delta_t(\hat{w}) + \tau\left(\vartheta\mathbf{A}^{k+1}\hat{w}^{k+1} + (1-\vartheta)\mathbf{A}^k\hat{w}^k\right) = \tau\delta_t^\vartheta(\mathbf{F}), \tag{B.24a}$$

$$\mathbf{M}\delta_t(\hat{\rho}) = b\mathbf{M}\delta_t^\vartheta(\hat{w}), \tag{B.24b}$$

$$\mathbf{M}\hat{w}(0) = \hat{w}_0, \tag{B.24c}$$

$$\mathbf{M}\hat{\rho}(0) = \hat{\rho}_0, \tag{B.24d}$$

for $i,j = 1,2,\ldots,N$ in each $k = 0,\ldots,n$ with $\tau = T/n$, $n \in \mathbb{N}$.

Hence, the system (B.24) is the Forward Euler scheme if $\vartheta = 0$ (conditionally stable), Crank-Nicolson scheme if $\vartheta = 1/2$ (unconditionally stable for linear systems), the Backward Euler scheme if $\vartheta = 1$.

If we consider $\vartheta = 1$ (Backward Euler) in (B.24), we have a system of "linear equations" respect to $\hat{w}^{k+1}$ (the system (B.23)), which can be solved using iterative algorithms Chen and Douglas (1991); Thomée (1984), and for example if $\mathcal{V}_0^h$ is the finite element space of piecewise linear functions the error $|\hat{w}^{k+1} - \hat{w}_h^{k+1}|$ in the L^2-norm is of order $\mathcal{O}(\tau + h^2)$ under appropriate smoothness assumptions on $\hat{w}$ and for τ small enough Chen and Douglas

(1991); Douglas (1961); Thomée (1984). We will consider in the next analysis the Crank-Nicholson discretization method in order to solve the system (B.24). However, we will need to be careful because, the linearization decreases the order of the time discretization error to $\mathcal{O}(\tau)$, giving $\mathcal{O}\left(\tau + h^2\right)$, but, this drawback can be overcome by using extrapolation techniques in the linearization of the coefficients. For this reason, combined with an appropriate extrapolation the Crank-Nicholson method can be used in order to produce an error of order $\mathcal{O}\left(\tau^2\right)$ Douglas (1961); Thomée (1984).

B.0.2.1 Static enamel geometry

We apply the theory developed in the above subsection to the specific examples developed in Chapter 4 using the Crank-Nicolson method, e.g., $\vartheta = 1/2$.

The assumption of the neglecting the effect of changes in the enamel geometry involves the constant values for $|\Omega|_0 = |\bar{\Omega}| - \pi\rho_0$, $|\partial E_p|_0 = 2\pi\rho_0$ and $\bar{D}_0 = a_1 - a_2\rho_0$ where $0 < \rho(x,0) = \rho_0 < 1$ is a fixed-constant value. In consequence, dividing all the equation (B.12) for $|\Omega|_0 > 0$ we go to get

$$\partial_t w = \partial_{x_1}\left(\frac{\bar{D}_0}{|\Omega|_0}\partial_{x_1} w\right) + \partial_{x_3}\left(\partial_{x_3} w\right) - \left(\frac{|\partial E_p|_0 R_1}{|\Omega|_0}\right) w, \qquad \text{in } V \times (0,T) \tag{B.25a}$$

$$\partial_t \rho = bw, \qquad \text{in } V \times (0,T) \tag{B.25b}$$

$$w|_{\Gamma_1} = g(x_1), \quad w|_{\Gamma_{2,3,4}} = 0 \qquad \text{in } (0,T) \tag{B.25c}$$

$$w(x,0) = w_0(x), \qquad \text{in } V \tag{B.25d}$$

$$\rho(x,0) = \rho_0 \qquad \text{in } V. \tag{B.25e}$$

In consequence, as particular case of the analysis made in the previous section, we will first present the semi-discrete approximation scheme where (B.25) is discretized only in space using the finite element method. Then we consider fully discrete approximation scheme where the time discretization is based on the Crank-Nicholson method.

Taking into consideration the same vectorial spaces $\mathcal{V}_0^h$ and $\mathcal{V}_V^h$ as finite-element subspaces of $\mathcal{V}_0$ and $\mathcal{V}_V$ correspondently, we can write the weak formulation for the problem (B.25) in the following form: Find $w_h, \rho_h : (0,T) \longrightarrow \mathcal{V}_V$ such that

$$\langle \partial_t w_h, \varphi\rangle + \langle \nabla w_h, \nabla\varphi\rangle = -m_0\langle w_h, \varphi\rangle, \qquad \forall \varphi \in \mathcal{V}_0, t \in (0,T) \tag{B.26a}$$

$$\langle \partial_t \rho_h, \varphi\rangle = b\langle w_h, \varphi\rangle, \qquad \forall \varphi \in \mathcal{V}_0, \tag{B.26b}$$

$$\langle w_h(\cdot,0), \varphi\rangle = \langle w_0, \varphi\rangle, \qquad \forall \varphi \in \mathcal{V}_0 \tag{B.26c}$$

$$\langle \rho_h(\cdot,0), \varphi\rangle = \langle \rho_0, \varphi\rangle \qquad \forall \varphi \in \mathcal{V}_0, \tag{B.26d}$$

where $\nabla = \left(\bar{D}_0/|\Omega|_0\right)^{1/2}\partial_{x_1}\hat{e}_1 + \partial_{x_3}\hat{e}_3$ and $m_0 = |\partial E_p|_0 R_1/|\Omega|_0$. Now, as (B.18) after the introduction of basis function in $\mathcal{V}_0^h$ and writing the solutions as a linear combination of the basis as (B.17), the system can be stated in matrix form

$$\mathbf{M}\frac{d\hat{w}}{dt} + \mathbf{A}\hat{w} = -m_0\mathbf{M}\hat{w}, \qquad t \in (0,T), \tag{B.27a}$$

$$\mathbf{M}\frac{d\hat{\rho}}{dt} = b\mathbf{M}\hat{w}, \qquad t \in (0,T), \tag{B.27b}$$

$$\mathbf{M}\hat{w}(0) = \hat{w}_0, \tag{B.27c}$$

$$\mathbf{M}\hat{\rho}(0) = \hat{\rho}_0 \tag{B.27d}$$

where the matrixes $\mathbf{M}$, $\mathbf{A}$ and the vectors $\hat{w}$, $\hat{\rho}$ are

$$\mathbf{M} = \left(\varphi_i, \varphi_j\right), \quad \mathbf{A} = \left(\nabla\varphi_i, \nabla\varphi_j\right), \quad \hat{w} = (w_1, w_2, \ldots, w_N)^T, \quad \hat{\rho} = (\rho_1, \rho_2, \ldots, \rho_N)^T, \tag{B.28a}$$

$$\hat{w}_0 = (w_0, \varphi_j), \quad \hat{\rho}_0 = (\rho_0, \varphi_j). \tag{B.28b}$$

Therefore, transforming the system equation (B.27) to Crank-Nicolson scheme, we ge:

Proposition B.3. *We can set out the Crank-Nicolson scheme associated to the equation* (B.25) *in the following form*

$$\left(\mathbf{M} + \frac{\tau}{2}(\mathbf{A} + m_0\mathbf{M})\right)\hat{w}^{k+1} = \left(\mathbf{M} - \frac{\tau}{2}(\mathbf{A} + m_0\mathbf{M})\right)\hat{w}^k, \tag{B.29a}$$

$$\mathbf{M}\left(\hat{\rho}^{k+1} - \frac{b}{2}\hat{w}^{k+1}\right) = \mathbf{M}\left(\hat{\rho}^k + \frac{b}{2}\hat{w}^k\right), \tag{B.29b}$$

$$\mathbf{M}\hat{w}(0) = \hat{w}_0, \tag{B.29c}$$

$$\mathbf{M}\hat{\rho}(0) = \hat{\rho}_0, \tag{B.29d}$$

for $k = 1, \ldots, n$.

Taking an appropriate φ, we can proof the unconditional stability of the scheme equation (B.29), Thomée (1984).

In addition, if we consider the boundary condition $w(x_1, 0, t) = 10^{-4}\cos(\pi x_1/2)$ of the Example 1, Chapter 4 and we denoting by $w_e(x,t) = 10^{-4}\cos(\pi x_1/2)e^{-2.25x_3}$ (proposal solution) and w_h like the numerical solution of the corresponding static problem in the scheme Proposition B.3, we can compare how good is our proposal solution $w_e(x,t)$ calculating the L^2-error when the number of elements in the finite-scheme increase as we depicted in Figure B.0.2.1

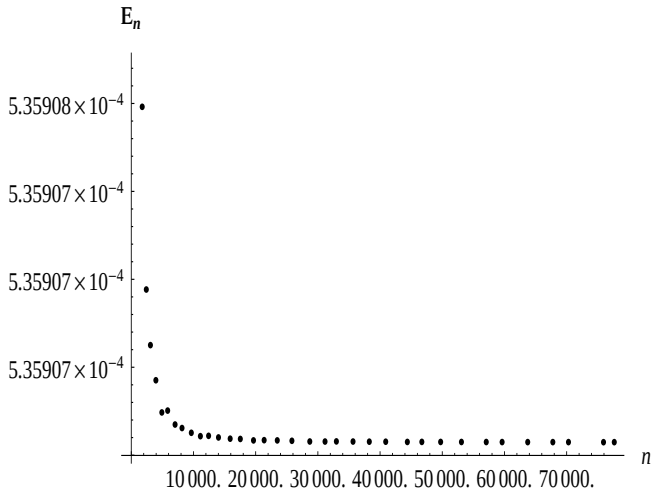

Figure B.3: The L^2-error denoted by $E_n = 10^4\|w_h - w_e\|_2$ between $w_e(x,t)$ and the numerical solution w_h computed by the resolution of the equation (B.29d).

B.0.3 Scheme in polar coordinates

In this section we consider the numerical formulation of system (B.10) on a sector of circular annulus

$$G_{1,2} = \{(r,\theta) : r_1 < r < r_2, |\theta| < \beta\} \tag{B.30}$$

depicted in the Figure 5.5 and Figure 5.9 with boundary

$$\Gamma_1 = \{(r,\theta) : r = r_1, |\theta| < \beta\}, \quad \Gamma_3 = \{(r,\theta) : r_2 < r < r_1, \theta = -\beta\}, \tag{B.31}$$

$$\Gamma_2 = \{(r,\theta) : r = r_2, |\theta| < \beta\}, \quad \Gamma_4 = \{(r,\theta) : r_2 < r < r_1, \theta = \beta\} \tag{B.32}$$

where $0 \leqslant r_1 < r < r_2$ and $\beta = \pi/4$.

In consequence, considering the polar transformation $x_1 = r\cos(\theta)$ and $x_3 = r\sin(\theta)$ into the equation (B.10) and multiplying the equation (B.10a) by r we get

$$r|\Omega|w_t = (r|\Omega|w_r)_r + \frac{1}{r}\partial_\theta\left(\bar{D}\partial_\theta\right)w + r|\partial E_p|(bw - R_1)w, \qquad (r,\theta) \in G,\ t \in (0,T) \tag{B.33a}$$

$$\partial_t \rho = bw, \qquad (r,\theta) \in G,\ t \in (0,T) \tag{B.33b}$$

$$w|_{\Gamma_1} = g(\theta), \quad w|_{\Gamma_{2,3,4}} = 0 \qquad t \in (0,T) \tag{B.33c}$$

$$w(r,\theta,0) = w_0(r,\theta), \qquad (r,\theta) \in G, \tag{B.33d}$$

$$\rho(r,\theta,0) = \rho_0(r,\theta) \qquad (r,\theta) \in G, \tag{B.33e}$$

where we denote $G = G_1$. We can obtain an equivalent approach for $G = G_2$ changing $w|_{\Gamma_1}$ by $w|_{\Gamma_2}$.

In order to find the discrete representation of the system (B.33), we consider the multiplication by a test function $\varphi(r,\theta)$ corresponding to the vectorial space $\mathcal{V}_0$ in the system (B.33) and using the integration by part take into account the Jacobian of the transformation, we arrive to the variational formulation in polar coordinates

$$\langle r|\Omega|\partial_t w, \varphi\rangle_G + \langle \nabla^r w, \nabla^r \varphi\rangle_G = F(\rho, w; r), \qquad \forall \varphi \in \mathcal{V}_0,\ t \in (0,T) \tag{B.34a}$$

$$\langle \partial_t \rho, \varphi\rangle_G = \langle bw, \varphi\rangle_G, \qquad \forall \varphi \in \mathcal{V}_0,\ t \in (0,T) \tag{B.34b}$$

$$\langle w(r,\theta,0), \varphi\rangle_G = \langle w_0(r,\theta), \varphi\rangle_G, \qquad \forall \varphi \in \mathcal{V}_0, \tag{B.34c}$$

$$\langle \rho(r,\theta,0), \varphi\rangle_G = \langle \rho_0(r,\theta), \varphi\rangle_G \qquad \forall \varphi \in \mathcal{V}_0, \tag{B.34d}$$

where likewise, we considered $|\Omega| = |\bar{\Omega}| - \pi\rho^2$, $|\partial E_p| = 2\pi\rho$, $\bar{D} = a_1 - a_2\rho$, $F(\rho, w; r) = r|\partial E_p|(bw - R_1)w$ and the symmetric operator

$$\nabla^r = (r|\Omega|)^{1/2}\partial_r \hat{e}_r + (\bar{D}/r)^{1/2}\partial_\theta \hat{e}_\theta \tag{B.35}$$

for carry on the corresponding transformations in the system (B.33) for obtain the variational formulation (B.4), with $w \in \mathcal{V}_G$.

Hence, taking into consideration $\mathcal{V}_G^h$ as subspace of $\mathcal{V}_G$ we can find $w_h : (0,T) \longrightarrow \mathcal{V}_G^h$ such that

$$\langle r|\Omega|_h \partial_t w_h, \varphi\rangle_G + \langle \nabla_h^r w_h, \nabla_h^r \varphi\rangle_G = F(\rho_h, w_h; r), \qquad \forall \varphi \in \mathcal{V}_0,\ t \in (0,T) \tag{B.36a}$$

$$\langle \partial_t \rho_h, \varphi\rangle_G = \langle bw_h, \varphi\rangle_G, \qquad \forall \varphi \in \mathcal{V}_0, t \in (0,T), \tag{B.36b}$$

$$\langle w_h(\cdot,0), \varphi\rangle_G = \langle w_0, \varphi\rangle_G, \qquad \forall \varphi \in \mathcal{V}_0, \tag{B.36c}$$

$$\langle \rho_h(\cdot,0), \varphi\rangle_G = \langle \rho_0, \varphi\rangle_G \qquad \forall \varphi \in \mathcal{V}_0, \tag{B.36d}$$

and again considering a basis $\{\varphi_i(r,\theta)\}_i^N$ of the corresponding vectorial space $\mathcal{V}_0^h$, we obtain the corresponding matrix form for the system (B.36)

$$\mathbf{B}(\hat{\rho}; r)\frac{d\hat{w}}{dt} + \mathbf{A}(\hat{\rho}; r)\hat{w} = \mathbf{F}(\hat{\rho}, \hat{w}; r), \qquad t \in (0,T) \tag{B.37a}$$

$$\mathbf{M}\frac{d\hat{\rho}}{dt} = b\mathbf{M}\hat{w}, \qquad t \in (0,T) \tag{B.37b}$$

$$\mathbf{M}\hat{w}(0) = \hat{w}_0, \tag{B.37c}$$

$$\mathbf{M}\hat{\rho}(0) = \hat{\rho}_0, \tag{B.37d}$$

where the matrix $\mathbf{M}$, $\mathbf{A}(\hat{\rho};r)$, $\mathbf{B}(\hat{\rho};r)$, $\mathbf{F}(\hat{\rho},\hat{w};r)$ are the corresponding matrixes to $\mathbf{M}$, $\mathbf{A}(\hat{\rho})$, $\mathbf{A}$, $\mathbf{B}(\hat{\rho})$, $\mathbf{F}(\hat{\rho},\hat{w})$ in cartesian coordinates under the polar transformation.

Finally, discretizing the temporal variable we can obtain the respective full scheme to (B.40) setting out the following proposition

Proposition B.4. *The discrete scheme associated to the system can be set out in the following form*

$$\delta_t^{\vartheta}(\mathbf{B})\,\delta_t(\hat{w}) + \tau\left(\vartheta\mathbf{A}^{k+1}\hat{w}^{k+1} + (1-\vartheta)\mathbf{A}^{k}\hat{w}^{k}\right) = \tau\delta_t^{\vartheta}(\mathbf{F}), \tag{B.38a}$$

$$\mathbf{M}\delta_t(\hat{\rho}) = b\tau\mathbf{M}\delta_t^{\vartheta}(\hat{w}), \tag{B.38b}$$

$$\mathbf{M}\hat{w}(0) = \hat{w}_0, \tag{B.38c}$$

$$\mathbf{M}\hat{\rho}(0) = \hat{\rho}_0, \tag{B.38d}$$

for $i,j = 1,2,\ldots,N$ *in each* $k = 0,\ldots,n$ *with* $\tau = T/n$, $n \in \mathbb{N}$.

Therefore, if $\vartheta = 0$ then (B.38) is the forward Euler scheme, if $\vartheta = 1/2$ then (B.38) is the Crank- Nicolson scheme and if $\vartheta = 1$ then (B.38) is the backward Euler scheme.

Static enamel geometry

Once again, without having under consideration the effects of changes in the enamel geometry, i.e., fixing $|\Omega|_0 = |\bar{\Omega}| - \pi\rho_0$, $|\partial E_p|_0 = 2\pi\rho_0$ and $\bar{D} = a_1 - a_2\rho_0$ where $0 < \rho(r,\theta,0) = \rho_0 < 1$, we can dividing all the equation (B.4) for $|\Omega|_0 > 0$ and consider a similar approach for (B.4), we get a particular matrix expression of (B.38)

$$\left(\mathbf{M}_r + \frac{\tau}{2}(\mathbf{A}_r + m_0\mathbf{M}_r)\right)\hat{w}^{k+1} = \left(\mathbf{M}_r - \frac{\tau}{2}(\mathbf{A}_r + m_0\mathbf{M}_r)\right)\hat{w}^{k}, \tag{B.39a}$$

$$\mathbf{M}\left(\hat{\rho}^{k+1} - \frac{b}{2}\hat{w}^{k+1}\right) = \mathbf{M}\left(\hat{\rho}^{k} + \frac{b}{2}\hat{w}^{k}\right), \tag{B.39b}$$

$$\mathbf{M}\hat{w}(0) = \hat{w}_0, \tag{B.39c}$$

$$\mathbf{M}\hat{\rho}(0) = \hat{\rho}_0, \tag{B.39d}$$

for $k = 1,\ldots,n$ and $i,j = 1,2,\ldots,N$, where the matrixes $\mathbf{M}$, $\mathbf{M}_r$ $\mathbf{A}_r$ and the vectors $\hat{w}$, $\hat{\rho}$ are

$$\mathbf{M} = \langle\varphi_i,\varphi_j\rangle_G, \quad \mathbf{M}_r = \langle r\varphi_i,\varphi_j\rangle_G, \quad \mathbf{A}_r = \langle\nabla^r\varphi_i,\nabla^r\varphi_j\rangle_G, \quad \hat{w} = (w_1,w_2,\ldots,w_N)^T, \tag{B.40a}$$

$$\hat{\rho} = (\rho_1,\rho_2,\ldots,\rho_N)^T, \quad \hat{w}_0 = (w_0,\varphi_j), \quad \hat{\rho}_0 = (\rho_0,\varphi_j). \tag{B.40b}$$

where $\nabla^r = r^{1/2}\partial_r\,\hat{e}_r + (\bar{D}_0/|\Omega|_0 r)^{1/2}\partial_\theta\,\hat{e}_\theta$.

Over again, considering the boundary condition $w|_{\Gamma_1} = 10^{-4}\cos(2\theta)$ of the Example 5, Chapter 5 and denoting by $w_e(r,\theta) = 10^{-4}\frac{K_1(2r)}{K_1(2)}\cos(2\theta)$ (proposal solution) and w_h like the numerical solution of the corresponding static problem in the scheme equation (B.39), we can compare how good is our proposal solution $w_e(r,\theta)$ calculating the L^2-error when the number of elements in the finite-scheme increase as we depicted in Figure B.0.3

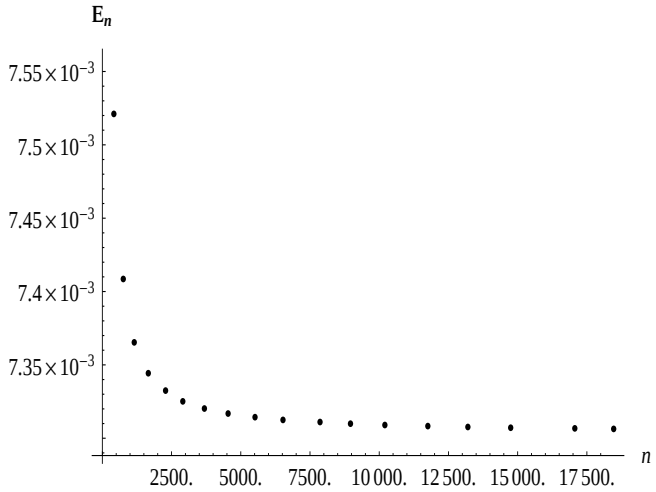

Figure B.4: The L^2-error denoted by $E_n = 10^4\|w_h - w_e\|_2$ between $w_e(r,\theta)$ and the numerical solution w_h computed by the resolution of the equation (B.39).

B.0.4 Domain Decomposition Algorithm

Let us consider a partition of V into two non-overlapping open sub-domains V_i, $i = 1,2$, and denote by $\Gamma^* := \bar{V}_1 \cap \bar{V}_2$ the common boundary between $\bar{V}_1$ and $\bar{V}_2$, and Γ_i, $i = 1,2,3,4,5,6$ the remaining boundaries. We define the domains as follow

$$V_1 = \{(x_1,x_3) : |x_1| < 1, \text{and } 0 < x_3 < \xi\} \text{ and } V_2 = \{(x_1,x_3) : |x_1| < 1, \text{and } \xi < x_3 < 3\} \quad \text{(B.41)}$$

where $\xi = 0.3$, see Figure B.5 and

$$\Gamma_1 = \{(x_1,x_3) : |x_1| < 1, x_3 = 0\}, \quad \Gamma_2 = \{(x_1,x_3) : x_1 = 1, 0 < x_3 < \xi\}, \quad \text{(B.42)}$$

$$\Gamma_3 = \{(x_1,x_3) : x_1 = 1, \xi < x_3 < 3\}, \quad \Gamma_4 = \{(x_1,x_3) : |x_1| < 1, x_3 = 3\}, \quad \text{(B.43)}$$

$$\Gamma_5 = \{(x_1,x_3) : x_1 = -1, \xi < x_3 < 3\}, \quad \Gamma_6 = \{(x_1,x_3) : x_1 = -1, 0 < x_3 < \xi\}, \quad \text{(B.44)}$$

$$\Gamma^* = \{(x_1,x_3) : |x_1| < 1, x_3 = \xi\}. \quad \text{(B.45)}$$

An iterative method for solving the model (5.3) can be obtained by applying a saddle point iterative algorithm such as Uzawa's method, to update the Lagrange multiplier function

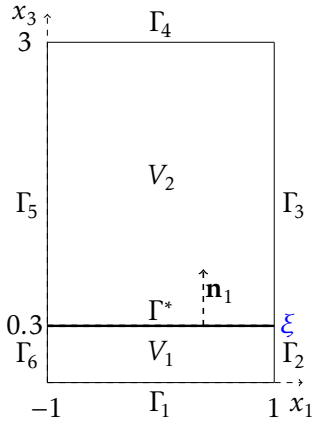

Figure B.5: Domains V_1 and V_2 with no-overlapping partitions.

$\mu(x)$, as described below. Let's consider μ^0 as starting guess and $\nu > 0$ a chosen step size such that where

Algorithm 4 For model (5.3)

for $n = 0, 1, .., m$ **do** ▷ $t_n = n\tau$ where $\tau = T/m$, $T = O(1)$
  for $k = 0, 1, ...$ until convergence **do** ▷ $w_1^{k+1,n+1}$ and w_2^{k+1} in parallel
    $|\Omega|^{n+1}\left((\delta_t(w_1^{k+1})\right) = \tau\nabla\cdot\left(|\Omega|^{n+1}\nabla w_1^{k+1,n+1}\right) + b^*|\partial E_p|^{n+1}w_1^{k+1,n+1}w_2^{k+1}$ in V_1;
    $w_1^{k+1,n+1} = Q^{n+1}(x_1)$ on Γ_1; ▷
    $\mathbf{n}_1\cdot\left(\nabla w_1^{k+1,n+1}\right) = -\mu^k$, on Γ^*;
    $w_1^{k+1,n+1} = 0$, on Γ_j; ▷ For $j = 2, 6$
    $w_1^{k+1,0} = 0$, in V_1;
    $0 = \nabla_g\cdot\nabla_g w_2^{k+1} - (1+\gamma)|\partial E_p|^{n+1}R_1 w_2^{k+1}$ in V_2;
    $w_2^{k+1} = 0$, on Γ_j; ▷ For $j = 3, 4, 5$
    $\mathbf{n}_1\cdot\left(\nabla w_2^{k+1}\right) = -\mu^k$, on Γ^*; ▷ $\mathbf{n}_2 = -\mathbf{n}_1$
    $\mu^{k+1,n+1} = \mu^{k,n+1} - \nu\left(w_1^{k+1,n+1} - w_2^{k+1}\right)$; ▷ Update of μ^{k+1}
  end for
  Output: $(w_1^{k,n}, w_2^{k,n})$
  $\rho^{n+1} - \rho^n = -\tau b^* w_2^{k,n}$, in V_2;
  $\rho^0 = \rho^0$, in V_2;
end for

$$\nabla_g = \left(\partial_{x_1}\left(\bar{D}^{n+1}\right)^{1/2}, \partial_{x_2}\left(\bar{D}^{n+1}\right)^{1/2}, \partial_{x_3}\left(|\Omega|^{n+1}\right)^{1/2}\right)$$

Appendix C

Tables

Table C.1: Summary of diffusion experiments

Author	**Species**	**Component**	D ($\mu m^2/h$),	$\lambda = (D/R)^{1/2}$ (μm),	$\lambda_b = (Dt_m)^{1/2}$ (μm),
Patel et al. (1987)	-	-	$0.9 \cdot 10^8$,	$0.3 \cdot 10^5$,	$0.3 \cdot 10^4$,
Bollet et al. (2004)	-	-	10^6	10^4,	10^3,
Van Dijk	-	-	$0.9 \cdot 10^6$	$0.3 \cdot 10^4$,	$0.3 \cdot 10^3$,
(Marthaler et al. (1960))	man	$[^{35}S]$	10^4	10^3,	10^2,
(Duckworth et al. (1967)		$^{18}F^-$	$0.9 \cdot 10^4$	$0.3 \cdot 10^3$,	$0.3 \cdot 10^2$,
(Braden et al. (1971))		$^{24}Na^+$	10^2	10^2,	10,
(Flim (et al. (1977))	cattle	$^{18}F^-$	10^2	10^2,	10,
		$^{45}Ca^{2+}$	1	10,	1,
(de Rcoy et al. (1980))		$^{32}PO_4$	1	10,	1,
		$^{32}PO_3F$	0.9	3,	0.3,

$R \sim 10^{-2} 1/h$ and $t_m \sim 1h$

Table C.2: Summary of thickness of outer enamel layer.

Author	**Article Pages (J. Pages)**	λ_o (μm),
Holly et al. (1968),	3 (321), 4 (322), 12 (330)	10 (2-20),
Shellis (1984),	4 (978),	4.9 ± 5.3,
		28.3 ± 3.6,
Yoshikawa et al. (1990),	4 (674)	30.6 ± 17,
		31.8 ± 19,
		35.4 ± 9,
		27.0 ± 7,
Fava et al. (1997),	-	7.25,

λ_o: measure of the thickness of outer enamel layer

Bibliography

Anderson, P., Levinkind, M., and Elliott, J. (1998). Scanning microradiographic studies of rates of in vitro demineralization in human and bovine dental enamel. *Archives of Oral Biology*, 43(8):649 – 656.

Avery, J., Steele, P., and Avery, N. (2002). *Oral Development and Histology*. Thieme Medical Publishers.

Bensoussan, A., Lions, J., and Papanicolaou, G. (2011). *Asymptotic Analysis for Periodic Structures*. AMS Chelsea Publishing Series. American Mathematical Society.

Bjrndal, L. (2008). The caries process and its effect on the pulp: The science is changing and so is our understanding. *Journal of Endodontics*, 34(7, Supplement):S2 – S5. Proceedings of the Joint Symposium Sponsored by the American Academy Of Pediatric Dentistry and the American Association Of Endodontists. Emerging Science in Pulp Therapy: New Insights Into Dilemmas and Controversies.

Bjrndal, L. and Thylstrup, A. (1995). A structural analysis of approximal enamel caries lesions and subjacent dentin reactions. *European Journal of Oral Sciences*, 103(1):25–31.

Bollet-Quivogne, F., Anderson, P., Dowker, S., and Elliott, J. C. (2005). Scanning microradiographic study on the influence of diffusion in the external liquid on the rate of demineralization in hydroxyapatite aggregates. *European Journal of Oral Sciences*, 113(1):53–59.

Bourgat, J. (1979). *Numerical Experiments of the Homogenization Method for Operators with Periodic Coefficients: Computing methods in applied sciences and engineering*. Lecture Notes in Mathematics. Springer Berlin Heidelberg.

Bourgat, J. and Dervieux, A. (1978). *Méthode d'homogénéisation des opérateurs à coefficients périodiques: étude des correcteurs provenant du développement asymptotique*. Rapports de recherche / Institut de recherche d'informatique et d'automatique. IRIA.

Chandra, S., Chandra, S., Chandra, M., Chandra, G., and Chandra, N. (2007). *Textbook of Dental and Oral Histology with Embryology and Multiple Choice Questions*. Jaypee Brothers Medical Publishers.

Chen, Z. and Douglas, J., J. (1991). Approximation of coefficients in hybrid and mixed methods for nonlinear parabolic problems. *Mat. Aplic. Comp.*, 10(10):137–160.

Conca, C., Natesan, S., and Vanninathan, M. (2001). Numerical solution of elliptic partial differential equations by bloch waves method. *Dep. Mat. Apl., Univ. Salamanca, Salamanca.*, page 63âĂŞ83.

Conca, C., Orive, R., and Vanninathan, M. (2002). Bloch approximation in homogenization and applications. *SIAM J. Math. Anal.*, 33(5):1166âĂŞ1198.

Daniel, D. E. and Shackelford, C. D. (1988). Disposal barriers that release contaminants only by molecular diffusion. *Nucl. Chem. Waste Manage.*, 8:299–305.

Douglas, J., J. (1961). *A survey of numerical methods for parabolic differential equations, in Advances in Computers*, volume 2 of *F. L. Alt, ed.* Academic Press, New York.

Dumont, E. (1995). Mammalian enamel prism patterns and enamel deposition rates. *Scanning Microscopy*, 9(2):429–442.

Dumont, E. (1996). Enamel prism morphology in molar teeth of small eutherian mammals. *Scanning Microscopy*, 10(2):349–370.

Ehrlich, H., K. P. D. K. and Pokrovsky, O. (2008). Principles of demineralization: Modern strategies for the isolation of organic frameworks: Part i. common definitions and history. *Micron*, 39(8):1062 – 1091.

Fabregas, L. R. I. and Rubinstein, J. (2013). A mathematical model for the progression of dental caries. *Mathematical Medicine and Biology*.

Fava, M., W. I. F. d. M. F. D. C. L. (1997). Prismless enamel in human non-erupted decidous moalr teeth: A scanning electron microscopy study. *Revista de Odontologia da Universidade de São Paulo*, 11.

Featherstone, J. (1977). Diffusion phenomena during artificial carious lesion formation. *Journal of Dental Research*, 56(4 suppl):D48–D52.

Gray, J. (1962). Kinetics of the dissolution of human dental enamel in acid. *Journal of Dental Research*, 41(3):633–645.

Hecht, F., Pironneau, O., Le Hyaric, A., and Ohtsuka, K. (2012). *Freefem++ Manual*. Laboratoire Jacques-Louis Lions, Université Pierre et Marie Curie.

Herrero, M. and López, J. (2005). Bone Formation: Biological Aspects and Modelling Problems. *Journal of Theoretical Medicine*, 6.

Holly, F. and Gray, J. (1968). Mechanism for incipient carious lesion growth utilizing a physical model based on diffusion concepts. *Archives of Oral Biology*, 13(3):319 – 333, IN23.

Hornung, U. (1997). *Homogenization and Porous Media*. Interdisciplinary applied mathematics. Springer Verlag.

Jeng, Y.-R., Lin, T.-T., and Shieh, D.-B. (2009). Nanotribological characterization of tooth enamel rod affected by surface treatment. *Journal of Biomechanics*, 42(14):2249 – 2254.

Keller, J. (1963). Conductivity of a medium containing a dense array of perfectly conducting spheres or cylinders or nonconducting cylinders. *Journal of Applied Physics*, 34(4):991–993.

Kidd, E. and Fejerskov, O. (2004). What constitutes dental caries? histopathology of carious enamel and dentin related to the action of cariogenic biofilms. *Journal of Dental Research*, 83(suppl 1):C35–C38.

Kudiyirickal, M. and Ivancaková, R. (2008a). Early enamel lesion part I. classification and detection. *Acta Medica (Hradec Kralove)*, 51(3):145–149.

Kudiyirickal, M. and Ivancaková, R. (2008b). Early enamel lesion part II. histomorphology and prevention. *Acta Medica (Hradec Kralove)*, 51(3):151–156.

Lions, P. (1990). On the schwartz alternating method iii: A variant for non-overlapping subdomains. *T.F. Chan et al. Eds. SIAM Phildelphia*, pages 202–231.

Maas, M. and Dumont., E. (1999). Built to last–a microscopic view of the morphology and evolution of primate dental enamel. *Evolutionary Anthropology*, 8(2):133–152.

Martin, B. (1994). Mathematical model for the mineralization of bone. *Journal of Orthopaedic Research*, 12(3):375–383.

Mathew, T. (2008). *Domain Decomposition Methods for the Numerical Solution of Partial Differential Equations*. Lecture notes in computational science and engineering. Springer.

Patel, M., Fox, J., and Higuchi, W. (1987a). Effect of acid type on kinetics and mechanism of dental enamel demineralization. *J Dent Res*, 66(9):1425–30.

Patel, M., Fox, J., and Higuchi, W. (1987b). Physical model for non-steady-state dissolution of dental enamel. *J Dent Res*, 66(9):1418–1424.

Pinchover, Y. and Rubinstein, J. (2005). *An Introduction To Partial Differential Equations*. Number v. 10 in An introduction to partial differential equations. Cambridge University Press.

Poole, D., Shellis, R., and Tyler, J. (1981). Rates of formation in vitro of dental caries-like enamel lesions in man and some non-human primates. *Archives of Oral Biology*, 26(5):413 – 417.

Quarteroni, A. and Valli, A. (1999). *Domain Decomposition Methods for Partial Differential Equations*. Numerical mathematics and scientific computation. Clarendon Press.

Quigley, R., Fernandez, F., and Yanful, E. (1987). *Ion Transfer by Diffusion Through Clayey Barriers*. Geotechnical Research Centre report. Geotechnical Research Centre, University of Western Ontario.

Radlanski, R. and Renz, H. (2004). A possible interdependency between the wavy path of enamel rods, distances of retzius lines, and mitotic activity at the cervical loop in human teeth: a hypothesis. *Medical Hypotheses*, 62(6):945–949.

Ripa, L., Gwinnett, A., and Buonocore, M. (1966). The âĂIJprismlessâĂİ outer layer of deciduous and permanent enamel. *Archives of Oral Biology*, 11(1):41 – IN5.

Rouhi, G., E. M. S. L. and Herzog, W. (2007). Modeling bone resorption using Mixture Theory with chemical reactions. *Journal of Mechanics of Materials and Structures*, 2(6).

Shellis, R. and Wilson, R. (2004). Apparent solubility distributions of hydroxyapatite and enamel apatite. *J Colloid Interface Sci*, 278(2):325–332.

Silva, E. and Ulm, F.-J. (2002). A bio-chemo-mechanics approach to bone resorption and fracture. In Karihaloo, B., editor, *IUTAM Symposium on Analytical and Computational Fracture Mechanics of Non-Homogeneous Materials*, volume 97 of *Solid Mechanics and Its Applications*, pages 355–366. Springer Netherlands.

Stumpf, M. and Porter, M. (2012). Critical truths about power laws. *Science*, 335(6069):665–666.

ten Cate, J. (1997). Review on fluoride, with special emphasis on calcium fluoride mechanisms in caries prevention. *Eur J Oral Sci*, 105(5 Pt 2):461–465.

Thomée, V. (1984). *Galerkin finite element methods for parabolic problems*. Number nos. 1053-1054 in Lecture notes in mathematics. Springer-Verlag.

Thylstrup, A. and Fejerskov, O. (1986). *Textbook of Cardiology*. Mosby, Incorporated.

van Dijk, J., Borggreven, J., and Driessens, F. (1983). Diffusion in mammalian tooth enamel in relation to the caries process. *Arch. Oral. Biol.*, 28(7):591–597.

Wu, M., Higuchi, W., Fox, J., and Friedman, M. (1976). Kinetics and mechanism of hydroxyapatite crystal dissolution in weak acid buffers using the rotating disk method. *J. Dent. Res.*, 55(3):496–505.

Zimmerman, S. (1966a). A mathematical theory of enamel solubility and the onset of dental caries: I. the kinetics of dissolution of powdered enamel in acid buffer. *The bulletin of mathematical biophysics*, 28(3):417–432.

Zimmerman, S. (1966b). A mathematical theory of enamel solubility and the onset of dental caries: II. some solubility equilibrium considerations of hydroxyapatite. *The bulletin of mathematical biophysics*, 28(3):433–441.

Zimmerman, S. (1966c). A mathematical theory of enamel solubility and the onset of dental caries: III. development and computer simulation of a model of caries formation. *The bulletin of mathematical biophysics*, 28(3):443–464.